UNIVERSITÀ DEGLI STUDI DI MILANO

Scuola di Dottorato in Scienze Biologiche e Molecolari

XXVIII Ciclo

Analysis of the *in vivo* function of Haspin kinase using Zebrafish as a model system: knockdown and knockout approaches

Guido Roberto Gallo

PhD Thesis

Scientific tutor: Prof. Paolo Plevani

Academic year: 2014-2015

SSD: BIO/11; BIO/06

Thesis performed at: Department of Biosciences, University of Milan and Department of Biology, Temple University, Philadelphia (USA)

INDEX

PART I

During my Ph.D. I worked on two distinct research projects. The first one has been related to conclude an ongoing work that began during my Master Degree internship under the supervision of Prof. Franco Cotelli and in collaboration with the research group directed by Prof. Paola Riva (Department of Medical Biotechnology and Translational Medicine, University of Milan). The project concerns the analysis of cardiac defects caused by the functional inactivation of Adap2 (protein involved in Neurofibromatosis type 1 microdeletion syndrome), during zebrafish development.

The second project is related to the main research topic that I wanted to address during the three years of my Ph.D. In fact, I was interested in analyzing the expression and function of the *haspin* gene during zebrafish embryonic development. This work represents a collaboration between Proff. Plevani and Muzi-Falconi group and the zebrafish unit led by Prof. Franco Cotelli at the Department of Biosciences, University of Milan. Part of the work related to this project was performed at Temple University, Philadelphia (USA) in collaboration with Dr. Gianfranco Bellipanni.

PROJECT 1

This project concerns the analysis of *adap2* gene expression and function during zebrafish embryonic development focusing, in particular, on cardiogenesis. The study of the *adap2* gene was of particular interest for me, as it had been previously reported to be potentially involved in Neurofibromatosis type 1 (NF1) microdeletion syndrome (Venturin *et al.,* 2005; data previously obtained at our collaborator's laboratory).

NF1 is an autosomal dominant pathology with an incidence of 1/3500 individuals. It is characterized by an increased risk of developing tumors, café-au-lait spots and multiple dermal neuro-fibromas (Huson and Hughes, 1994). This disease is caused by constitutional mutations of the *NF1* gene on chromosome 17 (17q11.2), which encodes a protein with a tumor suppressor function. 5-20% of NF1 patients carry a heterozygous deletion of 1,5 Mb (Mega base pairs) involving *NF1* and contiguous genes lying in its flanking regions (Jenne *et al.*, 2001; Venturin *et al.*, 2004). These patients are called microdeleted patients and present a more severe phenotype compared to the classic NF1 symptoms, probably caused by haploinsufficiency of one or more genes located in the deleted region. In particular, they show facial dysmorphisms, mental retardation and cardiovascular malformations (Venturin *et al.*, 2004; Venturin *et al*., 2005). By genotype-phenotype correlation analysis it was possible to identify the potential genes involved in

the characteristic phenotypes of NF1 microdeletion syndrome. Particularly, the research group directed by Prof. Paola Riva (Department of Medical Biotechnology and Translational Medicine, University of Milan), with whom we collaborated, had identified *ADAP2* (ArfGAP with dual PH domains 2) as a possible candidate for the onset of cardiovascular malformations in microdeleted patients. In fact, this gene is located in the deletion interval of 1,5 Mb flanking *NF1* and it is characterized by high levels of expression in human and mouse fetal heart, particularly during fundamental stages of cardiac morphogenesis (Venturin *et al*., 2005).

ADAP2 encodes a protein belonging to the GAPs (GTPase Activating Proteins) family, involved in membrane trafficking, cytoskeletal actin reorganization and cell motility (Hanck *et al*., 2004; Venkateswarlu *et al*., 2007).

Before our work, there were no studies about its function during embryonic development, and therefore we found particularly interesting to investigate *in vivo* the Adap2 role. We decided to use zebrafish (*Danio rerio*, Teleostea), a model system for the study of embryonic development in Teleostea and, in general, in Vertebrates. This little fish, thanks to its natural features, is also an excellent model for the analysis of cardiovascular system development (Weinstein *et al*., 1995; Kimmel *et al.*, 1995). Our work aimed to verify an involvement of Adap2 during cardiac morphogenesis in zebrafish in order to verify the hypothesis that this gene could be considered a candidate gene for the onset of cardiovascular malformations in NF1 microdeleted patients. Our findings have been published in the Journal of Medical Genetics in 2014, during my second year of Ph.D (part 2).

PROJECT 2

The study of the function of Haspin during zebrafish embryonic development represents my main Ph.D. project. We are still terminating the last experiments in order to write and submit the manuscript possibly on a high impact scientific Journal. I will develop in details the rationale and the results obtained on this research topic in the introduction of my thesis (Abstract, State of the art, Aim of the Project, Main results, Conclusions and future prospects, References).

ABSTRACT

The *Haspin* gene encodes an atypical serine/threonine mitotic kinase first discovered in mouse spermatocytes and preferentially expressed in tissues with a high rate of proliferating cells. Haspin acts at metaphase by phosphorylating threonine 3 of histone H3 (H3Thr3PH) and this modification allows the recruitment of the chromosomal passenger complex, a key factor required to orchestrate different steps of mitosis. In human cells, *HASPIN* depletion causes a decrease in H3Thr3 levels, resulting in premature loss of sister chromatid cohesion and in defects in chromosome alignment at metaphase. Haspin has been found in all eukaryotic organisms; however, up to know, its role during animal embryonic development has never been investigated. We decided to investigate its function and expression during zebrafish embryonic development and, to this aim, we took advantage of a morpholino (MO)-mediated knockdown approach and of the CRISPR-Cas9 knockout strategy.

We identified and cloned the zebrafish *haspin* ortholog, together with a previously unknown splicing isoform, and we clarified its expression pattern during embryogenesis and in some adult tissues. We demonstrated a relevant maternal contribution for the *haspin* transcript and important levels of zygotic expression in tissues with a high rate of proliferating cells, such as the developing brain and hematopoietic tissues. We also detected *haspin* transcript in the adult gonads and found that its expression is significantly switched on after injury during adult fin tissue regeneration.

Interestingly, after Haspin functional inactivation using two different MOs, a translation blocking (ATG MO) and a splicing one, we demonstrated that Haspin is involved in H3Thr3PH also in zebrafish. Moreover, microinjection of the *haspin* ATG MO results in high embryo mortality and severe defects during epiboly stages, indicating important alterations in cellular rearrangements and movements.

A *haspin* stable mutant line was generated by using the CRISPR-Cas9 technology: we isolated three different mutant *haspin* alleles, all causing the formation of premature stop codons. Although they do not show evident phenotypic alterations during embryogenesis, embryos carrying a homozygous genotype for these mutations are not able to reach the adulthood stage, showing a high rate of mortality in the first three weeks of larval development, indicating that Haspin is fundamental for larval survival and growth.

To conclude, we clarified various aspects of *haspin* expression pattern during zebrafish development and in adult organs. Even though we were not able yet to unambiguously define the phenotypic effect of Haspin functional inactivation by using a MO-mediated approach, we paved the way for the analysis of the effect of a complete *haspin* gene knockout during zebrafish development by generating a *haspin* stable KO line and by showing that this null mutant allele significantly affects larval survival and growth.

STATE OF THE ART

Cell cycle regulation during development

During embryogenesis, the process by which the embryo forms and develops, a proper control of the cell cycle is critical in many ways. Most importantly, there must be an accurate balance of both the steps that play a role during normal growth: cell division and cell differentiation. It is fundamental to ensure that adequate stem cell pools are maintained and, at the same time, that populations of cells start to acquire a specific fate, thus differentiating in the various types that will constitute all different tissues and organs.

To this end, a proper establishment of asymmetric cell divisions, depending on the correct distribution of polarization factors within the cell, is essential. Interestingly, epigenetics modifications, namely heritable changes in gene expression or function that do not alter primary DNA sequences, are one of the ways in which cells with identical genomes can be directed to either remain in an undifferentiated state or become specialized to acquire a particular function (Reik, 2007; Bonasio *et al.*, 2010).

Disruption in the regulation of cell division and differentiation may lead to cancer development and contribute to other pathologies such as birth defects, degenerative diseases, tissue dystrophy and infertility (Gonzalez, 2007; Knoblich, 2010; Wodarz and Näthke, 2007).

Another very important aspect of cell cycle regulation is the equal partition of the genetic material of the mother cells between the two daughter cells, that must both receive the correct complement of chromosomes. This may appear as a simple process, but the way this goal is actually accomplished is very complicated. A lot of different steps must take place in a coordinated manner, such as DNA replication, chromatin condensation and compaction, the establishment of a properly oriented mitotic spindles and the presence of control mechanisms, the so called cell cycle checkpoints, that monitor the ongoing of cellular division, arresting it if some abnormalities are detected (Clevers, 2005; Quyn *et al.*, 2010; Gray *et al.*, 2010). A key set of mitotic kinases is essential to orchestrate all these processes, as well as a balance with the competing action of protein phosphatases. Changes in many other cellular events also take place, including secretion patterns, organelle migration, cytoskeletal rearrangements and the disassembly and assembly of the nuclear membrane. The most critical problem for the cell is to coordinate a large number of processes in both space and time, with different activities being switched on and off at precise times and locations (Siller and Doe, 2009; Gönczy, 2008).

Finally, an accurate regulation of cell division is also fundamental in the adult organism, as there remains are a lot of tissues with a high rate of proliferating cells. In particular, a very critical event for the reproductive biology of an individual is the accuracy of meiosis, the cellular process that takes place in the gonads and generates haploid gametes from diploid precursors. A proper meiotic regulation is crucial, since errors occurring during this event, in particular during chromosome segregation in meiosis I, may lead to genetic problems and aneuploidy in the resulting egg and embryo (Hunt and Hassold, 2002).
Among all the molecules orchestrating the cell cycle identified so far, the Chromosomal Passenger Complex certainly plays a pivotal role in mitosis (Carmena *et al.*, 2012a).

The Chromosomal Passenger Complex-actors in play

The Chromosomal Passenger Complex (CPC) is considered as one of the master regulators of the cell cycle. It is able to control key mitotic events during almost every phase of cellular division, ensuring that two daughter cells can correctly be generated following the accurate distribution of the genetic material of the mother (Carmena *et al.*, 2012a).
The CPC can be ideally separated into two modules: a catalytic module and a chromosome-localization module. The first one comprises Aurora-B kinase and the highly conserved C-terminal domain of the INCENP protein (IN box), while the second one is composed of Survivin, Borealin and the INCENP amino terminus (Ruchaud *et al.*, 2007).
A proper coordination between all these different components is crucial for the beginning and the ongoing of mitosis. First of all, the INCENP protein has a structural role, constituting a scaffold on which the CPC is then assembled; it interacts with the three other members of the complex, thus providing the link between its two modules. Both Survivin and Borealin, indeed, bind the N-terminal portion of INCENP, forming a triple coiled-coil, while Aurora-B binds its C-terminal domain (Carmena *et al.*, 2012a).
Survivin, member of the inhibitor of apoptosis (IAP family) proteins, possesses a single baculovirus IAP repeat (BIR) domain, is able to bind the other three complex members and is phosphorylated by Aurora-B. It is mainly a chaperone protein, in fact, its most relevant activity is to contribute to the localization of the CPC on mitotic centromeres (Ruchaud *et al.*, 2007).
Borealin, also named Dasra-B, is a protein that was isolated in a proteomic study performed to identify components of the mitotic chromosome scaffold. It helps to stabilize the interactions between the other components of the CPC, participating in the three-helix

bundle that constitutes the CPC localization module with its N-terminal alpha helices. Moreover, like Survivin, also Borealin plays a role in the centromere targeting of the CPC.
Aurora-B is a Ser/Thr kinase protein very highly conserved from yeast to mammals and it is one of the most important coordinator of all the different processes occurring during cell division. The binding between Aurora-B and the C terminus domain of INCENP is important for the initial activation of the kinase; moreover, Aurora-B phosphorylates INCENP, thus creating a positive feedback activation loop (Carmena *et al.*, 2012a).

The Chromosomal Passenger Complex-activity during mitosis

During late S phase, the CPC initially localizes on pericentromeric heterochromatin (Cooke *et al.*, 1987; Hayashi-Takanaka *et al*., 2009; Monier *et al.*, 2007). The initial step required for the activation of the CPC is the phosphorylation of the threonine 3 of histone H3 carried out by the serine/threonine kinase Haspin (Wang *et al*., 2010). This particular phosphorylation is mainly observed at the inner centromeres region during prometaphase, and this residue is then recognized and bound by the BIR domain of the Survivin subunit, thus providing a binding site for CPC recruitment on mitotic centromeres (Niedzialkowska *et al.*, 2012; Kelly *et al.*, 2010). Another phosphorylation also contributes to the accumulation of the complex on the chromosomes: the kinase Bub1 phosphorylates histone H2A on threonine 120, thus leading to the recruitment of Shugoshins Sgo1 and Sgo2. After this process, this protein complex is able to interact with CDK1-phosphorylated Borealin, thus promoting an accumulation of CPC at centromeres (Yamagishi *et al.*, 2010; Wang *et al*., 2011; Kaur *et al.*, 2010).
The complex is thereby recruited on mitotic chromosomes, making feasible its cell division controller role, via its kinase module, initially activated by INCENP binding (Honda *et al.*, 2003; Kang *et al.*, 2001; Sessa *et al.*, 2005). First of all, Aurora-B phosphorylates H3 at serine 10; this modification is the most characteristic epigenetic marker for mitotic chromosomes and it is detectable all over the entire chromosome, as they start to condense during prophase (Hendzel *et al.*, 1997; Hsu *et al.*, 2000; Adams *et al.*, 2001). During mitosis, the most critical task carried out by Aurora-B is to monitor the correct kinetochore-microtubule attachments in the contest of a bipolar spindle thus identifying and correcting chromosomes that are not properly oriented (Lampson *et al.*, 2004). To this end, Aurora B controls different regulatory pathways: one of the most important acts by phosphorylating the microtubule depolymerase protein MCAK, whose main role is to mediate the disassembly and destabilization of microtubules attached to maloriented

chromosomes to allow a correct re-orientation (Lan *et al.*, 2004; Ohi *et al.*, 2004). Aurora-B is also involved in the regulation of the SAC (Spindle assembly checkpoint), namely the mechanism preventing separation of sister chromatids until each chromosome is properly attached to the microtubules of the mitotic spindle. The role of Aurora-B in regulating SAC activity has been demonstrated in different models, from fission yeast to human cells (Petersen *et al*., 2003; Kallio *et al.*, 2002). The CPC also plays an important role during late mitosis, when it re-localizes first to the central spindle microtubules, and then also to the equatorial complex, the area where the cleavage furrow is assembled to start cytokinesis (Ruchaud *et al.*, 2007; Carmena *et al.*, 2012a). It has been demonstrated that the CPC is fundamental for the regulation and completion of many processes taking place in this phase: anaphase chromatid compaction, anaphase spindle stabilization and cytokinesis. During this last process, CPC is required for contractile ring formation and abscission required for the separation of daughter cells during cytokinesis (Carmena *et al.*, 2012a; Kitagawa and Lee, 2015).

Several studies addressed the role played by some of the CPC proteins during animal embryonic development, also using zebrafish (*Danio rerio*, Teleostea), a little teleost fish whose use as a model to study embryogenesis has become crucial in the last 15 years.

Zebrafish as a model for the analysis of cell cycle and proliferation during development

Zebrafish is one of the most important models to study vertebrate developmental biology in general, but also for understanding the molecular mechanisms involved in several human diseases. The main advantages of this biological system are that this Teleost can be easily bred, has a short generation time and its embryos, generated by external fertilization, are transparent (Kimmel *et al.*, 1995; Westerfield, 1995). Moreover, zebrafish embryos, that are available in large numbers on a daily basis year round, develop outside the mother and thus allow the direct observation of all stages of embryonic development *in vivo*.

The first cellular divisions during zebrafish development are very rapid (15 minutes), as the cycle is biphasic (S-M); the divisions occur metasynchronously until the midblastula transition at the tenth cycle, which is approximately 3 hpf (hours post-fertilization). At this crucial stage, the cell cycle switches from the “embryonic” to the “adult” form: it lengthens, as zygotic transcription is activated, the cells become motile and the divisions begin to occur in an asynchronous manner (Kimmel *et al.*, 1995; Kane *et al.*, 1992; Kane and Kimmel, 1993). Moreover, the cell-cycle checkpoints become functional after this particular stage (Ikegami *et al.*, 1997a; Ikegami *et al.,* 1997b).

Zebrafish turned out to be a very good model not only to study cell cycle regulation, but also to address relevant issues about early vertebrate development in general. Indeed, studies of the developing zebrafish embryo have revealed important similarities to early cell divisions in other vertebrates such as *Xenopus* (Kimmel *et al.*, 1995). Moreover, the molecular pathways that regulate cell division are evolutionarily conserved in all eukaryotes. Finally, the finding that alterations in the mechanisms controlling cell cycle progression are linked to cancerogenesis and several degenerative diseases supports the importance to analyze in depth cell cycle progression in non-mammalian organisms to gain insights into many processes underlying human development and diseases.

Another reason to stress the relevance of zebrafish in studying early vertebrate development lies in the peculiar segregation of localized maternal determinants taking place during the very first cellular divisions. At these early stages, some determinants are already specified and localized, contributing to cell fate diversification. For instance, one of the earliest decisions involves a subset of maternal mRNAs and protein products, that are specifically segregated in a particular zone of the zebrafish oocyte cytoplasm, the germ plasm. Cells inheriting these determinants will give rise to the germ cell lineage, migrating finally to the gonads (Lesch and Page, 2012; Seervai and Wessel, 2013).

The CPC in the zebrafish model

The function and expression of the CPC components have been largely studied in different models. It has been reported that, surprisingly, Aurora B-null mouse embryos develop normally during the early cell divisions, but they die after implantation. It is believed that Aurora-C, highly expressed during early cell divisions, is responsible for CPC functions at pre-implantation stages (Fernandez-Miranda *et al.*, 2011). Incenp, survivin or borealin-deficient embryos display instead an earlier lethality (Cutts *et al*., 1999; Uren *et al.*, 2000; Yamanaka *et al.*, 2008).

For what is concerning the zebrafish model, two of the CPC components have already been well characterized: Survivin and Aurora-B (Nair *et al.*, 2013; Yabe *et al.*, 2009).

Several research groups demonstrated the existence of two different zebrafish *survivin* paralogs, named *birc5a* and *birc5b* (Ma *et al.*, 2007; Ma *et al.*, 2009; Delvaeye *et al.*, 2009). These studies demonstrated that *birc5a* is expressed both maternally and zygotically throughout development and a morpholino-mediated knockdown approach elucidated its role during late embryogenesis. In particular, *birc5a* morphants display evident defects concerning angiogenesis, neurodevelopment, cardiogenesis and

hematopoiesis (Delvaeye *et al.*, 2009). More recently, during a ENU-induced mutagenesis screening, a mutant for the *motley* allele was recovered, which was then found to correspond to *birc5b* (Nair *et al.*, 2013). *birc5b* is expressed exclusively maternally and, consistently, the *motley* mutation shows a precise maternal effect. Indeed, homozygous *motley* females develop into viable and fertile adults, but embryos from such females show a completely penetrant cell division defect, namely the complete absence of the cleavage furrow and abnormal mitotic spindle elongation with consequent death within 4hpf. *birc5b* mutants mature oocytes exhibit important defects during the completion of meiosis II and the cytoskeletal rearrangements involving astral microtubules and F-actin; these events are essential for the aggregation and reorganization of the germ plasm components occurring immediately after fertilization. Therefore, Birc5b is considered to be involved in the typical cell-cycle CPC activities, consistently with what observed in other model organisms (Nair *et al.*, 2013).

Studies on Aurora-B function during zebrafish development have also been carried out: a mutant model has been successfully characterized by Yabe and collegues, who were able to recover a mutation in the gene *cellular island (cei)*, encoding the zebrafish Aurora-B kinase homologue (Yabe *et al.*, 2009). This mutation turned out to have a maternal-effect: even though homozygous females are viable and develop normally to the adulthood stage, all embryos deriving from such mutant females are unviable, exhibiting a strong phenotype since the very early cellular divisions, namely the total lack of organized cleavage furrows and of furrow associated structures, thus resulting in the presence of an abnormally expanded syncytial region. The zebrafish Aurora-B kinase appears also to play an important role in germ plasm recruitment to the forming furrow, consistent with the lack of distal furrows (the region where the germ plasm granules accumulate) in *cei* mutant embryos (Yabe *et al.*, 2009).

The *HASPIN* gene and its discovery

The *haspin* gene was first isolated by Tanaka H. and collegues in 1998 after a functional screening performed using various germ cell-specific cDNAs from a cDNA library of mouse testis (Tanaka *et al.*, 1994; Tanaka *et al.*, 1999). Indeed, it was first identified as a haploid germ cell-specific nuclear protein expressed in spermatids and possessing an intrinsic Ser/Thr kinase activity, and the name of *haspin* stands for: haploid germ cell-specific nuclear protein kinase (Tanaka *et al.*, 1999). The gene encoding this protein in mouse was

first named *Gsg2* (*Germ cell specific gene 2*), and, given their first evidences, the authors suggested a role for it in cell cycle cessation and differentiation of haploid germ cells (Tanaka *et al.*, 1999).

A few years after, J.M.G. Higgins identified the human *HASPIN* ortholog, located within an intron of the integrin αE gene (Higgins, 2001a). This very important discovery was subsequently followed by the isolation of *haspin* family members in all eukaryotic organisms.

HASPIN in human cells

As anticipated above, the human *HASPIN* gene was identified while studying the different transcriptional mechanisms of the integrin αE gene based on the evidence of an alternative αE-derived transcript abundantly present particularly in the testis. Indeed, this transcript turned out to derive from a previously uncharacterized human *HASPIN* gene, included within an intron of the conventional integrin αE gene (Higgins, 2001a). Interestingly, human *HASPIN* is a peculiar gene as it lacks introns. Its coding sequence is composed of a single exon and the encoded protein shows 83% identity with the murine homologue for what is concerning the C-terminal region, while the level of conservation in the N-terminal region drops to 53% (Higgins, 2001b).

Northern blot analysis indicated that human *HASPIN* is expressed in a particularly abundant way in testis, but its transcript is detectable also in many other tissues, such as thymus, bone marrow, fetal liver and more weakly in spleen, intestine and lung (Higgins, 2001a). *HASPIN* is thus most abundantly expressed in gonads and in all tissues characterized by relevant levels of cellular proliferation and differentiation.

The protein encoded by *HASPIN* presents a serine/threonine C-terminal kinase domain; nevertheless, this particular HASPIN domain significantly differs from the one of classical eukaryotic kinases. In fact, for this reason, HASPIN kinases have been grouped in a divergent eukaryotic protein kinase superfamily, distinct from the Cdk family and other common sub-groups (Higgins, 2001b).

The structure of HASPIN serine/threonine kinase domain has been studied by crystallographic analysis by several groups. It presents a bi-lobed structure, common feature of a high number of eukaryotic protein kinase domains, but with some significant structural changes. Its peculiarity lies in the fact that it contains a certain number of specific-inserts, including additional β-hairpin, β-strand and α-helices possibly acting through the stabilization of structural elements which are usually mobile in other kinases

(Eswaran *et al.*, 2009; Villa *et al.*, 2009). In particular, one β-strand, together with other elements, appear to be important to stabilize the active conformation of the small lobe. Due to these observations, HASPIN was first believed to present a constitutively active kinase conformation, even in the absence of any activation loop phosphorylation (Villa *et al.*, 2009; Higgins, 2010). Moreover, it was demonstrated that its isolated kinase domain is active *in vitro* (Dai *et al.*, 2005; Eswaran *et al*., 2009). Moreover, HASPIN substrate recognition (and thus H3Thr3 phosphorylation) is strongly influenced by the methylation level of the neighboring lysine residue (H3-K4), with decreasing enzymatic activity on peptides with increasing methylation of H3-K4 (Eswaran *et al*., 2009).

HASPIN function during cell cycle

HASPIN has been mostly studied for what is concerning its role as a kinase. As already mentioned, HASPIN displays a Ser/Thr kinase activity and its best characterized and conserved function is to phosphorylate, other than itself, threonine 3 of histone H3 (Dai and Higgins, 2005; Dai *et al.*, 2005).

The post-translational modifications of histones dynamically occur during the cell cycle and are mostly confined within the N-terminal regions of the nucleosomal octamers, thus producing epigenetic modifications. Such modifications represent the so called “histone code”, which can be interpreted by effector proteins to play various roles in the control of the chromatin structure and in regulating gene expression (Sims and Reinberg, 2008; Koster *et al.*, 2015). Among such modifications, phosphorylation of threonine 3 of histone H3 (H3Thr3PH) plays a pivotal role in the regulation of cell cycle. As described previously, such phosphorylation event is essential for the recruitment and the correct positioning of Aurora-B and of the other components of the CPC, a key player for the correct progression of mitosis (Wang et *al.*, 2010). H3Thr3PH is first observed at late G2 or prometaphase on chromosome arms; during prometaphase, it becomes most concentrated at inner centromeres, while it can still be detected on chromosome arms as well. It then declines during anaphase and cannot be detected anymore in telophase cells (Dai *et al.*, 2006; Markaki *et al.*, 2009). The most classical mitotic marker and the best characterized histone phosphorylation event is the phosphorylation of serine 10 in Histone H3 by the mitotic kinase Aurora-B. This modification is detected in pericentromeric chromatin and on chromosome arms between late phase G2 and anaphase (Adams *et al.*, 2001; Crosio *et al.*, 2002). Unlike H3Thr3 phosphorylation, it is never observed at inner centromeres

(Hendzel *et al.*, 1997), indicating that these two fundamental histone modifications have distinct distributions throughout mitosis, although they overlap to some extent.

HASPIN role during mitosis has been deeply investigated in mitotically dividing tissue culture cell lines using RNAi or chemical inhibition. It was observed that *HASPIN* depleted cells display a defect in chromosome congression and a delay in exit from mitosis (Dai *et al.*, 2005; Dai *et al.*, 2006; Markaki *et al.*, 2009). *HASPIN* knock-down or inhibition results in chromosome misalignment at metaphase and consequently in the activation of the spindle assembly checkpoint (Fig. 1; Dai and Higgins, 2005; Dai *et al.*, 2005); HASPIN indeed appears to be involved in the positive regulation of centromeric cohesion (Dai *et al.*, 2009) and also in the establishment of a bipolar spindle (Dai *et al.*, 2009). On the other hand, HASPIN overexpression is able to prevent the normal dissociation of sister chromatids, thus causing mitotic delay (Dai *et al*., 2006; Yamagishi *et al.*, 2010; Huertas *et al.*, 2012).

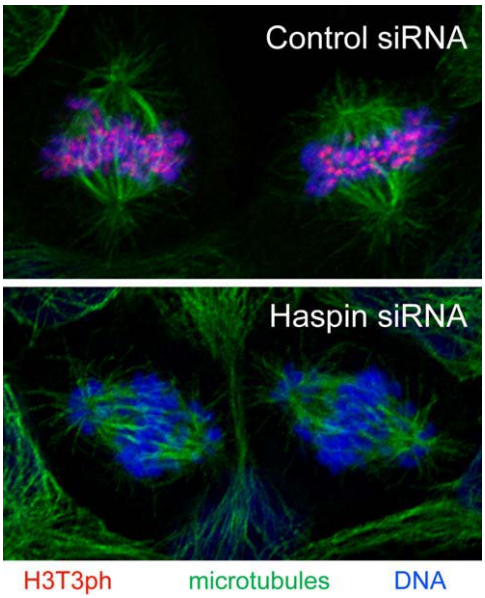

Fig. 1: RNAi experiments in human cell lines show Haspin role during cell division. Haspin depletion causes a decrease in the phosphorylation of H3Thr3 and leads to chromosome misalignment during mitosis. After Haspin depletion, the chromosomes are not correctly aligned at the metaphase plate but they are detectable also at spindle poles. Green: microtubules; blue: DNA; red: H3 phosphorylated at Thr3. (From Higgins, 2010).

Using a combination of biochemical, pharmacological and mass spectrometric approaches, it was recently discovered that HASPIN very likely has other direct substrates

in human cells, other than H3Thr3 and itself. In particular, another validated target of HASPIN kinase activity seems to be Ser137 of the histone variant macroH2A, a particular site involved in the stabilization of extranucleosomal DNA and in the activation or inhibition of transcription, suggesting that HASPIN might influence the phosphorylation state of proteins involved in regulating gene expression and splicing (Maiolica *et al.*, 2014).
Another *bona fide* HASPIN substrate isolated by this screening is Threonine 57 of CENP-T (Maiolica *et al.*, 2014), namely a component of the CCAN (constitutive centromere associated network), which plays a pivotal role in kinetochore assembly, mitotic progression and chromosome segregation (Gascoigne *et al.*, 2011).

Regulation of HASPIN activity during cell cycle

Two recent publications shed some light on how HASPIN activity is finely regulated during mitosis, deciphering, in particular, how the protein is kept inactive during interphase (Moutinho-Santos T. and Maiato H., 2014). Indeed, from previous information derived from the crystal structure of the protein, its kinase domain appeared to be in a constitutive active state. It has been recently discovered that HASPIN possesses an evolutionary conserved stretch of basic amino acid residues (named HBIS, Haspin basic inhibitory segment) located immediately upstream of the C-terminal kinase domain, which is able to inhibit HASPIN kinase activity. HBIS inhibition very likely acts through an allosteric, rather than competitive, mechanism and the multiple basic residues in the segment suggest a charge-based interaction with the kinase domain (Ghenoiu *et al.*, 2013).
This interaction is able to keep HASPIN in a completely inactive state during interphase, and the result of HASPIN activation, that is the accumulation of H3 phosphorylated at Thr3, is first detectable at the beginning of prophase. Particular sites, namely conserved consensus motifs of Cyclin-dependent kinase 1 (Cdk1) and Polo-like kinase-1 (Plk1), present in the N-terminal region of HASPIN, are involved in its initial activation (Zhou *et al.*, 2014). During prophase, the Cdk1/cyclinB complex specifically phosphorylates the corresponding N-terminal consensus site, thus generating a Plk1 recognition site (Fig. 2). Plk1 can then recognize and bind this site through its Polo Box domain (PDB), resulting in the phosphorylation of HASPIN at the particular motif S-T128-P in the human protein (Zhou *et al.*, 2014). This heavy N-terminal Plk1-dependent phosphorylation is able to relieve HASPIN inhibition; in fact, the HBIS loses affinity for the C-terminal kinase domain leading to an active conformation (Moutinho-Santos T. and Maiato H., 2014). Thus, HASPIN activity only starts when both active Cdk1 and Plk1 are present (Zhou *et al.*,

2014; fig. 2). Proceeding through mitosis, during prometaphase and metaphase, Aurora-B kinase also plays a major role in full HASPIN activation (Fig. 2). In fact, by phosphorylating HASPIN, Aurora B establishes a positive feedback loop ensuring that HASPIN is kept phosphorylated throughout mitosis, promoting the accumulation of H3Thr3 phosphorylation and, consequently, its own targeting, together with the other components of the CPC, at the centromeres (Carmena *et al.*, 2012a; Wang *et al.*, 2011; fig. 2). This positive feedback loop amplifies the initial HASPIN activation signal carried out by Cdk1 and Plk1 and it is essential for CPC recruitment and for the achievement of all its mitotic related functions, such as the activation of the spindle assembly checkpoint and the regulation of kinetochore-microtubule attachments (Wang *et al.*, 2010; De Antoni *et al.*, 2012). An additional positive feedback loop is also present; in fact, Aurora-B kinase contributes to Plk1 activation by phosphorylating its activation loop (Carmena *et al*., 2012b).

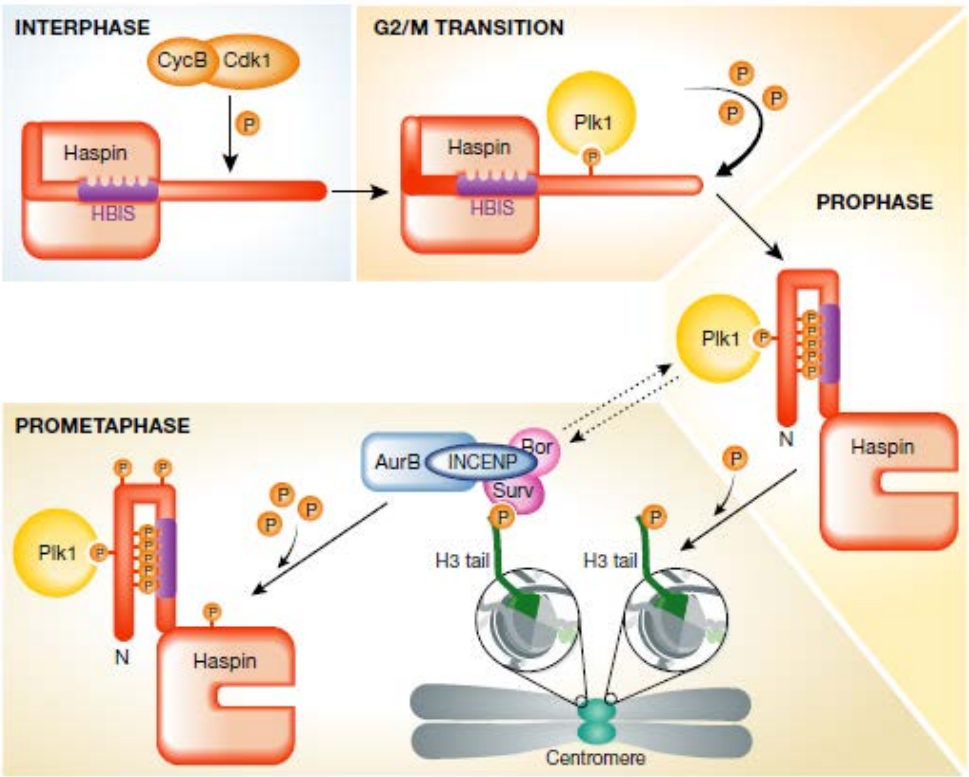

Fig. 2: Regulation of Haspin activity during mitosis. During interphase, HASPIN is kept inactive by interaction of HBIS with the kinase domain. At M-transition Cdk1/cyclin B complex phosphorylates HASPIN, generating a polo-box domain recognition site. At prophase Plk1 phosphorylates and activates HASPIN. Since prometaphase HASPIN is also phosphorylated by Aurora b (positive fedback loop). (Adapted from Moutinho-Santos and Maiato, 2014).

Haspin in mouse

As already mentioned, the mouse model is that in which the *Haspin* gene was initially discovered, thanks to a functional screening performed using a cDNA library prepared from male germ cells (Tanaka *et al.*, 1994, Tanaka *et al*., 1999).

Similarly to the human orthologue, the murine *Haspin* gene is located in intron 26 of the mouse integrin αE gene and the encoded protein shows 66% amino acid identity overall, while it increases to 83% identity in coincidence with the conserved protein kinase domain (Higgins, 2001b). The expression pattern of murine *Haspin* gene also correlates with the human one, its mRNA being significantly represented in all tissues with relevant rates of cellular proliferation and differentiation (such as thymus, bone marrow, fetal liver, spleen), even if the highest levels of expression are still detectable in testis (Higgins, 2001a).

Even if no work is present in the literature describing genetic murine models with the aim to evaluate Haspin role during animal embryogenesis, recent studies analyzed Haspin function during mouse oocytes maturation. Using chemical inhibition and overexpression approaches in mouse oocytes, the authors demonstrated that Haspin is involved in the regulation of meiosis in this model system (Nguyen *et al.*, 2014). Indeed, *Haspin* inhibition in oocytes causes a significant delay in the occurrence of meiotic resumption and maturation and important chromatin defects during metaphase I, namely misalignment and improper kinetochore-microtubule attachments at metaphase I, thus resulting in aneuploidy at metaphase II (Nguyen *et al.*, 2014). Moreover, *Haspin* depletion and, consequently, the alteration of H3Thr3PH levels, was shown to down-regulate the physiological accumulation of Aurora-C kinase, a CPC component of meiotic cells, along chromosomes, but not at kinetochores, during Metaphase I. Also the other components of the CPC were found to be mislocalized after *Haspin* depletion. This altered distribution was correlated with improper kinetochore-microtubule attachments and subsequent aneuploidy, suggesting that Haspin dependent Aurora-C localization along chromosomes arms could be involved in the correction of improper kinetochore-microtubule attachments during meiosis, unlike during mitosis, a process in which most of the regulation mechanism relies upon Aurora B-CPC (Nguyen *et al.*, 2014).

Additional work by Wang and colleagues further contributed to elucidate the characteristic protein expression pattern of H3Thr3PH and its function in mouse oocytes during meiotic maturation. It was demonstrated that in this model system, H3Thr3PH starts being detectable after germinal vesicle breakdown and then reaches a peak at Metaphase I; its localization was found to be dynamically aggregated between chromosome arms (Wang *et*

al., 2016). By inhibiting *Haspin*, and thus H3Thr3 phosphorylation, a delay in the resumption of meiosis and in chromatin condensation was observed. Moreover, the decrease in H3Thr3PH levels also compromised the spindle assembly checkpoint, causing the meiotic transition from pro-MI oocytes to MII oocytes even in the presence of non-aligned chromosomes, hence resulting in the aberrant segregation of genetic material (Wang *et al.*, 2016). According to this model, Haspin activity is essential for chromatin condensation and for the regulation of meiotic resumption and transition from meiosis I to meiosis II in mouse oocytes.

Haspin in budding yeast

Two *Haspin* paralogues, *ALK1* and *ALK2*, have been discovered in the *Saccharomyces cerevisiae* (Sc) yeast genome by a two-hybrid screen (Nespoli *et al.*, 2006). It was discovered that the levels of the proteins coded by these two genes peak in mitosis and in late S/G_2, respectively, and their phosphorylation is maximal in mitosis. Moreover, both proteins are hyperphosphorylated in response to DNA damage and overexpression of *ALK2* causes a mitotic arrest (Nespoli *et al.*, 2006).

Further studies were then perfomed in this experimental model, demonstrating that budding yeast cells lacking both *ALK1* and *ALK2* homologues are sensitive to microtubule depolymerizing drugs such as benomyl or nocodazole (Panigada *et al.*, 2013). In fact, it has been observed that deletion of *ALK1* and *ALK2* causes strong defects in the reorganization of polarization factors after a mitotic arrest. In particular, the authors found that cells lacking both *ALK1* and *ALK2* are characterized by an overly polarized actin distribution in the bud. Since the organization of the mitotic spindle is governed by actin, its altered distribution causes a defect in the orientation of the spindle, which is pulled in the bud, where it elongates in an aberrant way generating anucleated mothers and binucleated daughters (Fig. 3; Panigada *et al.*, 2013). These results suggest an important involvement of Haspin kinase in maintaining the correct localization of polarity factors during cell cycle. It is important to mention that in Sc yeast cells Thr3 of histone H3 is not phosphorylated. This assumption supports the notion that the phenotypes summarized above seem to be independent on histone phosphorylation and other targets need to be identified. Moreover, it will be extremely relevant to verify whether the polarization defects observed in yeast cells lacking Haspin activity can be extended to other eukaryotic organisms.

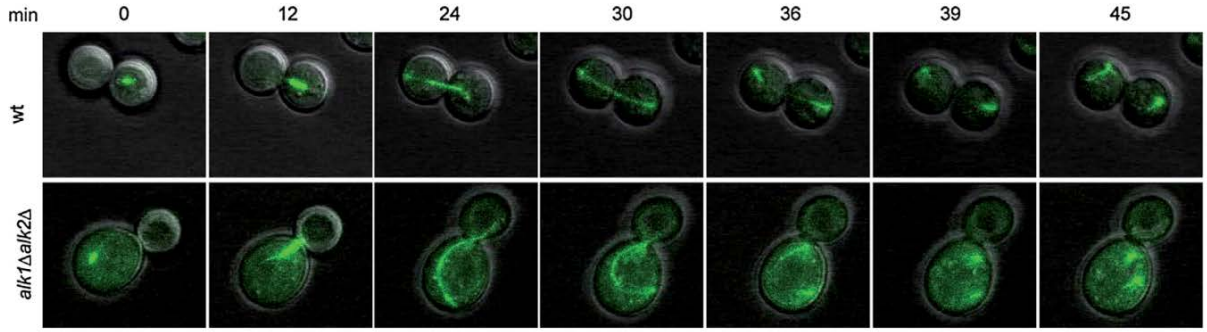

Fig. 3: Mitotic spindle orientation visualization during Sc yeast cells division (tubulin-GFP expressing strains). In the double ALK1 and ALK2 mutant (lane below), the mitotic spindle aberrantly elongates only in the bud cell, thus generating anucleated mothers and binucleated daughters. The time point of each photogram is indicated. (From Panigada *et al.*, 2013).

Haspin in *Arabidopsis thaliana*

Haspin role has been investigated also in the plant model *Arabidopsis thaliana*. The *A. thaliana haspin* ortholog was identified as a mitotic histone H3 threonine kinase, and it was shown to phosphorylate H3 at both Thr3 and Thr11 *in vitro* (Kurihara *et al.*, 2011).

It was then found that AtHaspin also plays an important role during plant embryonic patterning: indeed, *AtHaspin* mutant embryos often show alterations in the orientation of the division planes during the earliest cell divisions and *AtHaspin* depletion also causes pleiotropic phenotypes and defects in floral organs and vascular tissue at the whole plant level (Fig. 4; Ashtiyani *et al.*, 2011).

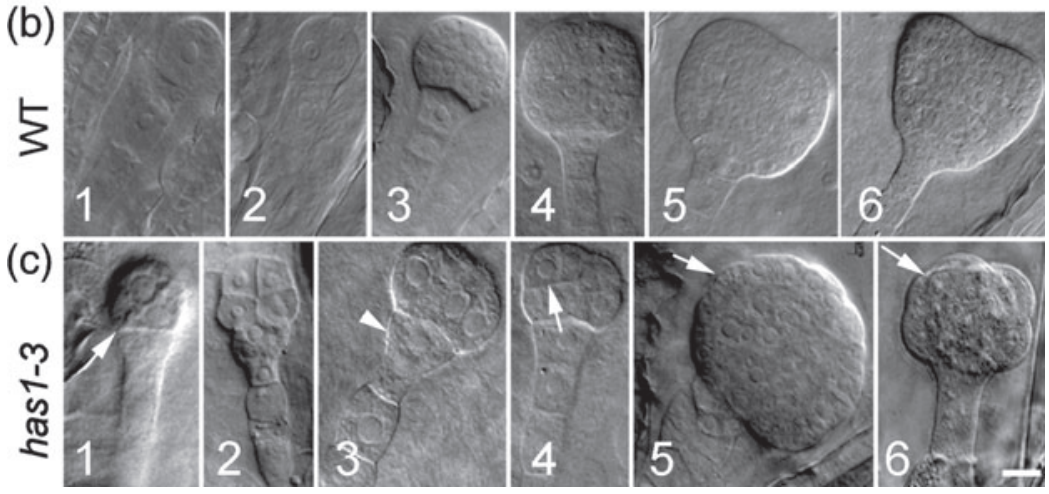

Fig. 4: Whole-mount analysis of embryo in wild type plants (b1–b6) and *Athaspin* mutants (c1–c6). *Athaspin* mutation causes defects during early cellular divisions. White arrows: abnormal cell divisions. White arrowhead: extra cell division. (From Ashtiyani *et al.*, 2011).

Further studies in plants showed that chemical inhibition of *AtHaspin* by using the 5-ITU molecule delays chromosome alignment and also alters the correct localization and activity of Aurora-3 kinase in Bright Yellow-2 cells, suggesting its involvement in Aurora-3 positioning at centromeres. Moreover, *AtHaspin* depletion also results in cytokinesis defects in these cell lines, resulting in binuclear cells with a partially formed cell plate and in alterations in the distribution of actin filaments (Kozgunova *et al.*, 2016).

Role of H3Thr3 phosphorylation in the *Drosophila* Male Germline

A very recent work highlighted a new and very interesting role of Haspin-dependent H3Thr3 phosphorylation during *Drosophila* male germline differentiation. In this system it has been shown that H3Thr3 phosphorylation by the Haspin kinase represents a transient mitotic mark able to distinguish sister chromatids carrying different epigenetic information, in this case pre-existing H3 instead of newly synthesized H3 (Xie *et al.*, 2015). The authors were able to distinguish between these two different modifications and they found that the phosphorylation of H3Thr3 can discriminate between pre-existing versus newly synthesized H3. This epigenetic modification occurs with different temporal patterns in these two histone populations, and according to this model it represents the mark by which asymmetric segregation of sister chromatids, one enriched in new histones and the other in the pre-existent ones, takes place during stem cell divisions (Xie *et al.*, 2015).

This work might open new interesting perspectives also in other models on the role of Haspin in the epigenetic regulation of germline differentiation, shading some light on the mechanisms controlling asymmetrical stem cells division.

AIM OF THE PROJECT

During my Ph.D. I focused my research work on the analysis of the function of the CPC related protein Haspin using zebrafish as a model system.

With our work, we aimed to address these main issues:

-How many *haspin* orthologs are present in zebrafish? Are the functional domains conserved compared to the human gene?

-What is the *haspin* expression pattern during zebrafish embryonic development? Is it maternal, zygotic or both?

-What is the role played by Haspin during embryo patterning in zebrafish? Does it have a maternal or a zygotic effect?

-Is its function similar to that described for other models in literature or is there a new different role during animal embryogenesis?

To our knowledge, this work represents the first attempt to characterize *in vivo* Haspin function and expression during zebrafish development. This aim is particularly interesting as, to our knowledge, no studies are currently underway on Haspin role during zebrafish embryogenesis, nor has its function during animal embryogenesis ever been investigated.

MAIN RESULTS

IDENTIFICATION OF THE *haspin* GENE IN ZEBRAFISH

First of all, we tried to identify the *haspin* ortholog in zebrafish by bioinformatics analysis of the genome database. Only one putative ortholog gene, previously annotated as *gsg2* on chromosome 1, was found. The corresponding transcript is 3525 bp long, including the un-translated regions; it is structured in 18 exons and encodes a protein composed of 1092 amino acids. A global alignment with the human protein shows 29% amino acidic identity and 40% similarity; however, in correspondence with the catalytic domain, it hits the highest local similarity score at 74% (Fig. 1A).

Even if the similarity score is apparently quite low, all the different functional domains appear to be present and highly conserved also in the zebafish protein: the STP motif, constituting the PBD (Polo Box domain) important for the activation of the protein and the HBIS auto-inhibitory segment as well as the C-terminal ser/thr kinase domain are all highly conserved (Fig. 1A,B).

Considering the fact that a lot of genes are duplicated in the zebrafish genome, we tried to look for other putative *haspin* isoforms by multiple alignments, using both the human and the zebrafish sequence as reference (we used both the full length protein coding sequence and the kinase domain only). As a result, we failed to detect in zebrafish any *haspin* paralog for this gene with a significative value of similarity; hence, to our knowledge, only one zebrafish h*aspin* ortholog is present and annotated in the genomic browser. In this work, we will refer to this gene as *haspin.*

haspin EXPRESSION PATTERN ANALYSIS

One of our main goals is to understand the *haspin* spatio-temporal expression pattern during zebrafish development. Hence, we first carried out semi quantitative RT-PCR assays on RNAs extracted from pools of wild type embryos at different stages of embryonic development to test the presence of the endogenous transcript at different time points. We designed specific *haspin* primers in order to amplify a fragment of 202 base pairs inside the coding sequence (Fig. 2A), and these primers were also tested on the whole zebrafish transcriptome to ensure that they would not give rise to possible aspecific

A AMINO ACID SIMILARITY

	Homo sapiens	*Homo sapiens* (kinase domain)	*Mus musculus* (kinase domain)
Danio rerio	40%		
Danio rerio (kinase domain)		74%	76%
Mus musculus (kinase domain)		93%	

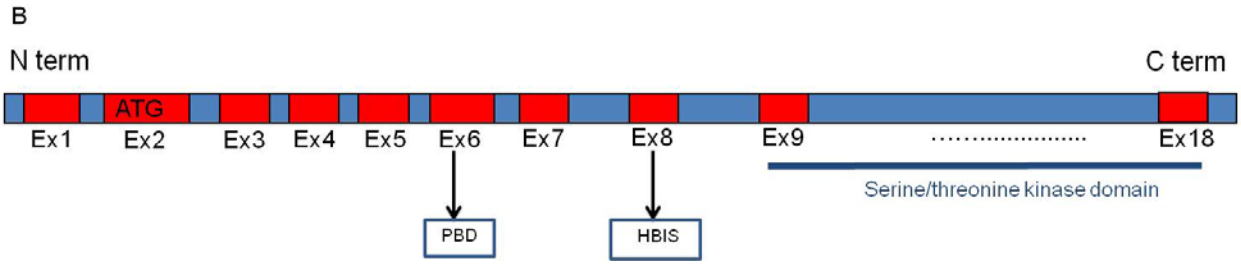

Fig. 1: Schematic representation of the zebrafish *haspin* sequence. (A) Table indicating amino acidic similarity between zebrafish and human protein and between zebrafish, human and mouse kinase domains. (B) Scheme of the different domains and conserved motifs within the zebrafish *haspin* ortholog. PBD: Polo box domain; HBIS: Haspin basic inhibitory segment. In red: exons; in blue: introns (not to scale).

amplification products. Using this approach, we assessed the temporal *haspin* expression pattern, and we found that the transcript is present at all developmental stages analyzed, starting from the very first cleavage stages (2-4 cells) to 3 dpf (days post-fertilization; Fig. 2B), showing both zygotic and maternal expression.

Next, to obtain a spatial expression pattern, we *in vitro* transcribed a specific *haspin* mRNA probe and carried out *in situ* hybridization assays. These experiments revealed a very intense and widespread *haspin* expression signal all over the embryo from the beginning of development to early segmentation stages, suggesting a significant maternal contribution (Fig. 2C-M). At later stages, namely late segmentation, the signal was still diffused, but began to preferentially localize in the developing dorsal neural tube at a periventricular level (Fig. 3A-D). At 24 hpf (hours post-fertilization) *haspin* was preferentially expressed in the cephalic region and in the caudal region of the ICM (Intermediate Cell Mass; Fig. 3E). In particular, histological sections of hybridized embryos and flat mount preparations showed probe labeling in correspondence with some particular anatomical districts such as retina, otic vesicles, and the periventricular portions of the developing brain structures (Fig. 3F,G).

At 2 dpf, the labeling was less intense, indicating a decreased level of expression, but we could still detect *haspin* signals in the cephalic region of the embryos and also in other tissues, such as the fin buds and the gut (Fig. 3H-L). We also conducted parallel assays at all stages analyzed using a sense probe, to make sure the labeling we were looking at was not due to probe trapping, and it turned out that our negative controls didn’t show any staining in the tissues where we detected *haspin* expression signal (supplemental fig. 1A-E).

In general, we can conclude that *haspin* hybridization signal was preferentially detected in tissues with a high rate of proliferating cells (Fig. 2-3).

haspin SEQUENCING AND CLONING

An essential step to define the *in vivo* function of Haspin was to clone its full length DNA sequence in a zebrafish expression vector with the aims to confirm the sequence we found annotated in the genomic browser and to *in vitro* transcribe the corresponding mRNA for overexpression studies.

In an the attempt to isolate the full length fragment by PCR performed on a tailbud stage cDNA, we were able to detected also an unexpected smaller DNA fragment. Cloning and

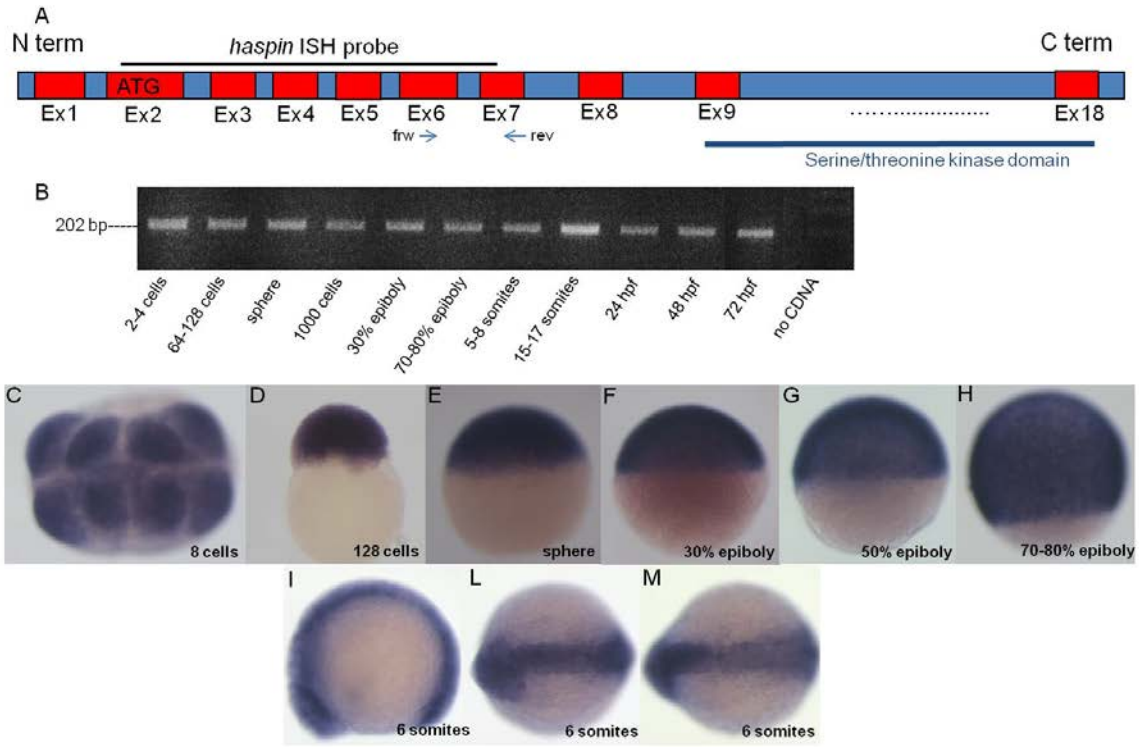

Fig. 2: Spatio-temporal expression pattern of zebrafish *haspin*. (A) Scheme of *haspin* sequence: the regions where we designed our probe for *in situ* hybridization (ISH) experiments (shown in C-M) and our primers for sqRT-PCR (shown in B), are indicated. In red: exons; in blue: introns (not to scale). (B) sqRT-PCR performed on total RNAs extracted from embryos at various stages of development, indicated in the figure. Negative control is shown in the right-most line. (C-M) Analysis of *haspin* early spatial expression pattern at early developmental stages, indicated in the figures. Hybridization signal is very widespread at these stages. (C, L, M) Dorsal view of the embryos. (D-I) Lateral view of the embryos.

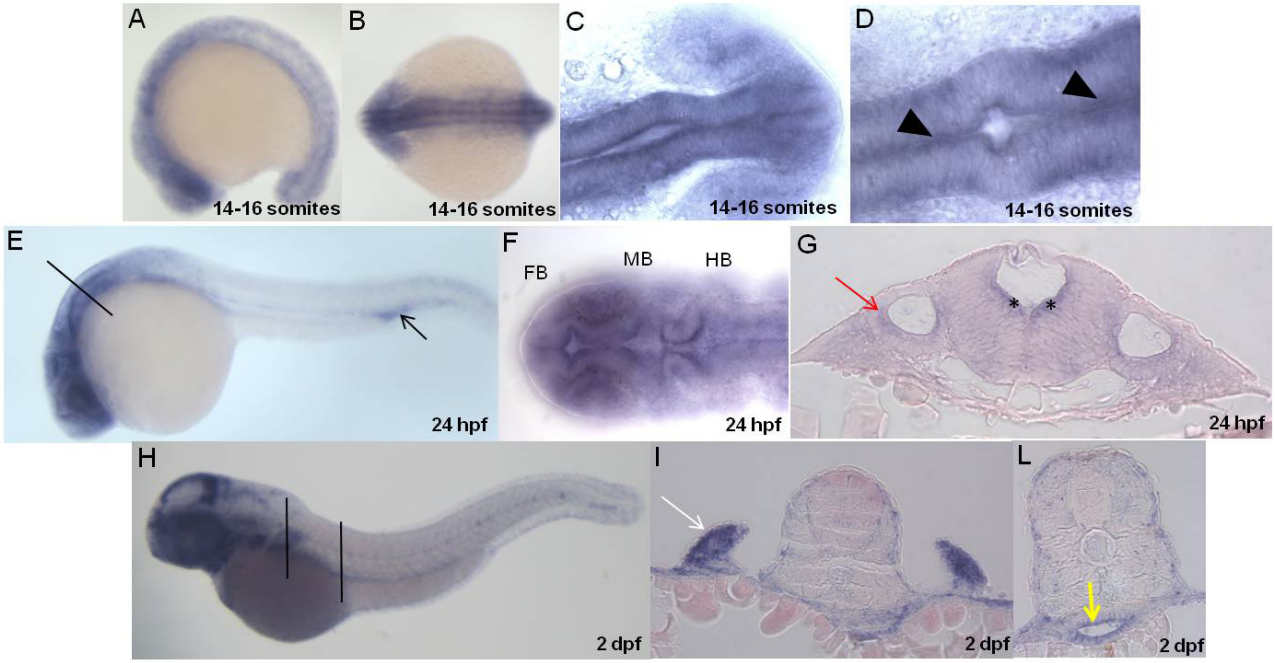

Fig. 3: Spatial expression pattern of zebrafish *haspin* at different developmental stages, indicated in the figures. (A-D) Late somitogenesis *haspin* expression pattern. (A) Lateral view of the embryo (B) Dorsal view of the embryo (C,D) Dorsal magnification from a flat mount preparation of hybridized embryos, showing expression in the developing dorsal neural tube. (E) Lateral view of a 24 hpf embryo oriented with the cephalic region to the left, showing expression in the nervous tissues and ICM. (F) Dorsal view of a flat mounted embryo oriented with the cephalic region, showing the stained neuromeres structures of the developing brain. (G) Histological section conducted according to the plane shown in figure E. (H) Lateral view of a 2 dpf embryo oriented with the cephalic region to the left. (I) Histological section conducted according to the plane showed in figure H, showing expression in the fin buds. (L) Histological section conducted according to the plane showed in figure H, showing expression in the gut. Black arrow: ICM (intermediate cell mass); FB: forebrain; MB: midbrain; HB: hindbrain; red arrow: otic vesicle; asterisk: periventricular portion of neural tube; white arrow: fin buds; yellow arrow: gut; black arrowheads: expression signal in the dorsal neural tube. Embryo developmental stage is indicated in each picture.

sequencing of this band revealed the presence of a new splicing variant, not previously annotated, lacking approximately 600 base pairs and corresponding to exon 6. The remaining DNA sequence of this clone was identical to the canonical one. Interestingly, exon 6, missing in the splicing isoform, contains the Polo box domain required for activation of the Haspin protein (Fig. 4A). We cloned and sequenced the full length coding fragments for both forms and found few differences respect to the sequences annotated in the genomic browser. These new sequences will be soon deposited in the appropriate DNA databank.

Next, we analyzed the temporal expression pattern of this newly identified splicing isoform variant at different developmental stages and also in adult organs, wondering if it could have a different temporal activation pattern with respect to the canonical one. To this end, we designed specific primers, a forward primer on exon 4 and a reverse primer on exon 7 (primers: zhaspsplscreen frw and rev; Fig. 4A), able to produce different amplification products in order to discriminate between the two isoforms (795 bp versus 201 bp). Even if the amplification obtained with these primers was not optimal, in this way we were able to detect the presence of the *haspin* splicing isoform at all developmental stages analyzed (from 2-4 cells to 3 dpf), except for the 5-8 somite stage, although in some of these stages we found a very faint band (Fig. 4B). The expression of the splicing isoform seems to be mostly zygotic.

For what concerns the expression analysis in adult organs, we tested the presence of both transcripts in eyes, ovary, testis and brain. For this particular experiment, we ordered a new set of primers, one forward on exon 5 and one reverse on exon 7 (zhaspsplscreenbis frw and rev; Fig. 5A), that turned out to work better than the previous ones, but we still need to repeat the same PCR experiments on cDNAs from the different embryonic developmental stages using these new oligonucleotides in order to obtain clearer results. We failed to identify either of the two forms in the eyes or in the brain, while the canonical transcript was present in both the ovary and the testis; in the latter, we also detected the presence of the *haspin* splicing variant (Fig. 5B).

Finally, we tested whether *haspin* might be overexpressed during tissue regeneration. In fact some zebrafish tissues, such as the heart and the fins, are able to regenerate in response to injuries. We thus performed sqPCR with *haspin* specific primers on cDNA retro-transcribed from total RNAs from a fin clipped from a wild type adult fish compared to a cDNA from the clipped growing blastema tissues 2 days after the first cut. Interestingly, *haspin* transcript appears to be strongly up-regulated during tissue regeneration (Fig. 5C).

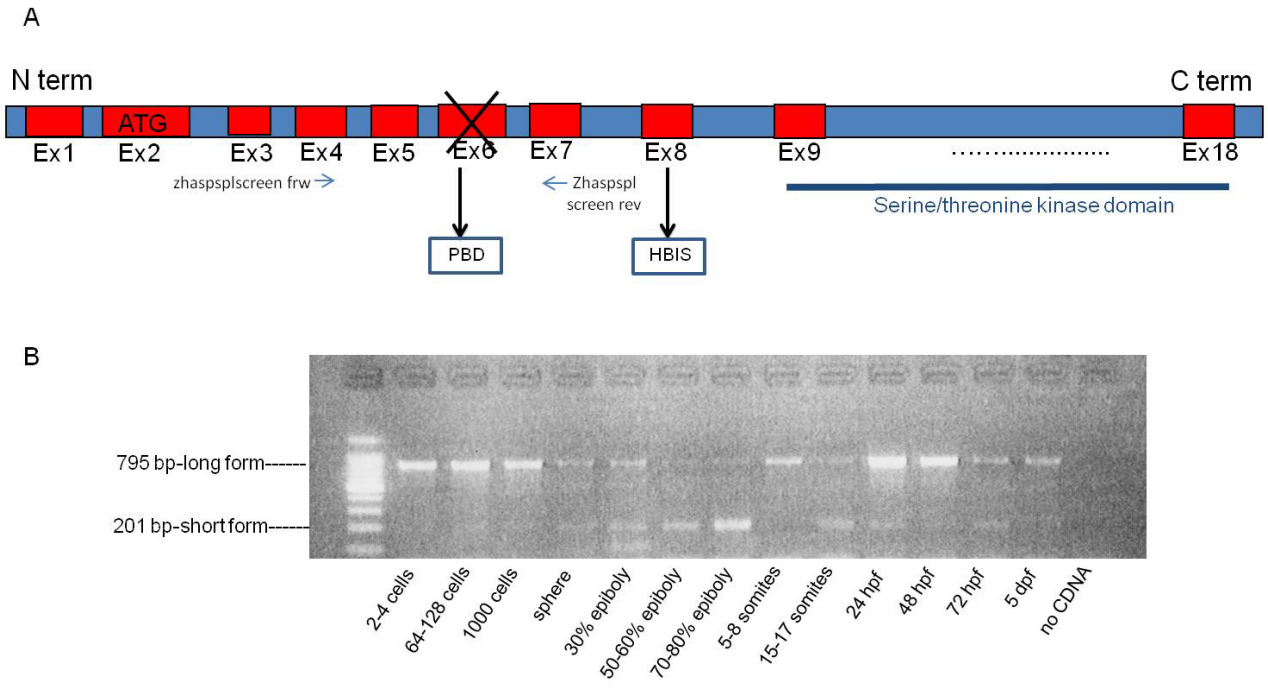

Fig. 4: Schematic representation of the newly identified zebrafish *haspin* splicing isoform and temporal expression pattern of both forms during embryogenesis. (A) The newly identified splicing isoform is identical to the canonical one except that it completely lacks exon 6, the one containing the polo box domain required for activation of the Haspin protein. PBD: Polo box domain; HBIS: Haspin basic inhibitory segment. In red: exons; in blue: introns (not to scale). (B) sqRT-PCR performed on total RNAs extracted from embryos at various stages of development, indicated in the figure. Primers used are indicated in figure 4A: they amplify a 795-bp fragment for the *haspin* canonical form and a 201-bp fragment for the splicing variant. Negative control is shown in the right-most line.

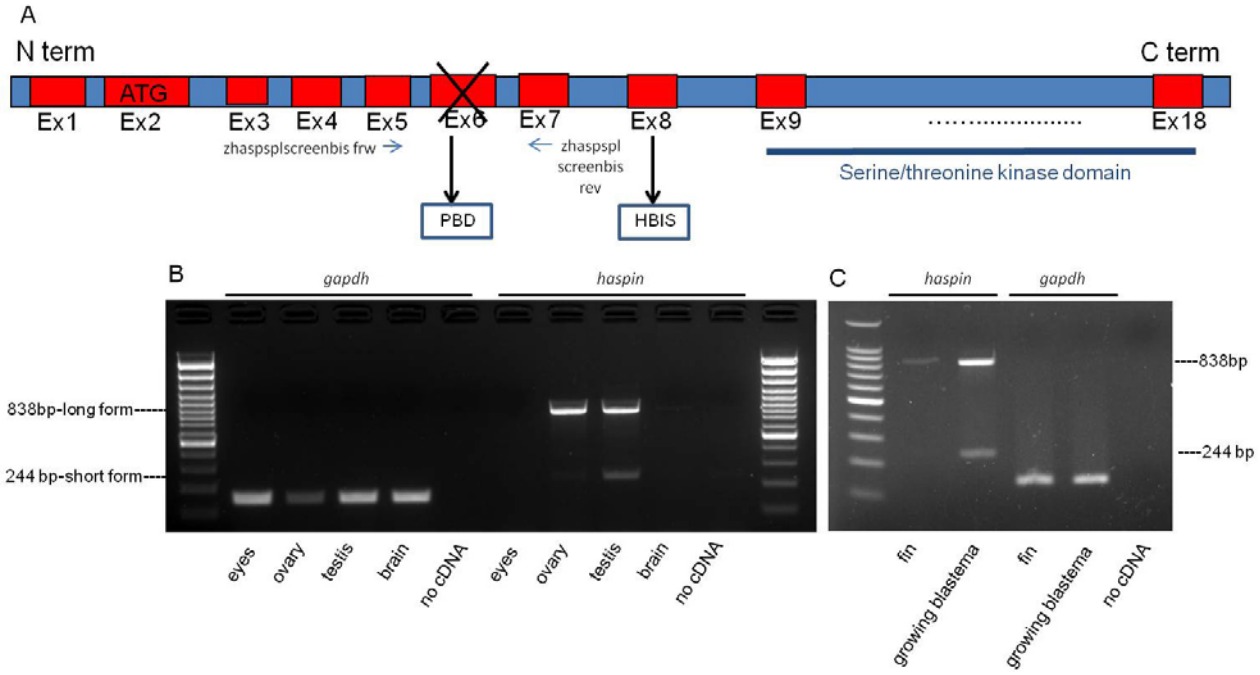

Fig. 5: Expression pattern of both *haspin* splicing forms in adult organs. (A) Representation of the newly identified splicing isoform with indication of the primers used for sqRT-PCR in fig. 5 B,C. PBD: Polo box domain; HBIS: Haspin basic inhibitory segment. In red: exons; in blue: introns (not to scale). (B) sqRT-PCR performed on total RNAs extracted from adult organs, indicated in the figure. Primers used are indicated in figure 5A: they amplify a 838-bp fragment for the *haspin* canonical form and a 244-bp fragment for the splicing variant. Primers for *gapdh* were used as a control to check cDNA quality. Expression of the canonical form is detected in ovary and testis; the splicing isoform is present only in the testis, even if a very faint band is detectable in the ovary as well. (C) sqRT-PCR performed on total RNAs extracted from a fin clipped from a wild type adult fish compared, in the second lane, to total RNAs from the clipped growing blastema tissues 2 days after the first cut; overexpression of both *haspin* forms was detected in the regenerating tissue. Primers for *gapdh* were used as a control to check cDNA quality. A negative control without cDNA is shown for every PCR mix.

Haspin FUNCTIONAL ANALYSIS

Given the encouraging and strong expression pattern of the gene during early embryogenesis and in different adult tissues, especially in those with high proliferation rates, we tried to evaluate the possible role played by Haspin during development and, to this end, we took advantage of both knockdown and knockout approaches.
As for the former approach, we used a morpholino (MO)-mediated functional inactivation while, to completely knockout the gene product, we generated a zebrafish *haspin* KO mutant using the CRISPR-Cas9 genome editing technique. This KO zebrafish line was generated at Temple University, Philadelphia (USA) thanks to the fruitful collaboration with Dr. Gianfranco Bellipanni.

MO-mediated knockdown analysis

We began our functional *haspin* analysis during zebrafish embryogenesis using the morpholino-mediated knockdown approach. Morpholino is a specific antisense oligonucleotide capable either of binding a region around the start codon of the endogenous mRNA of interest and thus blocking the correct translational process (ATG MO), or interfering with the physiological splicing event at a particular exon-intron junction, causing an exon skipping or an intron retention (Ekker, 2000; Nasevicius and Ekker, 2000). The former is able to target both maternal and zygotic transcripts, while the latter only affects zygotic mRNAs (that are synthesized after the midblastula transition stage), since maternal mRNAs are already mature upon fertilization of the embryos.
In parallel, a standard morpholino was always injected as a control (std-MO): this oligonucleotide has no target in zebrafish, and it is useful for discerning any aspecific effect on embryo development that may result from the injection technique itself. Morpholino-injected embryos are routinely identified as morphants.
For our analysis, we designed and tested two different types of MO: one ATG morpholino (*haspin* ATG MO) against the translation start codon, and one splicing morpholino (*haspin* spl MO) directed against the junction between exon 5 and intron 5/6, predicted to cause the skipping of the fifth exon and thus to alter the open reading frame of the mRNA. The localization of our morpholino targets on *haspin* coding sequence are shown in fig. 6.

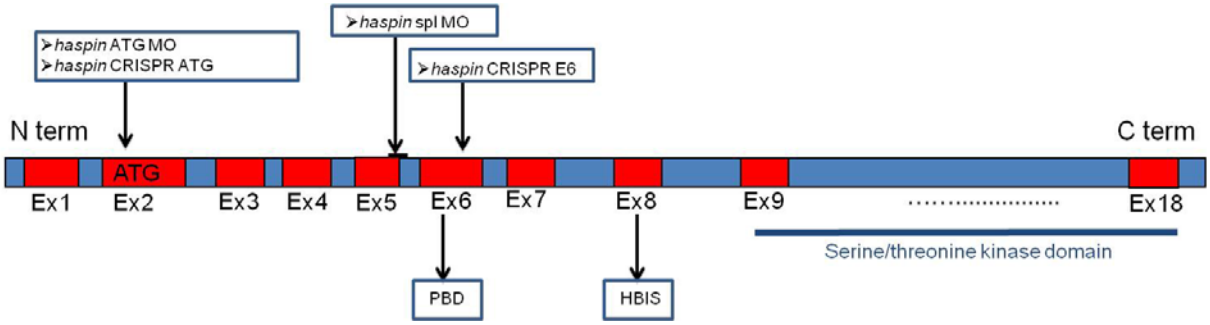

Fig. 6: Schematic representation of zebrafish *haspin* sequence with annotation of the targets designed for knockdown and knockout approaches. Features indicated in this figure: target sites of *haspin* ATG MO (translation blocking morpholino), h*aspin* spl MO (predicted to alter canonical splicing thus resulting in skipping of exon 5), *haspin* CRISPR ATG and *haspin* CRISPR E6 (See section "zebrafish *haspin* mutagenesis"). PBD: Polo box domain; HBIS: Haspin basic inhibitory segment. In red: exons; in blue: introns (not to scale).

1. Analysis of the effect of *haspin* ATG MO

We started our functional analysis by microinjecting 1-2 cells wild type embryos of the AB line with *haspin* ATG MO. First, we were interested in verifying whether Haspin was required for the phosphorylation of threonine 3 of histone H3 (H3Thr3PH) also in zebrafish model system. Hence, we prepared total protein extracts from std-MO and morphant embryos at 30% epiboly stage and analyzed them by western blotting to test the levels of H3Thr3PH with a specific antibody. The morpholino effects are dose-dependent and thus we analyzed their effect at various concentrations, namely 0.01 pmol/E (pmol/embryo), 0.05 pmol/E and 0.1 pmol/E. Even at the lowest dose, we observed a significant reduction in the phosphorylation signal of H3thr3 in morphants compared to control embryos and, as expected, the effect on this post-translational modification increased according to the MO dose injected in the embryos (Fig. 7). As controls, we used an actin antibody (loading control), an antibody against the total histone H3 population and another one recognizing specifically H3 phosphorylated at Ser10, a residue whose modification is not regulated by Haspin; this result was confirmed by 3 different experiments. Our results clearly indicate that also in zebrafish Haspin is controlling the modification of threonine 3 of histone H3.
Next, we asked whether *haspin* inactivation may cause some alterations at a phenotypic level during zebrafish early embryonic development, as we could expect by knocking down a protein known to be involved in the progression of cell cycle in other model systems and also considering the strong *haspin* expression levels at early stages of development.
At the low MO doses used to evaluate H3thr3PH levels we failed to identify any relevant effect during early development of morphants since their phenotype was comparable to that of controls in almost 100% of embryos. Therefore, we decided to increase the dose of injected morpholino up to to 0.5-1.0 pmol/E. Both doses caused a high rate of mortality during embryo development: almost 100% of the embryos failed to reach the 24 hpf stage. This high mortality rate is expected as a consequence of functional inactivation of a protein possibly involved in the regulation of the cell cycle, which is obviously crucial during the early stages of embryonic development.
We concluded that ATG MO has a very severe effect during the first hours of embryonic development and we decided to focus our attention on the analysis of epiboly and gastrulation stages in morphants injected with 0.5 pmol/E. We thus injected wild type AB embryos with 0.5 pmol/E *haspin* ATG MO, transferred them at their optimal temperature (28 °C) and monitored their development in comparison with std-morphants. We found that

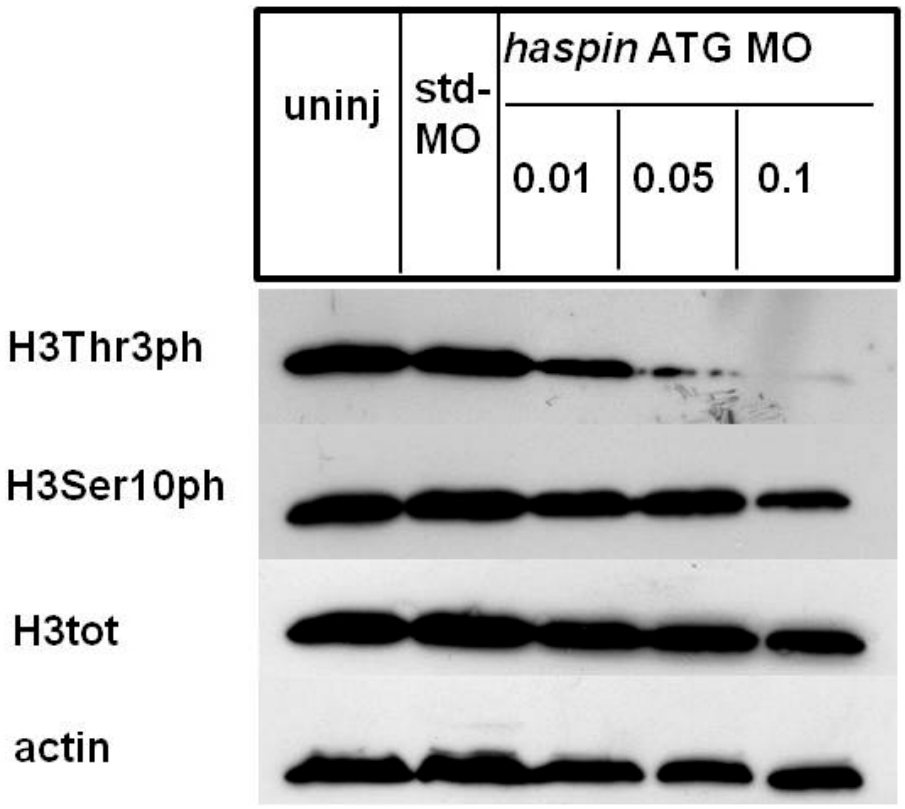

Fig. 7: Western blot assays performed on protein extracts from pools of embryos injected with *haspin* ATG MO at different doses (indicated on the different lanes as pmol/E) compared to std-MO embryos and uninjected. We observe a significant dose-dependent decrease in the signal of H3Thr3PH after *haspin* ATG MO injection. All pools of embryos processed in these experiments are at 30% epiboly stage.

haspin ATG morphants developed normally until the sphere stage; at the transition to dome stage, a very significant percentage of these embryos started exhibiting alterations in the normal processes of cell rearrangements and migration: the cells of the blastoderm appear less compact and start to lose adherence to the yolk below (Fig. 8C,E). The defect became more severe with the proceeding of epiboly: an irregular structure of the whole blastula was detected, cells appeared disorganized and lose more and more adherence to the yolk; they didn't manage to correctly and completely envelop it, as it happens during physiological epiboly, but they kept migrating in an anomalous way, generating a very severe epiboly phenotype (Fig. 8D,F). These embryos do not succeed to proceed during epiboly, and sometimes they remain arrested in gastrulation, showing evident gaps and spaces between the cells (Fig. 8G).

In an attempt to better characterize these early defects observed, we also performed *in situ* hybridization experiments with some classical epiboly markers in *haspin* morphants compared to control embryos. In particular, we evaluated the spatial expression pattern of *otx3*, *fgf8*, *goosecoid (gsc)* and *chordin (chd)* at 30-40% epiboly. We found important alterations in the expression pattern of all these markers, suggesting alterations in cellular rearrangements and movements occurring during epiboly: *otx3* and *chd* showed an ectopically expanded signal, while *gsc* and *fgf8* appeared to be decreased and, for *gsc*, more diffused (Fig. 9). These are the percentages of embryos exhibiting defects for each epiboly marker: 87% for *fgf8* (40/46), 84% for *otx3* (26/31), 91% for *gsc* (48/53), 76% for *chd* (19/25).

2. Analysis of the effect of *haspin* spl MO

Next, we were interested in evaluating the effect of *haspin* spl MO microinjection during embryonic development. In fact, with such morpholino, we had the chance to target exclusively zygotic transcripts.

First of all, we evaluated the efficiency of this morpholino by extracting RNA from *haspin* spl morphants. After retro-transcription, we were able to demonstrate by PCR amplification the presence of a shorter aberrant transcript; indeed, its length was compatible with the one expected after skipping of exon 5 of the ORF. Sanger sequencing confirmed this aberrant splicing event, and from the sequence we could conclude that it alters the correct reading frame of the coding sequence, generating a premature stop codon and, consequently, a truncated and therefore non-functional protein (supplemental fig. 2A,B).

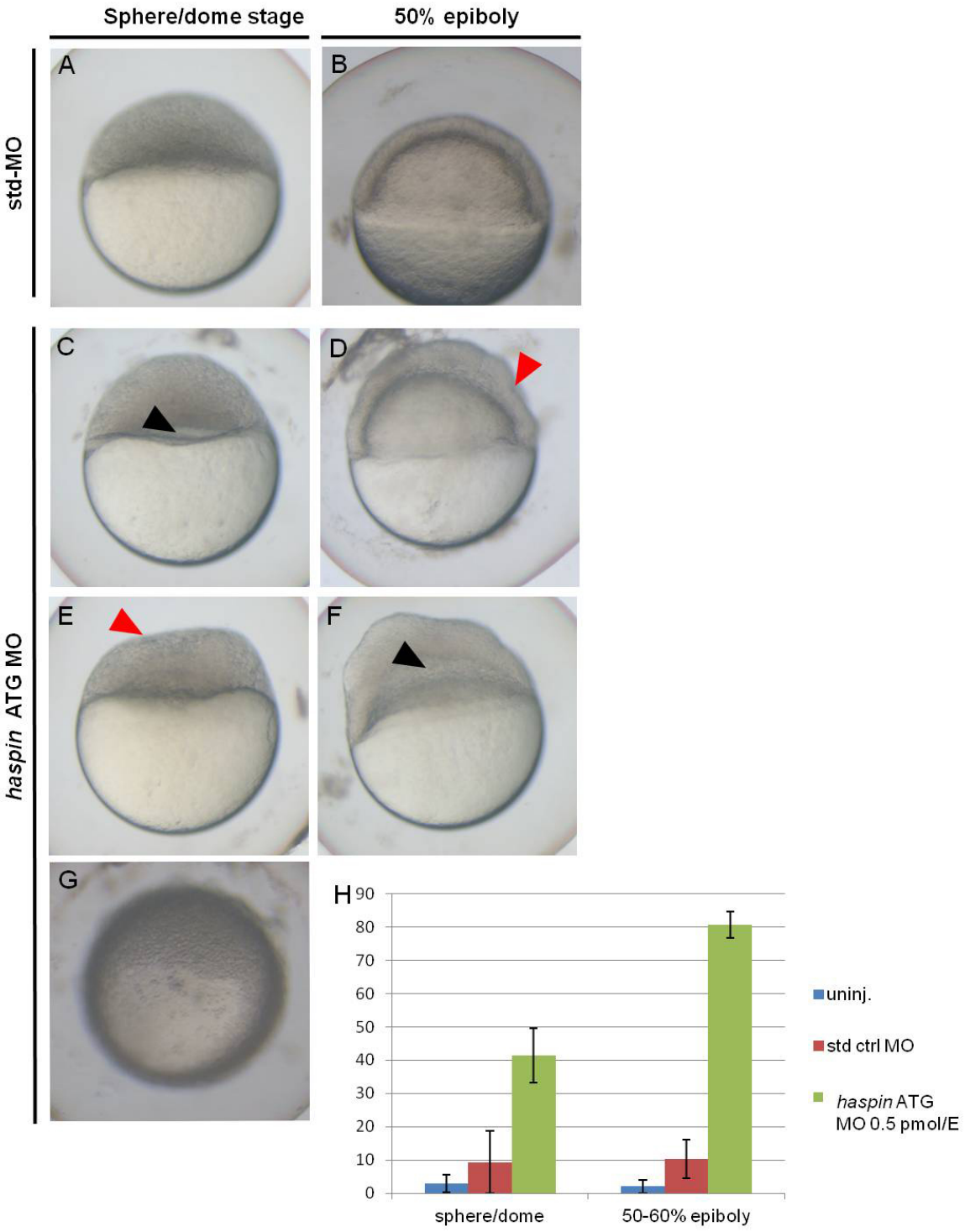

Fig. 8: Phenotypic effect of *haspin* ATG MO microinjection at early stages. (A,B) Lateral view of std-MO embryos at sphere/dome and 50% epiboly stages. (C,D) Lateral view of morphant embryos exhibiting a mild phenotype at the two different developmental stages. (E,F) Lateral view of morphant embryos exhibiting a more severe phenotype at the two different developmental stages. (G) Morphant embryo arrested in gastrulation, showing evident spaces between the cells. Red arrowheads: irregular structure of blastula/gastrula; black arrowheads: detachment of the blastoderm cells from the yolk below. All embryos were injected with 0.5 pmol/E for both MOs. (H) Percentages of embryos exhibiting epiboly defects at the two developmental stages analyzed.

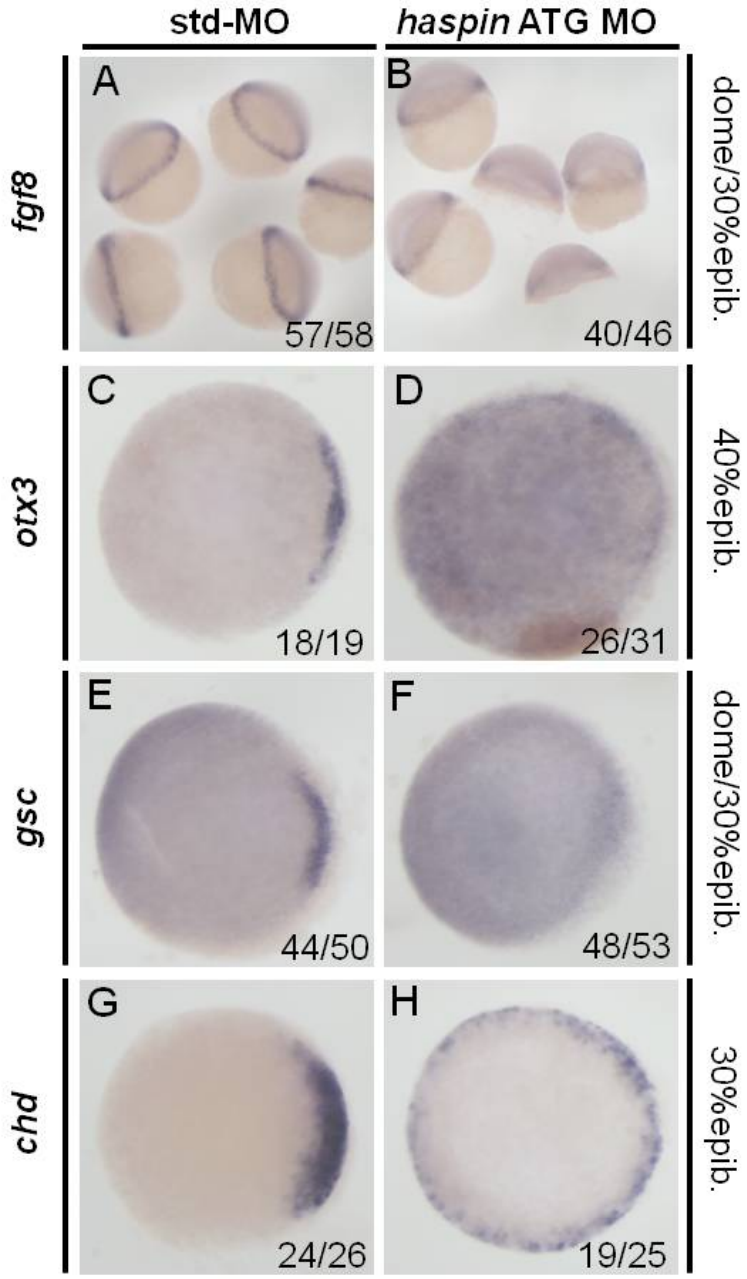

Fig. 9: Analysis of the expression pattern of some epiboly markers in *haspin* ATG morphants. (A,B): lateral view of group of *haspin* morphants and std-MO embryos hybridized with *fgf8* marker: the signal appears decreased in *haspin* morphants. (C,D) Dorsal view of embryos hybridized with *otx3:* in *haspin* morphants the signal is ectopically expanded. (E, F) Dorsal view of embryos hybridized with *gsc: haspin* morphants exhibit a weaker and more diffused signal. (G, H) Dorsal view of embryos hybridized with *chd:* in *haspin* morphants the signal appears ectopically expanded. Markers are indicated to the left; developmental stages are indicated to the right; the number of embryos exhibiting the expression pattern shown in each picture is indicated in the same picture.

We injected *haspin* spl MO in wild type AB embryos at different concentrations (starting from 0.5 pmol/E to 2 pmol/E) and monitored embryonic development at a phenotypic level. We did not find any alteration during the development of morphant embryos compared to controls. Spl morphants developed normally, even at the highest dose injected, and their survival rate in the first days after fertilization was not affected. The body axes were correctly formed, blood circulation was normal, somites were correctly patterned and the cephalic structured appeared normal (data not shown).

We then verified whether some molecular marker could be altered in these embryos, concentrating on the nervous system and the hematopoioetic tissues (where we found *haspin* to be preferentially expressed). Concerning the nervous system, we performed *in situ* hybridization experiments on morphants (1.5 pmol/E) compared to control embryos at 2 dpf using *fgf8* probe. At this stage, this probe labels a lot of different nervous structures, such as the midbrain-hindbrain boundary, the optic stalks, the retina, a part of the telencephalon and the anterior part of the ear. We could not detect any difference between morphants and controls concerning the expression pattern of this marker (data not shown).

We also tried to inject *haspin* spl MO at various doses, from 1.2 to 2 pmol/E, in the transgenic line *islet-1* EGFP, expressing EGFP under the promoter of *islet-1,* specific for the motor neurons of the hindbrain. We monitored morphants at 3 dpf and we failed to find any difference concerning the patterning of this neuronal population comparing them to control embryos (supplemental fig. 3A,B).

Since by *in situ* hybridization assays we found expression of *haspin* in the caudal region of the ICM, which is important for the hematopoiesis process, we asked whether *haspin* spl-MO could cause a decrease in the total number of blood cells. Hence, we stained 2 dpf morphants and control embryos with O-dianisidine in order to visualize hemoglobin and observe the amount of circulating erythrocytes. Also with this staining procedure we could not detect any difference between morphants and controls, as the levels of erythrocytes were comparable in both samples (supplemental fig. 3C,D).

Finally, we performed western blots with protein extracts from embryos injected with *haspin* spl MO (1 pmol/E) compared to control embryos, and we found out that also this MO caused a significant decrease in the signal of H3Thr3PH, at all developmental stages analyzed (from 50% epiboly to 24 hpf; supplemental fig. 2C).

We thus conclude that *haspin* spl MO microinjection does not cause any phenotypic defect during zebrafish embryonic development, even at the highest doses tested, but, as the ATG MO, it affects H3Thr3 phosphorylation levels.

Zebrafish *haspin* mutagenesis

In order to confirm the results of the MO-mediated knockdown approach, we generated a zebrafish stable mutant *haspin* line using the CRISPR-Cas9 system, a recent and very efficient mutagenesis technique that, nowadays, has made zebrafish gene targeting more affordable and has allowed many advanced genome engineering applications in this teleost fish (Blackburn *et al.,* 2013; Hwang *et al*., 2013). The CRISPR-Cas9 system takes advantage of a nucleic acid-based adaptive immune system very common in bacteria and archea to target and cleave foreign and potentially infective genetic material through a specific nuclease (Cas9). In zebrafish, as well as in other models, it is possible to target a desired sequence in the genome just by designing specific single guide RNAs (sgRNA) complementary to the target and co-injecting them with the *cas9* nuclease mRNA or protein. The sgRNAs will direct the nuclease to specifically cleave the sequence of interest, just using standard base-pairing rules, thus inducing a double strand break in the DNA filament. This DNA damage during zebrafish early development is usually repaired by the error prone non-homologous end joining (NHEJ) mechanism, that is very likely accompanied by small insertions or deletions (INDELs) of nucleotides at the targeted region, leading consequently to mutations (Hwang *et al*., 2013; Gagnon *et al*., 2014; Auer and Del Bene, 2014). The only requirement for the Cas9 nuclease to properly cleave its target is that the genomic target DNA sequence must be adjacent to a 3' NGG sequence, the so called PAM (protospacer adjacent motif): the cut usually occurs 3 base pairs upstream of the PAM site.

With this approach, our aim was to try to verify the results obtained by loss of function assays using MOs, and then to deepen our analysis, gaining more precise and specific insights into the Haspin role since the beginning of embryonic development by completely knocking out its gene.

We decided to target the genomic *haspin* sequence at two different sites: thus, we designed and *in vitro* synthesized two different sgRNAs: the first one is complementary to the ATG region of the gene (we will refer to it as CRISPR ATG), and the second one is more downstream, in correspondence to exon 6 (we will refer to it as CRISPR E6). We also synthesized *in vitro* the *cas9* mRNA (in particular the zebrafish optimized version with nuclear localization signals; Jao *et al.*, 2013) and co-injected it into 1 cell stage embryos together with our sgRNAs, doing parallel injections with both CRISPRs (F0 generation). The doses that we eventually used were 90 pgr/E cas9 mRNA together with 150 pgr/E

sgRNA: we found that these concentrations were not toxic for the embryos and did not cause any significant mortality rate or severe phenotypes.

Our CRISPRs target sequences are illustrated in fig. 6 while the pipeline that we followed for mutagenesis and fish raising and screening for mutations is shown in details in fig. 10. We injected F0 embryos from AB and Tubingen long-fin strains with the sgRNAs and *cas9* mRNA, thus generating genetically mosaic fish. We raised them to adulthood and consequently performed in-crosses of these fish to test for germline transmission, namely, to identify F0 founder fish carrying mutations in the germline and thus able to transmit it to their progeny. In order to do this, pools of about 15 dpf larvae from each F0 in-cross were processed for genomic DNA extraction. To detect the presence of possible INDELs, we performed PCR on genomic DNA using specific primers amplifying the region we targeted with our CRISPRs. The PCR products were then processed using the SURVEYOR Mutation Detection kit, a very useful method for mutation screening taking advantage of a particular nuclease that recognizes and cleaves mismatches due to the presence of single nucleotide polymorphisms or small insertions or deletions in heterozygosity (Fig. 10). For the positive PCR products, we always confirmed the result by direct Sanger sequencing, evaluating evidences of INDELs at the correct site, namely 3 base pairs upstream of the PAM motif.

After having isolated positive F0 founder fish, we kept in-crossing them in order to grow only clutches of embryos positive for our desired mutation (F1 generation). For the next step, namely the genotyping and isolation of adult F1 heterozygous fish, we extracted genomic DNA from their fins and then performed a screening in the same way we did for the F0 larvae (Surveyor kit and sequencing, after cloning of the PCR products of Surveyor positive samples). Once a heterozygous female and a heterozygous male were identified, they were in-crossed in order to generate the 25% of homozygous mutants in their progeny. This procedure allows us to assess the effect of the complete knockout of the gene of interest, to look for phenotypes, and to make clear genotype/phenotype correlations (Fig. 10).

We followed this pipeline for both CRISPRs injections. Unfortunately, for the CRISPR ATG we were not able to recover any mutant in the F1. However, we found some positive Surveyor results from the F0 germ-line transmission screening, but we could never confirm our results due to problems during Sanger sequencing. When we in-crossed those positive clutches to grow F1 adult fish, we could not find any heterozygous, even if we still had some positive results with the Surveyor mutation kit. We thus concluded that this CRISPR

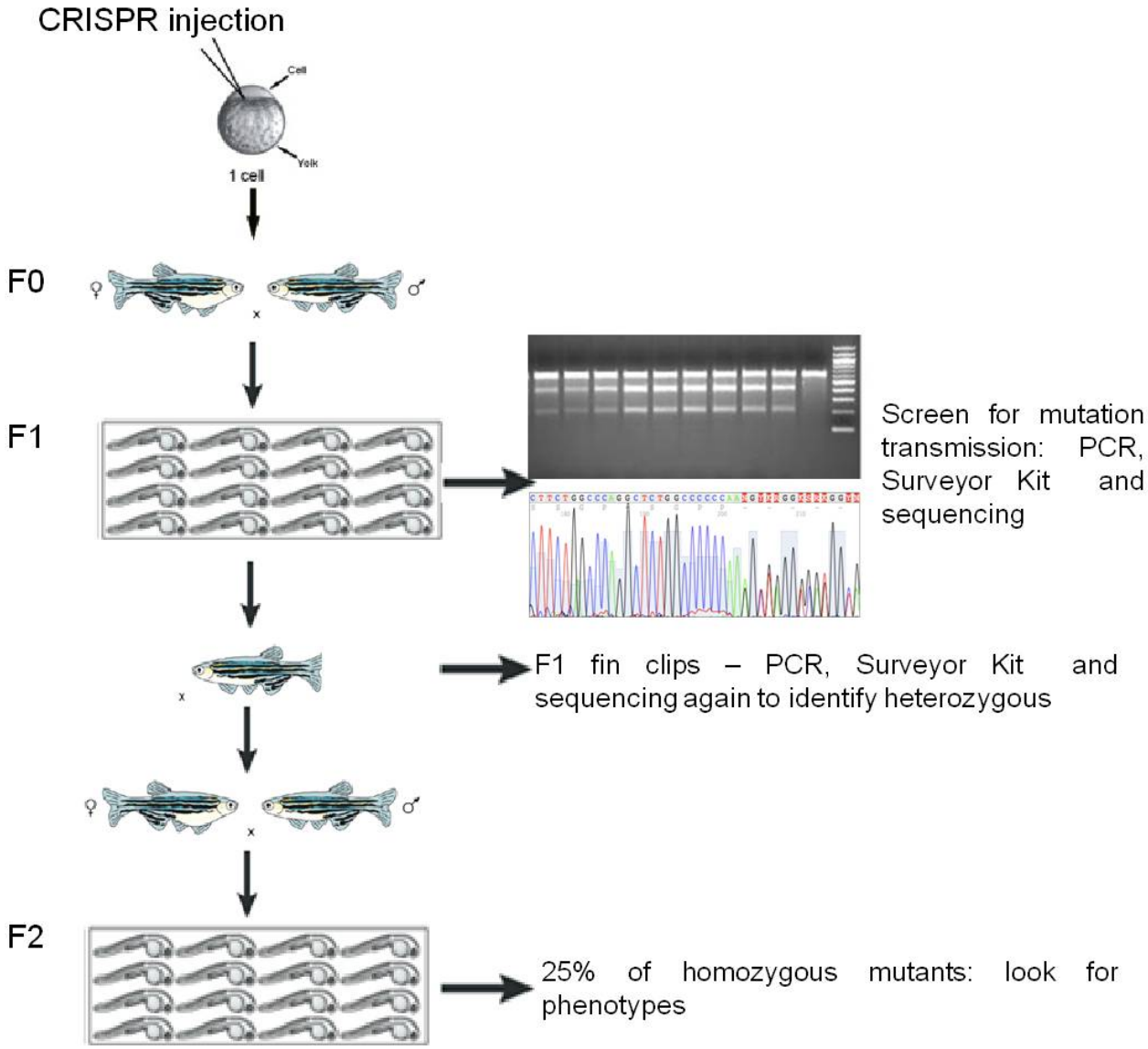

Fig. 10: Schematic representation of the pipeline we followed for mutagenesis by CRISPR-Cas9 system. F0 embryos injected with CRISPRs are genetically mosaic. They are grown to F0 adults and then different in-crosses are performed in order to test germline transmission of the mutation. Genomic DNA is extracted from pools of larvae from different clutches and PCR is performed using specific primers to amplify the region targeted by the CRISPR. PCR amplicons are tested with the Surveyor Mutation Detection kit, looking for mismatch-derived multiple bands, and positive results are then confirmed by Sanger sequencing, performed to detect evidences of insertions or deletions at the right target sites. Clutches positive for mutations are the grown to adults F1. Single F1 are tail-clipped and their genomic DNA is tested again with Surveyor Mutation Detection kit and then confirmed by Sanger Sequencing to identify heterozygous. Once a heterozygous female and a heterozygous male were identified, they were in-crossed in order to generate the 25% of homozygous mutants in their progeny (F2). Modified from Lawson and Wolfe, 2011.

targeting was not enough efficient to allow genome editing and eventually we discovered that the surveyor positive results we obtained from the F1 adult fin clips were caused by a polymorphism present in the CRISPR target region in the fish line we were using.
For what is concerning the CRISPR E6 instead, we managed to obtain a high efficiency of mutagenesis that allowed us to recover a good number of mutants, enough for our analysis.
We raised our F0 CRISPR injected mosaic fish to adulthood, and screened a total of 11 different in-crosses for germline transmission to the progeny. Sequencing results of 3 out of 5 total surveyor positive clutches of embryos derived from these in-crosses showed evidence of an INDEL at the target site (Fig. 11A,B). We thus identified 3 couples of founder F0 fish, able to transmit their mutation to the offspring. Next, we kept in-crossing these fishes in order to grow F1 generation to adulthood. For what is concerning the F1 screening, we analyzed 16 samples deriving from fin clips of single fish, and found in total 12 surveyor positive results (Fig. 12A). We proceeded with the sub-cloning and sequencing of 10 among those positive PCR products, and we were finally able to recover 8 heterozygous mutants, carrying mostly small INDELs (Fig. 12B). 2 of these turned out to have in frame insertions or deletions, while the other 6 (4 males and 1 female) carried small insertions or deletions all leading to frameshift mutations and, consequently, to a premature stop codon. Among these 6 fish, we found 3 different types of small INDELS, and we named these 3 different alleles *hasp*E6-1, *hasp*E6-2 and *hasp*E6-3 (Fig. 12B).
We then tried all different possibilities of in-crosses of these fish carrying the mutations of interest in order to generate 25% of homozygous mutants in the offspring, thus trying to evaluate the effect of a complete genetic knockout since the beginning of embryonic development. None of these in-crosses gave evident phenotypes during zygotic and larval development of the F2 offspring (first 5 days), and also the survival rate of embryos was not affected. To be sure that among the embryos we were monitoring there were actually homozygous mutants, we genotyped single F2 larvae at 5 dpf deriving from one of these in-crosses. From the sequences we found 4 homozygous mutants (-/-) out of 15 larvae: they were alive and phenotypically unaffected before lysis and genomic DNA extraction. This result proves that homozygous mutant embryos are viable and normal until, at least, the fifth day after fertilization. After that day, larvae cannot be kept in a petri dish in the embryo incubator anymore, but must be raised in the main system of the facility and they start to be fed. Hence, we decided to monitor larval development for all these in-crosses, to evaluate the occurrence of late defects in the homozygous mutants, that might cause a

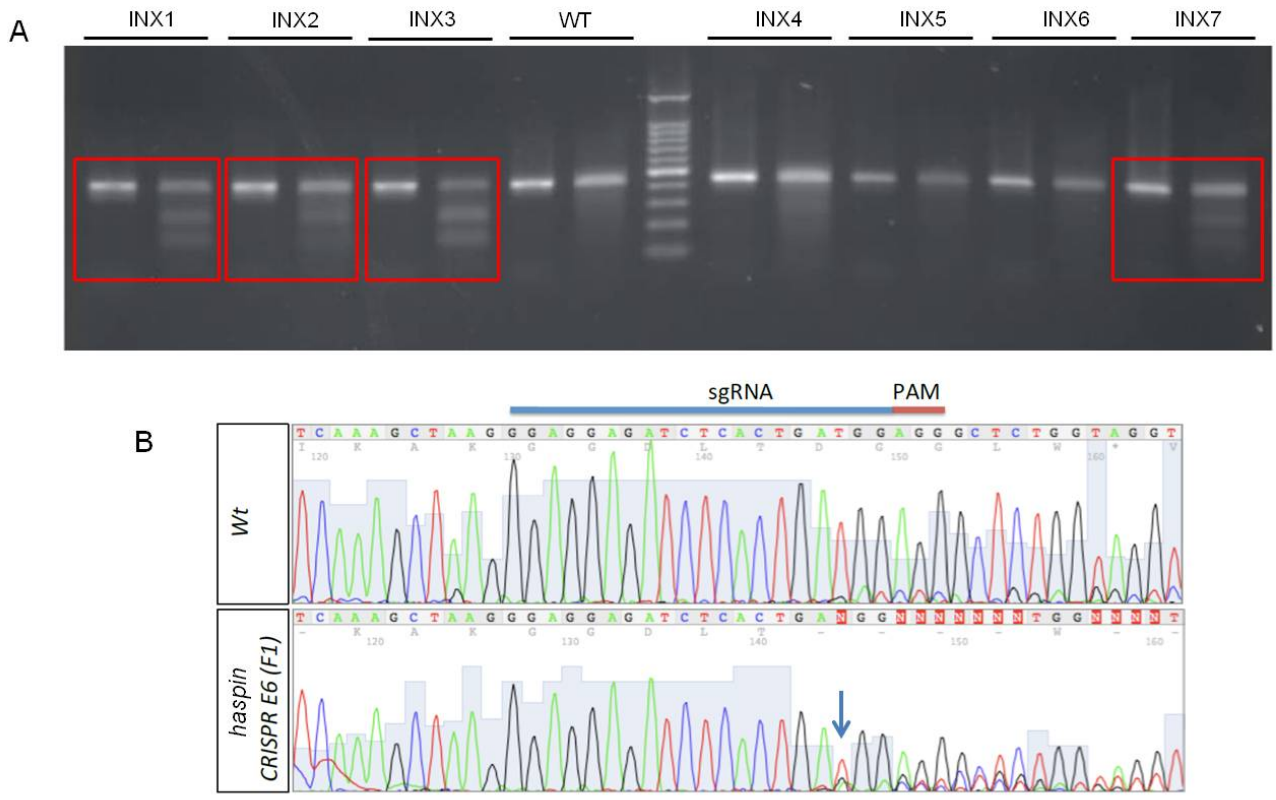

Fig. 11. Screening for mutation germline transmission in mosaic *haspin* CRISPRE6 F0 injected fish. (A) 2% agarose-gel electrophoresis conducted after surveyor nuclease processing of PCR samples performed on genomic DNA extracted from pools of F1 embryos (that derive from different in-crosses of the F0 mosaic generation). For each in-cross, a sample of undigested DNA is always loaded first as control. As negative control, wild type DNA is always digested as well. Samples containing mismatches derived from small insertions or deletions are cleaved by surveyor nuclease, thus resulting in multiple bands (highlited in red). The length of the digested fragments is compatible with a cleavage occurring 3 base pairs upstream of the PAM sequence. (B) Snapshot of the sequence obtained by a pool of F1 embryos positive for the SURVEYOR assay, compaired to the WT sequence. Blue arrow indicates the presence of an INDEL. Top blue line indicates the sgRNA, PAM sequence is in red.

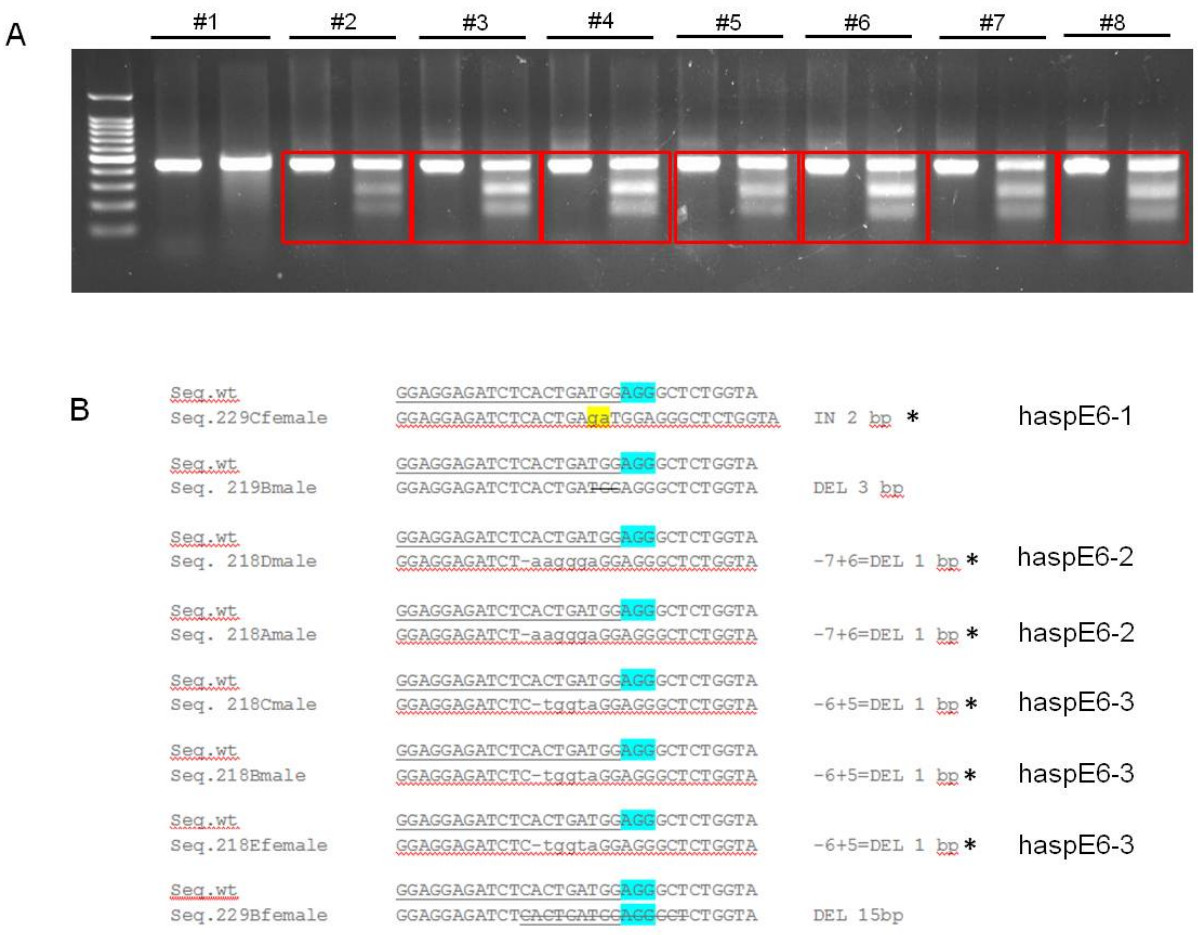

Fig. 12: Screening for heterozygous mutants among *haspin* CRISPR E6 adult F1 fish. (A) 2% agarose-gel electrophoresis conducted after surveyor nuclease processing of PCR samples amplified from genomic DNA of adult F1 fish fin clip samples (as described in fig. 11). Positive samples are highlited in red. (B) Out of 12 surveyor positive fin clips, we genotyped 10 samples and recovered 8 heterozygous mutants among these. Their sequence is shown in comparison to the wt sequence. Asterisks mark INDELs not multiple of 3 and thus leading to frameshift mutations; we verified they all resulted in premature stop codons and we named the different alleles as indicated in figure, grouping same mutations together. Underlined sequence: sgRNA; blue: PAM sequence; yellow: insertions.

different mortality rate compared to wild type or heterozygous situations. Everyday we collected any dead larva we could find in each tank, annotating the day of the death, and freezed it. When a reasonable number of dead larvae was collected from each tank, we proceeded with the lysis and genomic DNA extraction, in order to genotype each of them and verify if the dying fish were actually the homozygous mutants.

The results of these analysis are shown in fig. 13: in the different tanks we observed a trend of mortality from approximately 10% to 25% in the first three weeks of development, starting from 10 dpf. So far, for a group of dead fish collected from one of these in-crosses, we were able to genotype 5 dead larvae between 13 and 20 dpf, and we discovered that 4 out of 5 were homozygous mutants for *haspin* (Fig. 13). This is a first evidence indicating a differential survival rate between wild type fish and homozygous, suggesting that vey likely *haspin* knockout by CRISPR E6 results in mortality within the first month of development.

Moreover, we grew a F2 generation deriving from one of these in-crosses of two heterozygous fish to adulthood (around 3 months after fertilization). Our aim was to verify whether some of the homozygous fish deriving from that in-cross were able to reach the adult stage. Hence we tail clipped and genotyped 30 adult fish, from which we were not able to recover any adult homozygous mutant, but only wild type or heterozygous. This finding further indicates that none of the fish carrying a homozygous genotype for this mutation is able to reach the adulthood stage and that, interestingly, all of them die during the first weeks of development.

	initial number of larvae at 5 dpf	% mortality in the first 3 weeks	(-/-) among the dead larvae
incross HaspE6-1 xHaspE6-2	40	25	4 (-/-) out of 5 sequenced
incross HaspE6-3 xHaspE6-2	34	12	Still to sequence
incross HaspE6-1 xHaspE6-3	35	23	Still to sequence

Fig. 13: Table showing the mortality rate of larvae deriving from 3 different in-crosses of *haspin* heterozygous F1 adult fish. In this table we reported the initial number of alive larvae that are put in the main system of the facility starting from 5 dpf, their ortality rate in the first 3 weeks and the number of homozygous mutants, indicated as (-/-), that we recovered from the collected dead larvae. The heterozygous fish are named according to the mutated allele they carry (based on the nomenclature explained in fig. 12).

CONCLUSIONS AND FUTURE PROSPECTS

The *Haspin* gene, first discovered in male germ mice cells, encodes an atypical mitotic kinase which is important for the maintenance of chromosome cohesion (Dai and Higgins, 2005; Dai *et al.*, 2006). In mammalian cells, Haspin acts at metaphase as a serine/threonine kinase by phosphorylating threonine 3 of histone H3; this process allows the recruitment of the chromosomal passenger complex, which is required to regulate the metaphase to anaphase transition (Dai *et al.*, 2005). In human cells, *HASPIN* depletion causes premature loss of sister chromatid cohesion and defects in chromosome alignment at metaphase (Higgins, 2010; Wang *et al*., 2010). In *Arabidopsis thaliana*, Haspin is involved in the embryonic patterning of the plant (Ashtiyani *et al.*, 2011). Recently, it has been shown that Haspin activity is fundamental for meiosis I in mouse oocytes: in this model, indeed, its inhibition causes abnormalities in chromosome morphology and alignment, thus resulting in aneuploidy problems during metaphase II; Haspin kinase is also essential for chromatin condensation and for the regulation of meiotic resumption and transition from meiosis I to meiosis II (Nguyen *et al.*, 2014; Wang *et al.*, 2016).

Two haspin paralogs, *ALK1* and *ALK2*, have also been discovered in the budding yeast (Nespoli *et al.*, 2006). It was demonstrated that *ALK1* and *ALK2* do not appear to act through H3Thr3 phosphorylation, and their role is to organize actin cytoskeleton polarization in mitosis and to control mitotic spindle orientation (Panigada *et al.*, 2013).

During mitosis, a positive feedback loop in which Aurora B is involved ensures that HASPIN is kept phosphorylated and that its activity is restricted to this phase of the cell cycle (Wang *et al.*, 2011). Moreover, it has been demonstrated that Polo-like kinase 1 is required for initial activation of HASPIN in early mitosis (Zhou *et al.*, 2014). Interestingly, a recent work presents new possible HASPIN substrates in human cells, suggesting that its kinase activity might influence proteins involved in the regulation of gene expression (Maiolica *et al.*, 2014).

Summarizing, the atypical protein kinase Haspin has been found in all eukaryotic organisms, including vertebrates, arthropods, fungi and plants (Ashtiyani *et al.*, 2011; Higgins, 2010), suggesting a fundamental function. However, up to know, its role during animal embryonic development has never been investigated.

For this reason, in an effort between Proff. Paolo Plevani and Marco Muzi Falconi lab and the zebrafish unit of the University of Milan led by Prof. Franco Cotelli, we decided to investigate Haspin expression and its *in vivo* function during embryonic development using

zebrafish (*Danio rerio*, Teleostea), a little freshwater fish that has emerged in the past years as an ideal animal model to study basic events leading to embryo development and in modeling human diseases. Its embryos are translucent and fast growing and suitable for classical embryological studies as well as for more complex approaches. These characteristics make zebrafish one of the best models for genetic studies, suitable for both direct and reverse genetic experiments.

First of all, we managed to identify the zebrafish *haspin* ortholog on chromosome 1. Only one annotated gene encoding for *haspin* was detected in the genomic browser.

Since a lot of genes are duplicated in the zebrafish genome, in order to look for other possible *haspin* or *haspin*-like genes we carried out some bioinformatics research: in particular, we performed multiple alignments trying to use different reference sequences, such as the human HASPIN protein, the zebrafish Haspin protein and also the kinase domain only, but we could not find any other candidate *haspin* gene with a significant value of similarity. Hence, we conclude that, as far as we know now, only one form exists in the zebrafish genome.

The similarity score between human and zebrafish Haspin is overall quite low but, significantly, all the different functional domains and regulatory motifs are present in both organisms. More specifically, the STP motif constituting the PBD (Polo Box domain), important for the activation of the protein, the HBIS auto-inhibitory segment and the C-terminal ser/thr kinase domain are present in the fish protein and share a significant similarity with the human ortholog. This indicates that the functional and regulatory motifs are well conserved, thus suggesting relevant parallelisms on the importance of Haspin function in different eukaryotic organisms.

Moreover, while we were trying to clone the zebrafish full length DNA fragment isolated by PCR, we identified a smaller DNA fragment corresponding to an alternative, shorter transcript. We then cloned and sequenced this fragment and discovered the presence of a new a splicing variant that was not previously annotated in the genomic browser. Sequencing of this fragment revealed that is identical to the canonical gene, except that it is lacking a portion of ~600 base pairs constituting the sixth exon of the coding sequence.

Looking at the schematic representation of the different domains in the zebrafish *haspin* sequence, it was clear that the missing portion in this splicing variant corresponds exactly to the exon containing the STP motif constituting the PBD (Polo Box domain). The PBD is first phosphorylated by the Cdk1/cyclinB complex, thus creating a recognition site for Plk1, that binds and carries out the N-terminal phosphorylation of Haspin. This modification is

responsible for Haspin catalytic domain activation since, once Haspin is phosphorylated by Plk1, it loses its affinity for the auto-inhibitory domain (Moutinho-Santos T. and Maiato H., 2014). Therefore, Plk1 Haspin phosphorylation is fundamental for the activation of the protein and, as far as we know, a Haspin form lacking the PBD should be constitutive inactive, because the C-terminal kinase domain will be kept inactive by allosteric interaction with the auto-inhibitory segment (Ghenoiu *et al.*, 2013). Although we do not have yet any evidence about a possible role of this newly identified splicing isoform, we can speculate that it may act as a sort of “dominant negative”, since a constitutively inactive Haspin form could compete with the canonical one in the context of other activation processes, such as the phosphorylation carried out by Aurora B and the consequent positive feedback loop, thus decreasing and limiting the physiological levels of Haspin activity. In this scenario, this new Haspin form might play a role in some specific tissues in which high levels of Haspin activity may not be required, such as in non-proliferative tissues.

However, we cannot exclude the possibility that this splicing Haspin variant might be activated by different and still unknown regulatory mechanisms, and have different functions other than the canonical ones. This is a new open field and we are currently planning additional experiments to clarify the function of this new splicing isoform.

Concerning the temporal spatial expression of the *haspin* forms, we found that both of them display both a maternal and zygotic expression, as we were expecting given the data present in literature about the function of this protein during the regulation of the cell cycle in other models. The canonic *haspin* transcript is present in all developmental stages analyzed, starting from the 2-4 cells stage up to 3 dpf, and we were able to detect the shorter splicing variant in all stages except the 5-8 somites stage. The intensity of the band corresponding to the splicing variant was very faint in some stages, probably due to non optimal amplification of the shorter product; anyway, we are now repeating this experiment with a new set of primers. In any case, the expression of the splicing isoform appears to be mostly zygotic rather than maternal, showing an opposite trend compared to that of the canonical *haspin* form.

We then performed *in situ* hybridization experiments to clarify the spatial pattern of expression of the *haspin* gene at different stages of development. We found that the *haspin* hybridization signal was really intense and widespread all over the developing embryo, starting from the very first stages of cleavage (namely the 2-4 cells stage), proving a significantly abundant maternal contribution in the total level of this transcript. In

fact, during the first stages of zebrafish development, namely until the midblastula transition (at approximately 3 hpf), the zygotic transcription has not yet started and the embryo relies completely upon the maternally inherited mRNAs and proteins (Kimmel *et al.*, 1995). We then noticed that the expression level of *haspin* slightly decreases while progressing in the developmental program, but the transcript is present during all stages analyzed, namely up to 3 dpf. In particular, *haspin* expression is detectable is some specific tissues of the embryo, such as the caudal region of the ICM, the retina, the otic vesicles and the periventricular portions of the developing brain structures. At 2 dpf we could also detect a relevant presence of the transcript in the fin buds. This spatial expression pattern is interesting because all these regions exhibit high levels of proliferating cells, which is consistent with the literature data about *haspin* expression in other models (Higgins, 2001a), where the transcription of this gene is significantly enhanced in tissues with high proliferating rates.

Cellular divisions and proliferation are processes playing important roles also in some adult tissues. We thus wondered whether *haspin* transcript was also present in organs extracted from adult zebrafish individuals, trying to understand if it could be expressed either in adult tissues with high proliferation levels or in the gonads, where meiotic processes take place. We could not detect *haspin* transcript by sqRT-PCR assays either in the eyes or in the brain, but it was present in both ovary and testis, while the band corresponding to the shorter splicing variant was only found in the testis. Interestingly, Haspin has been shown to play an important role during oocytes maturation and meiotic resumption in mouse oocytes (Nguyen *et al.*, 2014; Wang *et al.*, 2016), and it is possible that this function may be conserved in the zebrafish gonads as well.

Furthermore, we demonstrated that *haspin* is overexpressed after injury during tissue regeneration; in fact, *haspin* expression is clearly detectable by performing sqRT-PCR on a growing blastema tissue sample cut from a previously clipped adult fin. This is a further demonstration that *haspin* transcription is significantly turned on in tissues with high proliferation rates, such as during regeneration.

Altogether, the particular *haspin* expression data in the zebrafish model system suggest a potential involvement of the protein in the regulation of cell cycle and proliferation, as well as during meiotic processes.

Concerning the Haspin functional characterization, we started our analysis taking advantage of a MO-mediated knockdown approach, by designing and testing both an ATG and a spl MOs.

By performing western blot assays using a specific antibody against H3Thr3PH on morphant embryos compared to controls, we were able to conclude that the microinjection of both MOs results in a significant decrease of the phosphorylation levels of threonine 3 of Histone H3, the most known Haspin substrate identified so far. We observed that MOs-dependent decrease of H3Thr3PH levels starts from the first stages of epiboly and, hence, we conclude that Haspin involvement in H3Thr3PH is conserved in the zebrafish model.
However, until now, we cannot unambiguously explain the phenotypic effects of Haspin inactivation during zebrafish embryonic development and we are testing various hypothesis.
The microinjection of the specific *haspin* ATG MO has a very severe phenotypic effect, because it interferes with epiboly and gastrulation processes and does not allow embryos to survive and to develop the organogenesis steps. Starting from the beginning of epiboly, *haspin* ATG morphants display a significant percentage of irregular blastoderm margin, cells are less compact and in some cases a gap between the blastoderm and the yolk is detectable. The morphants are not able to complete the epiboly process in a normal way and, being epiboly a crucial event during early embryogenesis, the mortality rate of these morphants almost reaches 100% within the first day of development.
This very dramatic effect of MO microinjection led us to hypothesize that the loss or a strong reduction of Haspin could somehow affect cellular adhesion and motility. In fact, morphants cells are not able to correctly migrate and envelope the yolk below during epiboly, and sometimes gaps between the cells and between the blastoderm and the yolk are detectable. Moreover, we also carried out *in situ* hybridization experiments in ATG morphants compared to std-MO control embryos using classical epiboly markers: we could demonstrate that the expression pattern of markers such as *otx3*, *fgf8*, *gsc* and *chd* is strongly altered after Haspin knockdown, confirming significant alterations in cellular rearrangements and movements during epiboly.
During our functional analysis, we also tested the effect of a splicing MO able to target the junction between exon 5 and intron 5/6, which is predicted to cause the skipping of the fifth exon thus altering the open reading frame of the mRNA. By RT-PCR performed on cDNA retro-transcribed from *haspin* splicing morphants we were able to clearly visualize the aberrant transcript, demonstrating that the exon 5 was skipped as expected, and Sanger sequencing of this amplicon demonstrated that, after this non-physiological splicing event, a frameshift event gives rise to a premature stop codon. Furthermore, we failed to detect any wild type transcript suggesting that, at the dose of spl-MO used for that assay (that

was equal or even lower than that used to evaluate possible phenotypic defects in the morphants), almost all or at least the great majority of the endogenous mRNA undergoes aberrant splicing, resulting in a very efficient knockdown. With this morpholino, also the shorter splicing isoform that we identified is targeted, as the exon/intron junction bound by the morpholino is present in both forms (exon 5-intron 5/6). Microinjection of the splicing MO, however, fails to cause any phenotypic alteration, and the nervous and hematopoietic markers analyzed were not altered in the morphants. Their survival rate was unaffected, also at high doses, although we were able to detect a decrease in the level of phosphorylation of threonine 3 of histone H3.

One hypothesis that very likely explains this discrepancy is that the particular and severe phenotype observed during epiboly might be due to loss or strong reduction of the maternally inherited *haspin* mRNA component. Indeed, this can be an interesting possibility, given the very relevant maternal expression of *haspin* during the early stages of zebrafish development documented both by RT-PCR and *in situ* hybridization assays, and the fact that splicing MO is not able to target mRNAs that are already mature. In any case, it appears that the decrease observed in the phosphorylation level of H3Thr3 and the epiboly phenotype resulting from *haspin* ATG MO microinjection are two distinct and separate effects. In fact, a decrease in the signal of H3Thr3PH is observed with *haspin* splicing MO, while embryos do not show any evident alteration during development. Haspin depletion, after all, has been already shown to have an effect not directly linked to histone modification in other models, such as in budding yeast. Indeed, in this system, *haspin* orthologs play a role in organizing actin cytoskeleton polarization during mitosis and in affecting mitotic spindle orientation, but in yeast cells Thr3 of histone H3 does not appear to be phosphorylated (Panigada *et al.*, 2013). However, we cannot formally exclude the hypothesis that the phenotype observed with the *haspin* ATG MO may be due to an aspecific MO-mediated effect. Indeed, it has been previously reported that MOs can in some cases lead to artifacts due to non-specific binding to some off-targets (Eisen and Smith, 2008; Schulte-Merker and Stainier, 2014).

We have not yet been able to rescue the ATG MO phenotype by co-injecting the morpholino and the *in vitro* synthesized mRNA encoding the zebrafish *haspin* canonical form, even if we are still performing trials in order to test the optimal dose of transcript to inject. Our rescue assays might not be simple to plan, as it usually is when dealing with long transcripts (like the 3279-bp full length zebrafish *haspin* mRNA), but we intend to

increase the dose of injected mRNA aiming to verify a rescue of the epiboly phenotype observed with *haspin* ATG MO.

To date, the most known and reported MO off-target effect is related to the activation of a non-physiological p53 isoform-mediated apoptosis cascade (Robu *et al.*, 2007). To exclude such possibility, we performed sqRT-PCR experiments on cDNAs retro-transcribed from ATG morphants at different doses, including the highest dose used for the phenotypic analysis, using specific primers for amplifying the non physiological p53 isoform, and using as internal controls also β-actin and the p53 canonical form. Even if this was not a strictly quantitative assay, we did not detect any significant increase in the intensity of the bands for the non-physiological p53 isoform in morphant samples, that would have been compatible with possible overexpression of this non-specific target, even in those injected with the highest doses (data not shown). This result strongly suggests that microinjection of the ATG MO does not result in the activation of this apoptotic pathway. However, we cannot formally exclude that *haspin* ATG MO may have other unpredictable off-target effects.

The hypothesis that the ATG MO phenotype may be specific and related to the depletion of maternal *haspin* transcripts, however, is also supported by the analysis of *haspin* mutants generated by CRISPR-Cas9 technology. We have been able to obtain six mutant fish carrying an heterozygous mutation in exon 6, in all cases leading to a frameshift mutations and thus to a premature stop codon. The homozygous mutant embryos, confirmed by sequencing and derived from in-crosses of these fish, did not exhibit any phenotype during early embryonic and larval development, similarly to what was observed after *haspin* spl-MO microinjection. In terms of maternal and zygotic contribution, the mutants that we analyzed reflect a condition comparable to that occurring after a spl MO microinjection; indeed, we generated a zygotic mutant in which the heterozygous mother carries one wild type copy of the *haspin* allele, thus the maternal contribution of determinants for embryos early development is not affected; this might be sufficient for them to normally proceed through the first stages of epiboly. However, we observed that homozygous *haspin* mutant embryos are not able to reach the adulthood stage, although they do not show any evident alteration during embryogenesis. It is very likely that all of them (or almost all of them) die within the first 3 weeks of development, starting from ~9 dpf.

This important evidence clearly indicates that *haspin* does play a role during larval or late embryogenesis stages. The first month of development is indeed the most critical for larval

survival rate, in particular around 14 and 30 dpf, and it is possible that *haspin* mutants will suffer from defects linked to previous mild problems during organogenesis that do not allow them to grow to the adulthood stage.
At 5 dpf zebrafish larvae have completed their morphogenesis, the swim bladder is inflated and the swimming is active, as well as other behaviours such as the seeking of prey and the feeding (Kimmel *et al.*, 1995). It is possible that *haspin* mutants exhibit some defects compromising their motility and thus their capacity of swimming and seeking of prey and, for this reason, they may be able to reach less food and progressively starve to death. They might also have mild defects in jaw joints movements, and this could result in feeding problems as well, or in some internal organs such as the gut, pancreas or kidney, that could affect their metabolism and nutrients assimilation, not allowing them to grow and reach the adulthood stage as their wild type and heterozygous siblings.

The work described in this Ph.D. thesis can be considered as the first *in vivo haspin* characterization using the zebrafish model and, in general, during animal embryonic development. We identified and cloned the zebrafish *haspin* ortholog, together with a new previously unknown splicing isoform, and we clarified its expression pattern during embryogenesis and in some adult tissues. To begin understanding the role played by this mitotic kinase during development, we generated a *haspin* stable mutant line, and also took advantage of a MO-mediated knockdown approach. However, we still have to address some open questions that will allow us to unequivocally shed light on Haspin function during zebrafish development.
To definitely exclude that the phenotype observed with the *haspin* ATG MO may be linked to off-target effects, we will design another ATG MO at a different, more downstream site, and/or we will target only the 5'UTR sequence and we will verify whether the same effect during epiboly will be observed. If we succeed in obtaining the same phenotype, possibly even at a difference degree of penetrance, we will be more confident about the specificity of the functional inactivation assays described here. So far, we have not been able to rescue the epiboly phenotype by coinjecting the *haspin* canonic mRNA together with the morpholino, but we are planning to try again increasing the dose of mRNA injected. We also plan to verify by western blotting at least a rescue of the H3Thr3 phosphorylation level by coinjecting the transcript with both of our MOs since they both cause a similar decrease in H3Thr3 phosphorylation.

We wish to clarify the function of the newly identified splicing isoform as well: to this aim, we will perform functional assays such as overexpression trials. With respect to the canonical *haspin* form, we will verify the rescue of the epiboly phenotype and that of the decreased H3Thr3 phosphorylation levels by coinjecting its transcript together with the MOs in parallel experiments.

To complete our work, we will also need to fully characterize our KO mutants. We need to perform western blot assays on protein extracts derived from single embryos among the offspring of two of our heterozygous fish, followed by genotyping of all of these embryos, to evaluate if the ones carrying a -/- genotype also show a decrease in H3Thr3PH levels. This result would also further confirm what we observed by MOs microinjection.

Our next aim will be then to clarify why the larvae carrying a -/- genotype start to die at ~9-10 dpf and cannot reach the adulthood stage. As I mentioned above, it is possible that they go through some mild alterations during organogenesis taking place in the first days of development, that might later lead to a significant decrease in the survival rate. To this end, we will perform *in situ* hybridization assays at 5 dpf using molecular markers to visualize possible alterations in some internal organs fundamental for larval growth and survival, such as liver, kidney, gut and pancreas, as well as specific markers for different specific neuronal populations, considering the *haspin* expression pattern during development.

REFERENCES

- Adams R. R., H. Maiato, W. C. Earnshaw, and M. Carmena, “Essential roles of Drosophila inner centromere protein (INCENP) and aurora B in histone H3 phosphorylation, metaphase chromosome alignment, kinetochore disjunction, and chromosome segregation.,” *J. Cell Biol.*, vol. 153, no. 4, pp. 865–80, 2001.

- Adams R. R., H. Maiato, W. C. Earnshaw, and M. Carmena, “Essential roles of Drosophila inner centromere protein (INCENP) and aurora B in histone H3 phosphorylation, metaphase chromosome alignment, kinetochore disjunction, and chromosome segregation.,” *J. Cell Biol.*, vol. 153, no. 4, pp. 865–80, 2001.

- Ashtiyani R. K., A. M. B. Moghaddam, V. Schubert, T. Rutten, J. Fuchs, D. Demidov, F. R. Blattner, and A. Houben, “AtHaspin phosphorylates histone H3 at threonine 3 during mitosis and contributes to embryonic patterning in Arabidopsis,” *Plant J.*, vol. 68, no. 3, pp. 443–454, 2011.

- Auer T. O. and F. Del Bene, “CRISPR/Cas9 and TALEN-mediated knock-in approaches in zebrafish,” *Methods*, vol. 69, no. 2, pp. 142–150, 2014.

- Bellipanni G., T. Murakami, O. G. Doerre, P. Andermann, and E. S. Weinberg, “Expression of Otx homeodomain proteins induces cell aggregation in developing zebrafish embryos.,” *Dev. Biol.*, vol. 223, no. 2, pp. 339–53, 2000.

- Blackburn P. R., J. M. Campbell, K. J. Clark, and S. C. Ekker, “The CRISPR system--keeping zebrafish gene targeting fresh,” *Zebrafish*, vol. 10, no. 1, pp. 116–118, 2013.

- Carmena M., M. Wheelock, H. Funabiki, and W. C. Earnshaw, “The chromosomal passenger complex (CPC): from easy rider to the godfather of mitosis.,” *Nat. Rev. Mol. Cell Biol.*, vol. 13, no. 12, pp. 789–803, 2012a.

- Carmena M., X. Pinson, M. Platani, Z. Salloum, Z. Xu, A. Clark, F. Macisaac, H. Ogawa, U. Eggert, D. M. Glover, V. Archambault, and W. C. Earnshaw, “The chromosomal passenger complex activates Polo kinase at centromeres.,” *PLoS Biol.*, vol. 10, no. 1, p. e1001250, 2012b.

- Clevers H., “Stem cells, asymmetric division and cancer.,” *Nat. Genet.*, vol. 37, no. 10, pp. 1027–8, 2005.

- Cooke C. A., M. M. Heck, and W. C. Earnshaw, “The inner centromere protein (INCENP) antigens: movement from inner centromere to midbody during mitosis.,” *J. Cell Biol.*, vol. 105, no. 5, pp. 2053–67, 1987.

- Crosio C., G. M. Fimia, R. Loury, M. Kimura, Y. Okano, H. Zhou, S. Sen, C. D. Allis, and P. Sassone-corsi, “Mitotic Phosphorylation of Histone H3 : Spatio-Temporal Regulation by Mammalian Aurora Kinases Mitotic Phosphorylation of Histone H3 : Spatio-Temporal Regulation by Mammalian Aurora Kinases,” vol. 22, no. 3, pp. 874–885, 2002.

- Cutts S. M., K. J. Fowler, B. T. Kile, L. L. Hii, R. A. O’Dowd, D. F. Hudson, R. Saffery, P. Kalitsis, E. Earle, and K. H. Choo, “Defective chromosome segregation, microtubule bundling and nuclear bridging in inner centromere protein gene (Incenp)-disrupted mice.,” *Hum. Mol. Genet.*, vol. 8, no. 7, pp. 1145–55, 1999.

- Dai J. and J. M. G. Higgins, “Haspin: A mitotic histone kinase required for metaphase chromosome alignment,” *Cell Cycle*, vol. 4, no. 5, pp. 665–668, 2005.

- Dai J., A. V Kateneva, and J. M. G. Higgins, “Studies of haspin-depleted cells reveal that spindle-pole integrity in mitosis requires chromosome cohesion.,” *J. Cell Sci.*, vol. 122, no. Pt 22, pp. 4168–76, 2009.

- Dai J., B. A. Sullivan, and J. M. G. Higgins, “Regulation of Mitotic Chromosome Cohesion by Haspin and Aurora B,” *Dev. Cell*, vol. 11, no. 5, pp. 741–750, 2006.

- Dai J., S. Sultan, S. S. Taylor, and J. M. G. Higgins, “The kinase haspin is required for mitotic histone H3 Thr 3 phosphorylation and normal metaphase chromosome alignment,” *Genes Dev.*, vol. 19, no. 4, pp. 472–488, 2005.

- De Antoni A., S. Maffini, S. Knapp, A. Musacchio, and S. Santaguida, “A small-molecule inhibitor of Haspin alters the kinetochore functions of Aurora B.,” *J. Cell Biol.*, vol. 199, no. 2, pp. 269–84, 2012.

- Delvaeye M., A. De Vriese, F. Zwerts, I. Betz, M. Moons, M. Autiero, and E. M. Conway, “Role of the 2 zebrafish survivin genes in vasculo-angiogenesis, neurogenesis, cardiogenesis and hematopoiesis.,” *BMC Dev. Biol.*, vol. 9, p. 25, 2009.

- Detrich H. W., M. W. Kieran, F. Y. Chan, L. M. Barone, K. Yee, J. A. Rundstadler, S. Pratt, D. Ransom, and L. I. Zon, “Intraembryonic hematopoietic cell migration during vertebrate development.,” *Proc. Natl. Acad. Sci. U. S. A.*, vol. 92, no. 23, pp. 10713–7, 1995.

- Eisen J. S. and J. C. Smith, “Controlling morpholino experiments: don’t stop making antisense.,” *Development*, vol. 135, no. 10, pp. 1735–43, 2008.

- Ekker S. C., “Morphants: a new systematic vertebrate functional genomics approach.,” *Yeast*, vol. 17, no. 4, pp. 302–306, 2000.

- Eswaran J., D. Patnaik, P. Filippakopoulos, F. Wang, R. L. Stein, J. W. Murray, J. M. G. Higgins, and S. Knapp, “Structure and functional characterization of the atypical human kinase haspin” *Proc. Natl. Acad. Sci. U. S. A.*, vol. 106, no. 48, pp. 20198–20203, 2009.

- Fernández-Miranda G., M. Trakala, J. Martín, B. Escobar, A. González, N. B. Ghyselinck, S. Ortega, M. Cañamero, I. Pérez de Castro, and M. Malumbres, “Genetic disruption of aurora B uncovers an essential role for aurora C during early mammalian development.,” *Development*, vol. 138, no. 13, pp. 2661–72, 2011.

- Gagnon J. A., E. Valen, S. B. Thyme, P. Huang, L. Ahkmetova, A. Pauli, T. G. Montague, S. Zimmerman, C. Richter, and A. F. Schier, “Efficient mutagenesis by Cas9 protein-mediated oligonucleotide insertion and large-scale assessment of single-guide RNAs,” *PLoS One*, vol. 9, no. 5, pp. 5–12, 2014.

- Gascoigne K. E., K. Takeuchi, A. Suzuki, T. Hori, T. Fukagawa, and I. M. Cheeseman, “Induced ectopic kinetochore assembly bypasses the requirement for CENP-A nucleosomes.,” *Cell*, vol. 145, no. 3, pp. 410–22, 2011.

- Ghenoiu C., M. Wheelock, and H. Funabiki, “Autoinhibition and polo-dependent multisite phosphorylation restrict activity of the histone H3 kinase haspin to mitosis,” *Mol. Cell*, vol. 52, no. 5, pp. 734–745, 2013.

- Gönczy P., “Mechanisms of asymmetric cell division: flies and worms pave the way.,” *Nat. Rev. Mol. Cell Biol.*, vol. 9, no. 5, pp. 355–66, 2008.

- Gonzalez C., “Spindle orientation, asymmetric division and tumour suppression in Drosophila stem cells.,” *Nat. Rev. Genet.*, vol. 8, no. 6, pp. 462–72, 2007.

- Gray R. S., K. J. Cheung, and A. J. Ewald, “Cellular mechanisms regulating epithelial morphogenesis and cancer invasion.,” *Curr. Opin. Cell Biol.*, vol. 22, no. 5, pp. 640–50, 2010.

- Hanck T., R. Stricker, F. Sedehizade, and G. Reiser, “Identification of gene structure and subcellular localization of human centaurin alpha 2, and p42IP4, a family of two highly homologous, Ins 1,3,4,5-P4-/PtdIns 3,4,5-P3-binding, adapter proteins.,” *J. Neurochem.*, vol. 88, no. 2, pp. 326–36, 2004.

- Hayashi-Takanaka Y., K. Yamagata, N. Nozaki, and H. Kimura, “Visualizing histone modifications in living cells: spatiotemporal dynamics of H3 phosphorylation during interphase.,” *J. Cell Biol.*, vol. 187, no. 6, pp. 781–90, 2009.

- Hendzel M. J., Y. Wei, M. A. Mancini, A. Van Hooser, T. Ranalli, B. R. Brinkley, D. P. Bazett-Jones, and C. D. Allis, “Mitosis-specific phosphorylation of histone H3 initiates primarily within pericentromeric

heterochromatin during G2 and spreads in an ordered fashion coincident with mitotic chromosome condensation.," *Chromosoma*, vol. 106, no. 6, pp. 348–60, 1997.

- Higgins J. M. G. , "Haspin: A newly discovered regulator of mitotic chromosome behavior," *Chromosoma*, vol. 119, no. 2, pp. 137–147, 2010.

- Higgins J. M. G., "Haspin-like proteins : A new family of evolutionarily conserved putative eukaryotic protein kinases," pp. 1677–1684, 2001b.

- Higgins J. M. G., "The Haspin gene : location in an intron of the Integrin a E gene , associated transcription of an Integrin a E-derived RNA and expression in diploid as well as haploid cells," vol. 267, pp. 55–69, 2001a.

- Honda R., R. Körner, and E. A. Nigg, "Exploring the functional interactions between Aurora B, INCENP, and survivin in mitosis.," *Mol. Biol. Cell*, vol. 14, no. 8, pp. 3325–41, 2003.

- Hsu J. Y., Z. W. Sun, X. Li, M. Reuben, K. Tatchell, D. K. Bishop, J. M. Grushcow, C. J. Brame, J. A. Caldwell, D. F. Hunt, R. Lin, M. M. Smith, and C. D. Allis, "Mitotic phosphorylation of histone H3 is governed by Ipl1/aurora kinase and Glc7/PP1 phosphatase in budding yeast and nematodes.," *Cell*, vol. 102, no. 3, pp. 279–91, 2000.

- Huertas D., M. Soler, J. Moreto, A. Villanueva, A. Martinez, A. Vidal, M. Charlton, D. Moffat, S. Patel, J. McDermott, J. Owen, D. Brotherton, D. Krige, S. Cuthill, and M. Esteller, "Antitumor activity of a small-molecule inhibitor of the histone kinase Haspin," *Oncogene*, vol. 31, no. 11, pp. 1408–1418, 2012.

- Hunt P. A. and T. J. Hassold, "Sex matters in meiosis.," *Science*, vol. 296, no. 5576, pp. 2181–3, 2002.

- Huson S. M. and R. C. Huges, "The neurofibromatosis: a clinical and pathogenetic overview". London: Chapman and Hall, (1994).

- Hwang W. Y., Y. Fu, D. Reyon, M. L. Maeder, S. Q. Tsai, J. D. Sander, R. T. Peterson, J. R. Yeh, and J. K. Joung, "Efficient genome editing in zebrafish using a CRISPR-Cas system," *Nat Biotechnol*, vol. 31, no. 3, pp. 227–229, 2013.

- Ikegami R., A. K. Rivera-Bennetts, D. L. Brooker, and T. D. Yager, "Effect of inhibitors of DNA replication on early zebrafish embryos: evidence for coordinate activation of multiple intrinsic cell-cycle checkpoints at the mid-blastula transition.," *Zygote*, vol. 5, no. 2, pp. 153–75, 1997a.

- Ikegami R., J. Zhang, A. K. Rivera-Bennetts, and T. D. Yager, "Activation of the metaphase checkpoint and an apoptosis programme in the early zebrafish embryo, by treatment with the spindle-destabilising agent nocodazole.," *Zygote*, vol. 5, no. 4, pp. 329–50, 1997b.

- Jao L.-E., S. R. Wente, and W. Chen, “Efficient multiplex biallelic zebrafish genome editing using a CRISPR nuclease system.,” *Proc. Natl. Acad. Sci. U. S. A.*, vol. 110, no. 34, pp. 13904–9, 2013.

- Jenne D. E., S. Tinschert, E. Stegmann, H. Reimann, P. Nürnberg, D. Horn, I. Naumann, A. Buske, and G. Thiel, “A common set of at least 11 functional genes is lost in the majority of NF1 patients with gross deletions.,” *Genomics*, vol. 66, no. 1, pp. 93–7, 2000.

- Kallio M. J., M. L. McCleland, P. T. Stukenberg, and G. J. Gorbsky, “Inhibition of aurora B kinase blocks chromosome segregation, overrides the spindle checkpoint, and perturbs microtubule dynamics in mitosis.,” *Curr. Biol.*, vol. 12, no. 11, pp. 900–5, 2002.

- Kane D. A. and C. B. Kimmel, “The zebrafish midblastula transition.,” *Development*, vol. 119, no. 2, pp. 447–56, 1993.

- Kane D. A., R. M. Warga, and C. B. Kimmel, “Mitotic domains in the early embryo of the zebrafish.,” *Nature*, vol. 360, no. 6406, pp. 735–7, 1992.

- Kang J., I. M. Cheeseman, G. Kallstrom, S. Velmurugan, G. Barnes, and C. S. Chan, “Functional cooperation of Dam1, Ipl1, and the inner centromere protein (INCENP)-related protein Sli15 during chromosome segregation.,” *J. Cell Biol.*, vol. 155, no. 5, pp. 763–74, 2001.

- Kaur H., M. E. Bekier, and W. R. Taylor, “Regulation of Borealin by phosphorylation at serine 219.,” *J. Cell. Biochem.*, vol. 111, no. 5, pp. 1291–8, 2010.

- Kelly A. E., C. Ghenoiu, J. Z. Xue, C. Zierhut, H. Kimura, and H. Funabiki, “Survivin reads phosphorylated histone H3 threonine 3 to activate the mitotic kinase Aurora B.,” *Science*, vol. 330, no. 6001, pp. 235–9, 2010.

- Kimmel C. B., W. W. Ballard, S. R. Kimmel, B. Ullmann, and T. F. Schilling, “Stages of embryonic development of the zebrafish.,” *Dev. Dyn.*, vol. 203, no. 3, pp. 253–310, 1995.

- Kitagawa M. and S. H. Lee, “The chromosomal passenger complex (CPC) as a key orchestrator of orderly mitotic exit and cytokinesis.,” *Front. cell Dev. Biol.*, vol. 3, p. 14, 2015.

- Knoblich J. A., “Asymmetric cell division: recent developments and their implications for tumour biology,” *Nat. Rev. Mol. Cell Biol.*, vol. 11, no. 12, pp. 849–860, 2010.

- Koster M. J. E., B. Snel, and H. T. M. Timmers, “Genesis of chromatin and transcription dynamics in the origin of species,” *Cell*, vol. 161, no. 4, pp. 724–736, 2015.

- Kozgunova E., T. Suzuki, M. Ito, T. Higashiyama, and D. Kurihara, “Haspin has Multiple Functions in the Plant Cell Division Regulatory Network,” *Plant Cell Physiol.*, vol. 57, no. 4, pp. 848-861, 2016.

- Kurihara D., S. Matsunaga, T. Omura, T. Higashiyama, and K. Fukui, “Identification and characterization of plant Haspin kinase as a histone H3 threonine kinase.,” *BMC Plant Biol.*, vol. 11, no. 1, p. 73, 2011.

- Lampson M. A., K. Renduchitala, A. Khodjakov, and T. M. Kapoor, “Correcting improper chromosome-spindle attachments during cell division.,” *Nat. Cell Biol.*, vol. 6, no. 3, pp. 232–7, 2004.

- Lan W., X. Zhang, S. L. Kline-Smith, S. E. Rosasco, G. A. Barrett-Wilt, J. Shabanowitz, D. F. Hunt, C. E. Walczak, and P. T. Stukenberg, “Aurora B phosphorylates centromeric MCAK and regulates its localization and microtubule depolymerization activity.,” *Curr. Biol.*, vol. 14, no. 4, pp. 273–86, 2004.

- Lawson N. D. and S. A. Wolfe, “Forward and Reverse Genetic Approaches for the Analysis of Vertebrate Development in the Zebrafish,” *Dev. Cell*, vol. 21, no. 1, pp. 48–64, 2011.

- Lesch B. J. and D. C. Page, “Genetics of germ cell development.,” *Nat. Rev. Genet.*, vol. 13, no. 11, pp. 781–94, 2012.

- Ma A. C. H., M. I. S. Chung, R. Liang, and A. Y. H. Leung, “The role of survivin2 in primitive hematopoiesis during zebrafish development.,” *Leukemia*, vol. 23, no. 4, pp. 712–20, 2009.

- Ma A. C. H., R. Lin, P.-K. Chan, J. C. K. Leung, L. Y. Y. Chan, A. Meng, C. M. Verfaillie, R. Liang, and A. Y. H. Leung, “The role of survivin in angiogenesis during zebrafish embryonic development.,” *BMC Dev. Biol.*, vol. 7, p. 50, 2007.

- Maiolica A., M. de Medina-Redondo, E. M. Schoof, A. Chaikuad, F. Villa, M. Gatti, S. Jeganathan, H. J. Lou, K. Novy, S. Hauri, U. H. Toprak, F. Herzog, P. Meraldi, L. Penengo, B. E. Turk, S. Knapp, R. Linding, and R. Aebersold, “Modulation of the chromatin phosphoproteome by the Haspin protein kinase.,” *Mol. Cell. Proteomics*, vol. 13, no. 7, pp. 1724–40, 2014.

- Markaki Y., A. Christogianni, A. S. Politou, and S. D. Georgatos, “Phosphorylation of histone H3 at Thr3 is part of a combinatorial pattern that marks and configures mitotic chromatin.,” *J. Cell Sci.*, vol. 122, no. Pt 16, pp. 2809–19, 2009.

- Monier K., S. Mouradian, and K. F. Sullivan, “DNA methylation promotes Aurora-B-driven phosphorylation of histone H3 in chromosomal subdomains.,” *J. Cell Sci.*, vol. 120, no. Pt 1, pp. 101–14, 2007.

- Moutinho-santos T. and H. Maiato, “Plk1 puts a (Has)pin on the mitotic histone code” *EMBO reports,* vol. 15, no. 3, pp. 203–204, 2014.

- Nair S., F. Marlow, E. Abrams, L. Kapp, M. C. Mullins, and F. Pelegri, “The chromosomal passenger protein birc5b organizes microfilaments and germ plasm in the zebrafish embryo.,” *PLoS Genet.*, vol. 9, no. 4, p. e1003448, 2013.

- Nasevicius A. and S. C. Ekker, “Effective targeted gene ‘knockdown’ in zebrafish.,” *Nat. Genet.*, vol. 26, no. 2, pp. 216–20, 2000.

- Nespoli A., R. Vercillo, L. Di Nola, L. Diani, M. Giannattasio, P. Plevani, and M. Muzi-Falconi, “Alk1 and Alk2 are two new cell cycle-regulated haspin-like proteins in budding yeast,” *Cell Cycle*, vol. 5, no. 13, pp. 1464–1471, 2006.

- Nguyen A. L., A. S. Gentilello, A. Z. Balboula, V. Shrivastava, J. Ohring, and K. Schindler, “Phosphorylation of threonine 3 on histone H3 by haspin kinase is required for meiosis I in mouse oocytes.,” *J. Cell Sci.*, vol. 127, no. 23, pp. 5066–78, 2014.

- Niedzialkowska E., F. Wang, P. J. Porebski, W. Minor, J. M. G. Higgins, and P. T. Stukenberg, “Molecular basis for phosphospecific recognition of histone H3 tails by Survivin paralogues at inner centromeres.,” *Mol. Biol. Cell*, vol. 23, no. 8, pp. 1457–66, 2012.

- Ohi R., T. Sapra, J. Howard, and T. J. Mitchison, “Differentiation of cytoplasmic and meiotic spindle assembly MCAK functions by Aurora B-dependent phosphorylation.,” *Mol. Biol. Cell*, vol. 15, no. 6, pp. 2895–906, 2004.

- Panigada D., P. Grianti, A. Nespoli, G. Rotondo, D. GalloCastro, R. Quadri, S. Piatti, P. Plevani, and M. Muzi-Falconi, “Yeast haspin kinase regulates polarity cues necessary for mitotic spindle positioning and is required to tolerate mitotic arrest,” *Dev. Cell*, vol. 26, no. 5, pp. 483–495, 2013.

- Petersen J. and I. M. Hagan, “S. pombe aurora kinase/survivin is required for chromosome condensation and the spindle checkpoint attachment response.,” *Curr. Biol.*, vol. 13, no. 7, pp. 590–7, 2003.

- Quyn A. J., P. L. Appleton, F. A. Carey, R. J. C. Steele, N. Barker, H. Clevers, R. A. Ridgway, O. J. Sansom, and I. S. Näthke, “Spindle orientation bias in gut epithelial stem cell compartments is lost in precancerous tissue.,” *Cell Stem Cell*, vol. 6, no. 2, pp. 175–81, 2010.

- Robu M. E., J. D. Larson, A. Nasevicius, S. Beiraghi, C. Brenner, S. A. Farber, and S. C. Ekker, “P53 Activation By Knockdown Technologies,” *PLoS Genet.*, vol. 3, no. 5, pp. 787–801, 2007.

- Ruchaud S., M. Carmena, and W. C. Earnshaw, “Chromosomal passengers: conducting cell division.,” *Nat. Rev. Mol. Cell Biol.*, vol. 8, no. 10, pp. 798–812, 2007.

- Schulte-Merker S. and D. Y. R. Stainier, “Out with the old, in with the new: reassessing morpholino knockdowns in light of genome editing technology,” *Development*, vol. 141, pp. 3103–3104, 2014.

- Seervai R. N. H. and G. M. Wessel, “Lessons for inductive germline determination.,” *Mol. Reprod. Dev.*, vol. 80, no. 8, pp. 590–609, 2013.

- Sessa F., M. Mapelli, C. Ciferri, C. Tarricone, L. B. Areces, T. R. Schneider, P. T. Stukenberg, and A. Musacchio, “Mechanism of Aurora B activation by INCENP and inhibition by hesperadin.,” *Mol. Cell*, vol. 18, no. 3, pp. 379–91, 2005.

- Siller K. H. and C. Q. Doe, “Spindle orientation during asymmetric cell division.,” *Nat. Cell Biol.*, vol. 11, no. 4, pp. 365–74, 2009.

- Sims R. J. and D. Reinberg, “Is there a code embedded in proteins that is based on post-translational modifications?,” *Nat. Rev. Mol. Cell Biol.*, vol. 9, no. 10, pp. 815–820, 2008.

- Tanaka H., Y. Yoshimura, M. Nozaki, K. Yomogida, J. Tsuchida, Y. Tosaka, T. Habu, T. Nakanishi, M. Okada, H. Nojima, and Y. Nishimune, “Identification and characterization of a haploid germ cell-specific nuclear protein kinase (Haspin) in spermatid nuclei and its effects on somatic cells,” *J. Biol. Chem.*, vol. 274, no. 24, pp. 17049–17057, 1999.

- Tanaka H., Y. Yoshimura, Y. Nishina, M. Nozaki, H. Nojima, and Y. Nishimune, “Isolation and characterization of cDNA clones specifically expressed in testicular germ cells.,” *FEBS Lett.*, vol. 355, no. 1, pp. 4–10, 1994.

- Thisse B. and C. Thisse, “In situ hybridization on whole-mount zebrafish embryos and young larvae,” *Methods Mol. Biol.*, vol. 1211, pp. 53–67, 2014.

- Uren A. G., L. Wong, M. Pakusch, K. J. Fowler, F. J. Burrows, D. L. Vaux, and K. H. Choo, “Survivin and the inner centromere protein INCENP show similar cell-cycle localization and gene knockout phenotype.,” *Curr. Biol.*, vol. 10, no. 21, pp. 1319–28, 2000.

- Venkateswarlu K., K. G. Brandom, and H. Yun, “PI-3-kinase-dependent membrane recruitment of centaurin-alpha2 is essential for its effect on ARF6-mediated actin cytoskeleton reorganisation.,” *J. Cell Sci.*, vol. 120, no. Pt 5, pp. 792–801, 2007.

- Venturin M., A. Bentivegna, R. Moroni, L. Larizza, and P. Riva, “Evidence by expression analysis of candidate genes for congenital heart defects in the

NF1 microdeletion interval.," *Ann. Hum. Genet.*, vol. 69, no. Pt 5, pp. 508–16, 2005.

- Venturin M., P. Guarnieri, F. Natacci, M. Stabile, R. Tenconi, M. Clementi, C. Hernandez, P. Thompson, M. Upadhyaya, L. Larizza, and P. Riva, "Mental retardation and cardiovascular malformations in NF1 microdeleted patients point to candidate genes in 17q11.2." *J. Med. Genet.*, vol. 41, no. 1, pp. 35–41, 2004.

- Villa F., P. Capasso, M. Tortorici, F. Forneris, A. de Marco, A. Mattevi, and A. Musacchio, "Crystal structure of the catalytic domain of Haspin, an atypical kinase implicated in chromatin organization" *Proc. Natl. Acad. Sci.*, vol. 106, no. 48, pp. 20204–20209, 2009.

- Wang F., J. Dai, J. R. Daum, E. Niedzialkowska, B. Banerjee, P. T. Stukenberg, G. J. Gorbsky, and J. M. G. Higgins, "Histone H3 Thr-3 phosphorylation by Haspin positions Aurora B at centromeres in mitosis.," *Science*, vol. 330, no. 6001, pp. 231–5, 2010.

- Wang F., N. P. Ulyanova, M. S. van der Waal, D. Patnaik, S. M. A. Lens, and J. M. G. Higgins, "A positive feedback loop involving Haspin and Aurora B promotes CPC accumulation at centromeres in mitosis.," *Curr. Biol.*, vol. 21, no. 12, pp. 1061–9, 2011.

- Wang Q., H. Wei, J. Du, Y. Cao, N. Zhang, X. Liu, X. Liu, D. Chen, and W. Ma, "H3 Thr3 Phosphorylation Is Crucial for Meiotic Resumption and Anaphase Onset in Oocyte Meiosis," *Cell Cycle*, vol. 15, no. 2, pp. 213-224, 2016.

- Weinstein B. M., D. L. Stemple, W. Driever, and M. C. Fishman, "Gridlock, a localized heritable vascular patterning defect in the zebrafish.," *Nat. Med.*, vol. 1, no. 11, pp. 1143–7, 1995.

- Westerfield M. "The Zebrafish book". *Eugene, OR: University of Oregon Press*., 1995.

- Wodarz A. and I. Näthke, "Cell polarity in development and cancer.," *Nat. Cell Biol.*, vol. 9, no. 9, pp. 1016–24, 2007.

- Xie J., M. Wooten, V. Tran, B. C. Chen, C. Pozmanter, C. Simbolon, E. Betzig, and X. Chen, "Histone H3 Threonine Phosphorylation Regulates Asymmetric Histone Inheritance in the Drosophila Male Germline," *Cell*, vol. 163, no. 4, pp. 920–933, 2015.

- Yabe T., X. Ge, R. Lindeman, S. Nair, G. Runke, M. C. Mullins, and F. Pelegri, "The maternal-effect gene cellular island encodes aurora B kinase and is essential for furrow formation in the early zebrafish embryo.," *PLoS Genet.*, vol. 5, no. 6, p. e1000518, 2009.

- Yamagishi Y., T. Honda, Y. Tanno, and Y. Watanabe, “Two histone marks establish the inner centromere and chromosome bi-orientation.,” *Science*, vol. 330, no. 6001, pp. 239–43, 2010.

- Yamanaka Y., T. Heike, T. Kumada, M. Shibata, Y. Takaoka, A. Kitano, K. Shiraishi, T. Kato, M. Nagato, K. Okawa, K. Furushima, K. Nakao, Y. Nakamura, M. M. Taketo, S. Aizawa, and T. Nakahata, “Loss of Borealin/DasraB leads to defective cell proliferation, p53 accumulation and early embryonic lethality.,” *Mech. Dev.*, vol. 125, no. 5–6, pp. 441–50, 2008.

- Zhou L., X. Tian, C. Zhu, F. Wang, and J. M. Higgins, “Polo-like kinase-1 triggers Histone phosphorylation by Haspin in mitosis,” *EMBO Rep.*, vol. 15, no. 3, pp. 273–281, 2014.

ACKNOWLEDGEMENTS

I wish to thank my PhD supervisor Prof. Paolo Plevani, together with Prof. Marco Muzi Falconi from the yeast group at the University of Milan, and Prof. Franco Cotelli from the zebrafish unit, for their support and mentorship.
I wish to thank Dr. Gianfranco Bellipanni for his essential help and supervision during the mutant line generation, and not only, and the Sbarro Institute directed by Prof. Antonio Giordano in Philadelphia for hosting me.
A special acknowledgement goes to my lab colleagues at the University of Milan for their continuous and fundamental help.

PART II – Published Paper

JMG Online First, published on April 7, 2014 as 10.1136/jmedgenet-2013-102240

ORIGINAL ARTICLE

ADAP2 in heart development: a candidate gene for the occurrence of cardiovascular malformations in NF1 microdeletion syndrome

Marco Venturin,[1] Silvia Carra,[2] Germano Gaudenzi,[2] Silvia Brunelli,[3] Guido Roberto Gallo,[2] Silvia Moncini,[1] Franco Cotelli,[2] Paola Riva[1]

ABSTRACT

Background Cardiovascular malformations have a higher incidence in patients with NF1 microdeletion syndrome compared to NF1 patients with intragenic mutation, presumably owing to haploinsufficiency of one or more genes included in the deletion interval and involved in heart development. In order to identify which genes could be responsible for cardiovascular malformations in the deleted patients, we carried out expression studies in mouse embryos and functional studies in zebrafish.

Methods and results The expression analysis of three candidate genes included in the NF1 deletion interval, *ADAP2*, *SUZ12* and *UTP6*, performed by in situ hybridisation, showed the expression of *ADAP2* murine ortholog in heart during fundamental phases of cardiac morphogenesis. In order to investigate the role of *ADAP2* in cardiac development, we performed loss-of-function experiments of zebrafish *ADAP2* ortholog, *adap2*, by injecting two different morpholino oligos (*adap2*-MO and UTR-*adap2*-MO). *adap2*-MOs-injected embryos (morphants) displayed in vivo circulatory and heart shape defects. The molecular characterisation of morphants with cardiac specific markers showed that the injection of *adap2*-MOs causes defects in heart jogging and looping. Additionally, morphological and molecular analysis of *adap2* morphants demonstrated that the loss of *adap2* function leads to defective valvulogenesis, suggesting a correlation between *ADAP2* haploinsufficiency and the occurrence of valve defects in NF1-microdeleted patients.

Conclusions Overall, our findings indicate that *ADAP2* has a role in heart development, and might be a reliable candidate gene for the occurrence of cardiovascular malformations in patients with NF1 microdeletion and, more generally, for the occurrence of a subset of congenital heart defects.

INTRODUCTION

NF1 microdeletion syndrome (MIM 613675) is a rare disorder caused by the haploinsufficiency of *NF1* and contiguous genes. NF1-microdeleted patients carry a heterozygous deletion of 17q11.2 region typically spanning about 1–1.4 Mb.[1 2] NF1 microdeletion syndrome is often characterised by a more severe phenotype compared to the one observed in NF1 with intragenic mutation.[3] Comparing the clinical phenotype between NF1-microdeleted patients and the whole NF1 population, we found that cardiovascular malformations (CVM) are significantly more frequent in NF1 patients with microdeletion syndrome than in those with neurofibromatosis caused by intragenic mutation.[4] The CMVs found in the NF1-deleted patients include pulmonic stenosis, atrial/ventricular septal defects and valve defects, and show an incidence of 18% versus 2.1% displayed by NF1 patients with intragenic mutation.[4 5]

The higher incidence of CVMs in NF1-microdeleted patients is most likely dependent on the haploinsufficiency of genes lying in the deletion interval, presumably involved in heart morphogenesis. Our previous search for candidate genes by northern blotting and RT-PCR analysis evidenced that three genes encompassed by NF1 microdeletion, *SUZ12*, *ADAP2* (formerly *CENTA2*) and *UTP6* (formerly *C17ORF40*) are highly expressed in human fetal heart and during the early developmental stages of mouse embryonic heart,[6] thus deserving further analysis.

SUZ12 (*Suppressor of Zeste 12 Homolog (Drosophila)*) is the human ortholog of the Drosophila *Su(z)12* polycomb gene, encoding a protein which is implicated in developmental mechanisms in Drosophila.[7] Mice lacking *Suz12* are not viable and die around 7.5 days post-coitum (dpc), displaying severe developmental and proliferative defects.[8]

ADAP2 (*ArfGAP with Dual PH domains 2*) encodes a protein named Centaurin-α-2, which belongs to the centaurins protein family. Centaurin-α-2 is recruited to the plasma membrane where it specifically regulates actin cytoskeleton remodelling via ARF6, indicating an important role in exocytosis and cell motility.[9] Moreover, it was recently shown to interact with microtubules and to increase their stability.[10]

UTP6 (*small subunit (SSU) processome component, homologue (yeast)*) is the human homologue of yeast *SSU processome component*. The *UTP6* gene is essential for efficient pre-rRNA processing[11] and seems to be involved in the positive regulation of apoptosis.[12]

Here, we investigated the spatio-temporal expression profile of *ADAP2*, *SUZ12* and *UTP6* murine orthologs during mouse embryonic and fetal development by in situ hybridisation. Based on this analysis, we held *ADAP2* the most interesting candidate gene for CVMs occurrence and used zebrafish as a model organism to investigate in vivo the role of *adap2*, the *ADAP2* zebrafish ortholog, during vertebrate heart development by loss-of-function experiments.

▸ Additional material is published online only. To view please visit the journal online (http://dx.doi.org/10.1136/jmedgenet-2013-102240).

[1]Dipartimento di Biotecnologie Mediche e Medicina Traslazionale, Università degli Studi di Milano, Milan, Italy
[2]Dipartimento di Bioscienze, Università degli Studi di Milano, Milan, Italy
[3]Dipartimento di Scienze della Salute, Università degli Studi di Milano-Bicocca, Monza (MB), Italy

Correspondence to
Dr Marco Venturin, Dipartimento di Biotecnologie Mediche e Medicina Traslazionale, Università degli Studi di Milano; Via Viotti 3/5, Milan 20133, Italy; marco.venturin@unimi.it
Dr Paola Riva, Dipartimento di Biotecnologie Mediche e Medicina Traslazionale, Università degli Studi di Milano; Via Viotti 3/5 Milan 20133, Italy; paola.riva@unimi.it

MV, SC, GG, FC and PR contributed equally to this study.

Received 19 December 2013
Revised 7 March 2014
Accepted 10 March 2014

To cite: Venturin M, Carra S, Gaudenzi G, *et al*. *J Med Genet* Published Online First: [*please include* Day Month Year] doi:10.1136/jmedgenet-2013-102240

RESULTS

Expression analysis of *Suz12*, *Utp6* and *Adap2* genes in mouse reveals that *Adap2* is expressed during key stages of heart development

In order to elucidate the expression pattern of *Suz12*, *Utp6* and *Adap2* genes in mouse, we performed in situ hybridisations using whole mounts at different stages of development, ranging from 7.5 to 11.5 dpc.

The gene which revealed the most interesting expression pattern was *Adap2*, since it was visible in heart between 9 and 10.5 dpc (figure 1) during fundamental phases of cardiac morphogenesis, namely heart looping (beginning at 8 dpc), endocardial cushion formation (10 dpc), and septation of the outflow tract, atria, and ventricles (10.5 dpc). In particular, the strongest *Adap2* mRNA hybridisation signal was seen in the heart atria and ventricles at 9.5 dpc (figure 1E), but its expression in the heart was visible as of 9 dpc (figure 1C) and was still present in the atria and ventricles at 10.5 dpc (figure 1F). We also performed in situ hybridisations on cryosections of 15.5 dpc embryos in order to assess if *Adap2* transcript is also present in the heart during the later stages of fetal cardiac development. Our experiments demonstrated that the expression of *Adap2* in the heart continues to be maintained at least until 15.5 dpc, in the ventricles and atria (figure 1H).

Conversely, *Suz12* evidenced a more spatially and temporally restricted expression in heart, with a clear hybridisation signal only at 10.5 dpc in the atrium, while *Utp6* revealed no expression in heart at any analysed stages (see online supplementary figure S1).

Based on this evidence, we held *ADAP2* the most interesting candidate gene for CVMs occurrence, and we used zebrafish as a model organism to investigate in vivo its role during vertebrate heart development.

adap2, the *ADAP2* zebrafish ortholog, is required for proper cardiac morphogenesis

In order to explore the spatio-temporal expression pattern of *adap2*, the *ADAP2* zebrafish ortholog (Ensembl Gene ID: ENSDARG00000070565), we performed RT-PCR and whole-mount in situ hybridisation assays. *adap2* transcript was detected by RT-PCR at all analysed stages, from cleavage up to 120 hpf (hours post-fertilisation), as well as in the oocytes, indicating that the gene is maternally and zygotically expressed. Furthermore, *adap2* mRNA was present in all analysed adult tissues, including heart (see online supplementary figure S2). Whole-mount in situ hybridisation (WISH) revealed that *adap2* transcript was present in the heart at 2 dpf (days post-fertilisation) and 3 dpf stages, in the region corresponding to bulbus arteriosus (see online supplementary figure S2).

In order to investigate the potential role of *adap2* during zebrafish heart development in vivo, we performed loss-of-function experiments by injecting two independent translation-blocking morpholinos (*adap2*-MO and UTR-*adap2*-MO) which target the region surrounding *adap2* translation start codon and the 5′-UTR region, respectively. The injection of a control morpholino (std-MO) with no targets in zebrafish was used as control of the microinjection. At 2 dpf, most of embryos injected with 0.3 pmol of *adap2*-MO (morphants), unlike std-MO injected embryos, displayed blood circulation defects and curved tail (figure 2). Lower doses caused no circulatory defects. For the analysis of injected embryos, we focused our attention on 2 dpf, stage at which the circulation is surely started and the cardiac looping occurred in control embryos. At this stage, 61% (n=94) of embryos injected with 0.3 pmol/embryo of *adap2*-MO showed one or more blood circulatory defects, such as the total loss of circulation (21%), accumulation of blood cells in the trunk and/or tail region (48%) and blood stases in the head (13%) (figure 2D–F,G). All these circulatory defects were noticed in both *adap2* morphants which showed a body axis comparable with that of control embryos and morphants which displayed a bent tail phenotype (71%, n=94). The injection of the second translation-blocking MO, UTR-*adap2*-MO, caused in vivo qualitatively similar defects to the first injected MO, though with a different penetrance (see online supplementary figure S3).

To rule out that circulation defects could be caused by alterations of vascular development, we carried out *adap2* loss-of-function experiments in the tg(*flk1*:EGFP) zebrafish transgenic line,[13] where EGFP expression is controlled by the endothelial-specific *flk1* promoter (see online supplementary figures S4 and S5). At 2 dpf, *adap2* knocked-down embryos revealed no gross defects in vascular development, with correct development of main axial vessels, dorsal aorta (DA) and cardinal vein (CV), indicating a normal vasculogenesis. Weak defects in intersomitic vessels (Se) were observed only in those embryos with a marked curved tail, suggesting that these alterations were likely caused by structural defects of body axis rather than by angiogenesis abnormalities.

The evidence that two independent morpholinos gave the same in vivo phenotypes confirmed the specificity of the *adap2* morpholinos. Consequently, we present here data obtained on embryos injected with the *adap2*-MO, which we indicate as *adap2* morphants.

The evidence that circulatory defects in *adap2* morphants were not caused by vascular defects suggested that they were most likely derived from an abnormal heart development and functionality. To test this hypothesis, we injected *adap2*-MO or std-MO in embryos belonging to the tg(*gata1*:dsRed)^{sd2};tg(*flk1*:EGFP)^{S843} double transgenic line,[14] in which erythrocytes are labelled in red and endothelial cells are labelled in green; we observed the injected embryos under a confocal microscope (figure 3). At 2 dpf, control embryos displayed a normal heart morphology (figure 3A), while *adap2* morphants showed a reduction of atrioventricular (AV) canal bending, a partial lack of atrium and ventricle separation, as well as a reduced ventricle size (figure 3B,C). All analysed embryos displayed blood circulation.

The in vivo analysis of *adap2* phenotype in morphants prompted us to investigate their heart morphology by a molecular approach, through whole-mount in situ hybridisation assays with the cardiac-specific marker *cmlc2* (*cardiac myosin light chain 2*) (figure 4, see online supplementary tables S1 and S2). At 26 hpf, std-MO-injected embryos showed the linear cardiac tube correctly positioned ventrally in the left region of the embryo (left jog) (figure 4A). On the contrary, only 39% (n=59) of *adap2*-MO-injected embryos displayed, at the same stage, the correct leftward cardiac jogging (figure 4B), while another 39% showed no jog, with the heart tube situated centrally along the midline of the embryo (figure 4C). Finally, the remaining 22% of *adap2* morphants was characterised by an inverted cardiac jogging (right jog) (figure 4D). At 2 dpf, std-MO-injected embryos hybridised with the *cmlc2*-specific probe presented a normal S-shaped heart with the ventricle positioned on the right of the atrium, indicating a correct D-looping process (figure 4E). Differently, only 22% (n=49) of *adap2* morphants showed a heart morphology comparable to control embryos (figure 4F). The remaining *adap2*-injected

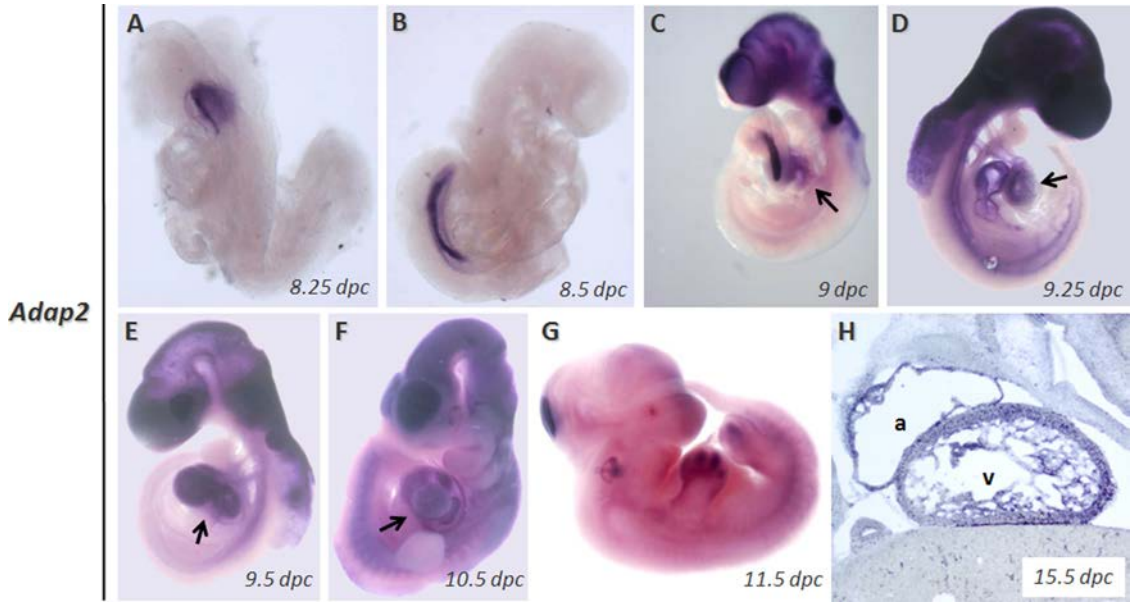

Figure 1 Expression of *Adap2* in whole-mount mouse embryos and mouse cryosections. (A–G) Whole-mount in situ hybridisation on embryos from 8.25 dpc to 11.5 dpc with an *Adap2* specific probe. (A) 8.25 dpc, expression at the midbrain/hindbrain boundary. (B) 8.5 dpc, expression in the gut tube. (C) 9 dpc, expression in forebrain, midbrain, hindbrain, heart (arrow), otic vesicles, gut tube. (D) 9.25 dpc, expression in forebrain, midbrain, hindbrain, otic vesicles, heart (arrow), posterior part of the gut tube. (E) 9.5 dpc, expression in forebrain, midbrain, hindbrain, otic vesicles, heart (arrow), gut tube. (F) 10.5 dpc, expression in forebrain, midbrain, hindbrain, otic vesicles, heart (arrow), gut tube. (G) 11.5 dpc expression in midbrain, inner ear, forelimbs, weakly in hindlimbs. (H) In situ hybridisation on cryosection of a 15.5 dpc embryo showing *Adap2* expression in heart atrium (a) and ventricle (v).

embryos displayed either an intermediate phenotype with reduced looping (18%), or absence of looping with a completely linear heart tube (47%), or a reversed heart looping with the ventricle on the left of the atrium (12%) (figure 4G–I). Moreover, whole-mount in situ hybridisation assays with the ventricle-specific marker *vmhc (ventricular myosin heavy chain)* evidenced, at 2 dpf, a marked reduction of ventricle size in 64% (n=39) of *adap2* morphants, confirming the in vivo observations (see online supplementary figure S6). The reduction of ventricle size was observed regardless of the heart looping phenotype (D-loop, no loop or reversed loop). Notably, the percentage of embryos showing reduced ventricle size was similar in *adap2* morphants with or without blood circulation, 65% (n=29) and 60% (n=10) respectively, suggesting no relation between this defect and circulatory complications.

adap2 loss-of-function affects AV valve development

In order to shed light on the effect of *adap2* knockdown on cardiac functionality, we analysed AV valve formation in zebrafish by carrying out histological sections of AV valve in std-MO and *adap2*-MO-injected embryos at different developmental stages. At 3 dpf stage, control embryos displayed correctly formed endocardial cushions in the AV canal connecting the two cardiac chambers (figure 5A). The *adap2* morphants morphologically more similar to std-MO-injected embryos still showed proper heart morphology with normal endocardial cushions, the only evident defect being a mild reduction of ventricle size, as already evidenced (figure 5B). In *adap2*-injected embryos which in vivo showed an intermediate phenotype (bent tail and presence of blood circulation), a visible alteration of the endocardial cushions was observed, with a marked disorganisation of the cellular elements that will be forming the mature AV valve (figure 5C). Embryos with severe phenotype, that is, curved tail and absent circulation, showed serious alterations in the heart morphology, making impossible any consideration on endocardial cushion formation (figure 5D). The histological analysis of std-MO-injected embryos at 5 dpf evidenced a properly developed mature valve, recognisable as two flap-like structures in correspondence to the AV canal (figure 5E). At this stage, *adap2*-MO-injected embryos showing an in vivo mild phenotype were already characterised by evident defects of mature AV valve, whose cells resulted disorganised and poorly compact (figure 5F). The morphology of mature valves in morphants with curved phenotype and with blood circulation appeared more compromised, structurally disorganised, without the typical valvular shape and with cells irregularly disposed (figure 5G). Finally, the most affected *adap2* morphants showed severe cardiac malformations: the heart appeared essentially as a linear-shaped structure, without a clear separation between the two chambers, and consequently it was impossible to analyse mature cardiac valve conformation (figure 5H). Moreover, longitudinal histological sections of *adap2* morphants at 5 dpf evidenced an endocardial detachment from the myocardial layer notably in the atrial chamber (figure 5F,G).

To characterise at molecular level the cardiac AV valve defects displayed by embryos as a consequence of *adap2* functional inactivation, we analysed, by means of in situ hybridisation experiments, the expression pattern of two markers, *bmp4* (*bone morphogenetic protein 4*) and *notch1b* (*notch homolog 1b*), which at 2 dpf are specifically expressed within the myocardial and endocardial component of AV canal, respectively (figure 6A,E). At 2 dpf stage, 91% (n=46) of control embryos showed a *bmp4*-specific hybridisation signal precisely marking the myocardial component of AV canal, as expected (figure 6B). Differently, 51% (n=41) of *adap2*-MO-injected embryos displayed a disorganised and ectopically expanded *bmp4*-specific expression domain, notably as the ventricular chamber is concerned (figure 6C,D). These defects were observed in all the

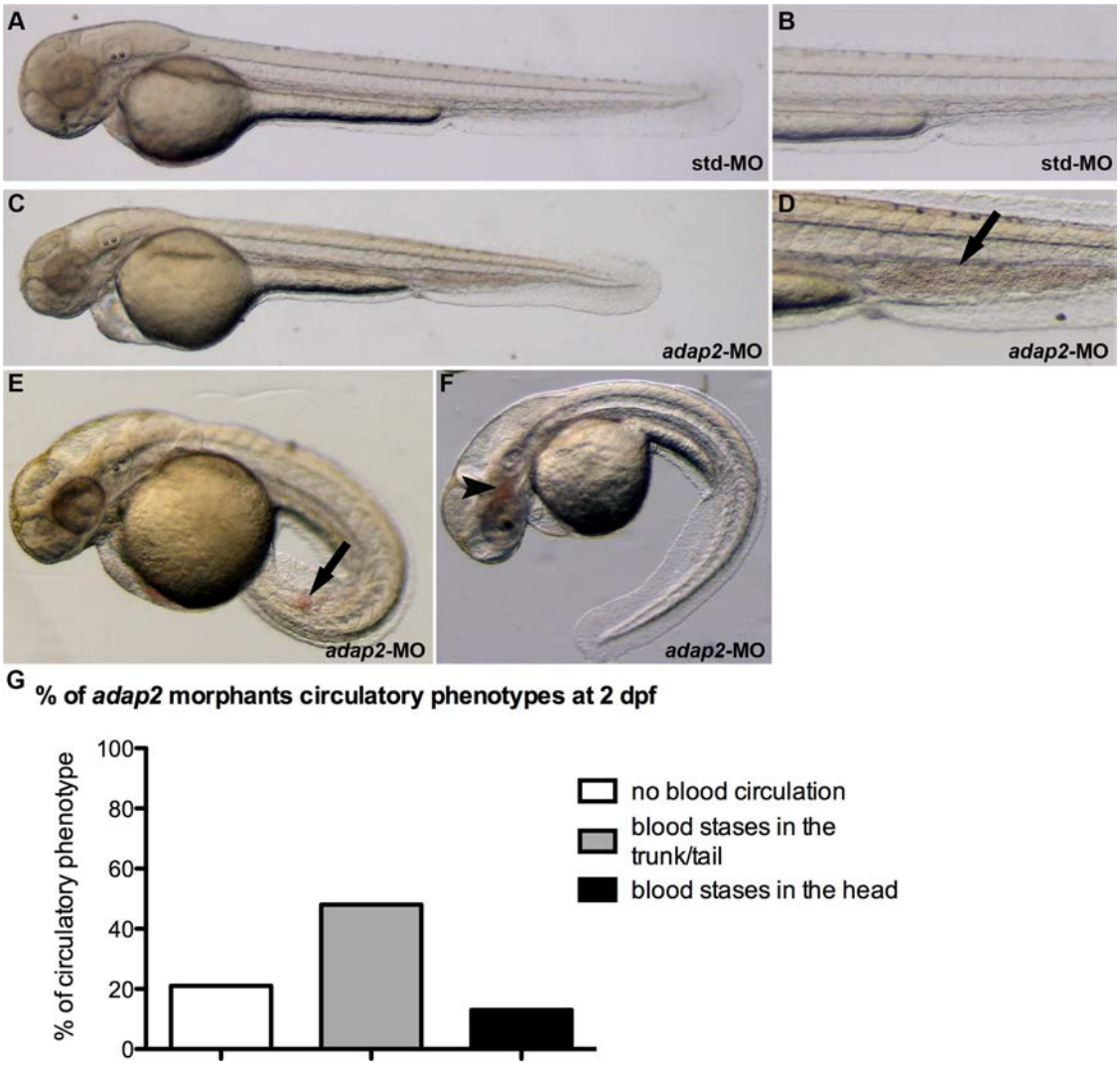

Figure 2 *adap2* knockdown causes circulation defects in zebrafish. (A) Lateral view and (B) detailed image of the trunk-tail region of std-MO-injected embryos at 2 dpf. (C, E and F) Lateral view and (D) detailed image of the trunk-tail region of *adap2*-MO-injected embryos at 2 dpf. Anterior to the left. Black arrows: blood stases in the tail region; arrowhead: blood stasis in the head. (G) Percentage of circulation defects in *adap2* morphants at 2 dpf (n=94): 21% of the *adap2* morphants displayed no blood circulation, 48% blood stases in the trunk-tail region and 13% blood stases in the cephalic region.

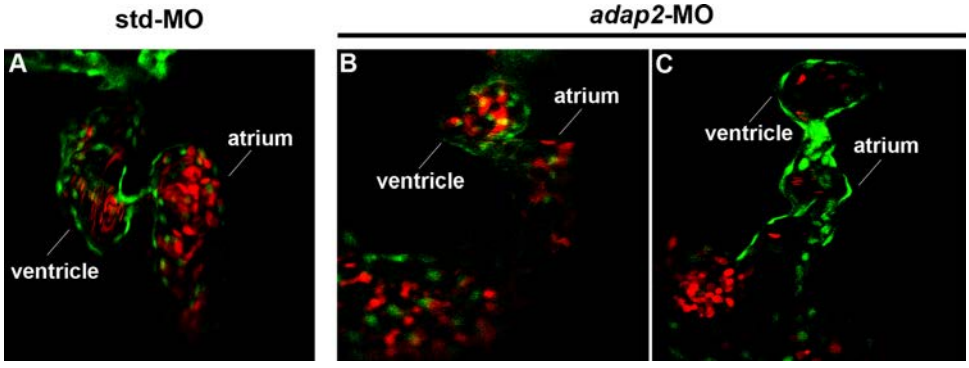

Figure 3 *adap2* loss-of-function affects normal heart morphogenesis in zebrafish. The hearts of double transgenic tg(*gata1*:dsRed)^{sd2};tg(*flk1*:EGFP)^{S843} embryos injected with std-MO or *adap2*-MO were examined in vivo by confocal microscopy at 2 dpf. Erythrocytes and endocardium are labelled in red and green, respectively. Confocal images of the heart in (A) std-MO-injected embryo, in (B) *adap2* morphant displaying normal morphology and in (C) *adap2*-MO-injected embryo with bent tail. All analysed embryos presented blood circulation.

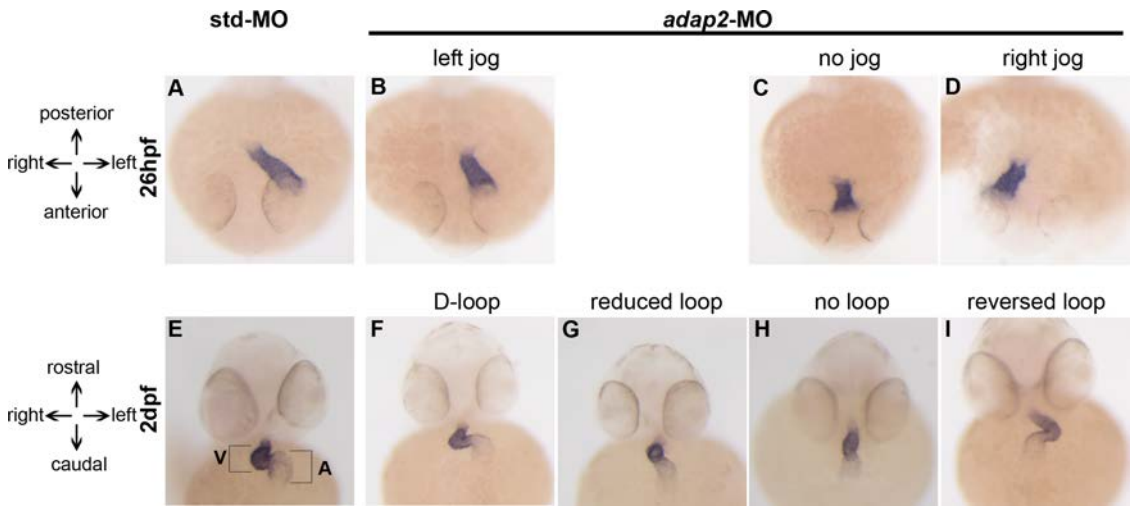

Figure 4 *adap2* loss-of-function experiments perturb zebrafish heart jogging and heart looping. Analysis of *cmlc2* expression by in situ hybridisation was performed on std-MO and *adap2*-MO-injected embryos at 26 hpf and 2 dpf. The heart position in injected embryos was scored as left jog (normal; A and B), no jog (C) and right (reversed) jog (D) at 26 hpf and as D-loop (normal; E and F), reduced loop (G), no loop (H) and reversed loop (I) at 2 dpf. V: ventricle; A: atrium. (A–D) Dorsal views through the head, anterior to the bottom; (E–I) frontal views, head to the top.

phenotypic classes of heart development. Similar results were obtained from the analysis of *notch1b* marker at the same stage, with 49% (n=43) of *adap2*-MO-injected embryos displaying an expanded and disorganised *notch1b* expression pattern (figure 6G,H). All these data highlight *adap2* function in fundamental processes of zebrafish cardiac morphogenesis, notably heart jogging, heart looping, determination of ventricular size and AV valve formation.

Overall, our findings provide compelling evidence that *ADAP2* is involved in heart development, pointing to it as the most plausible candidate gene for the occurrence of congenital CVMs in NF1 microdeletion syndrome and, more generally, for the occurrence of sporadic and familial congenital CVMs.

DISCUSSION

Microdeletion syndromes are a group of disorders characterised by the deletion of a chromosomal segment spanning multiple disease genes, each potentially contributing to the phenotype independently. Microdeletion syndromes are often characterised by a complex clinical and behavioural phenotype resulting from the imbalance of normal dosage of genes located in that particular chromosomal segment.[15]

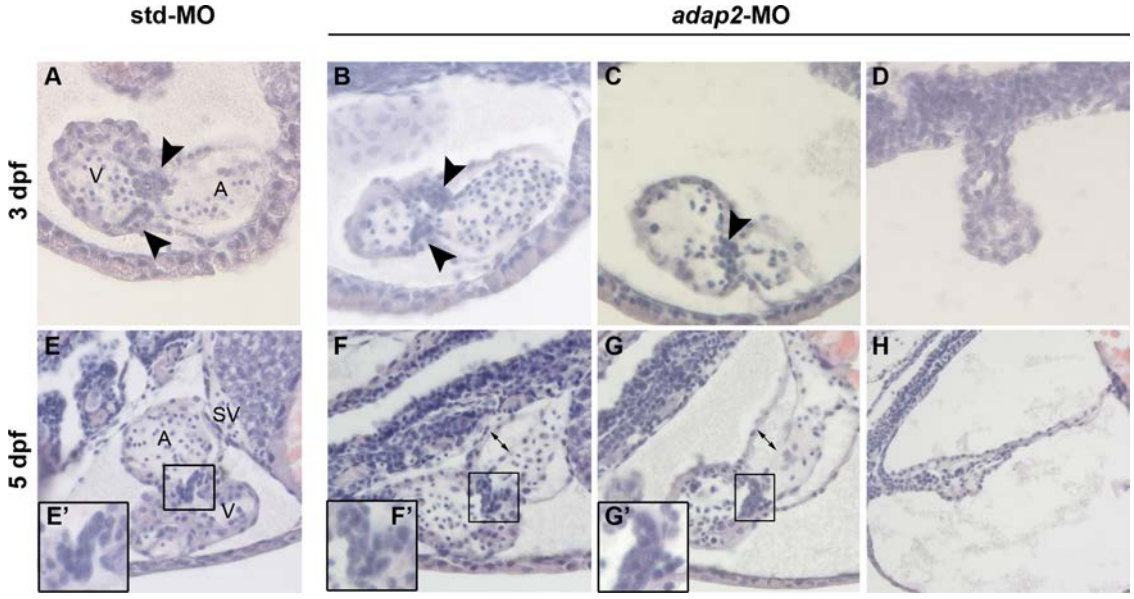

Figure 5 *adap2* knockdown impairs the normal endocardial cushions and mature valve formation. Histological sections of std-MO and *adap2*-MO-injected embryos at 3 dpf (transversal sections) and 5 dpf (longitudinal sections) stained with haematoxylin and eosin. (A and E) Heart sections of control embryos at 3 dpf (A) and 5 dpf, with magnification of the valve region (E). (B and F) Heart sections of *adap2* morphants with blood circulation and morphology comparable to controls at 3 dpf (B) and 5 dpf, with magnification of the valve region (F). (C and G) Heart sections of *adap2* morphants with blood circulation and bent tail at 3 dpf (C) and 5 dpf, with magnification of the valve region (G). (D and H) Heart sections of *adap2* morphants with no blood circulation and curved tail at 3 dpf (D) and 5 dpf, with magnification of the valve region (H). Arrowheads: endocardial cushions; double arrows: extracellular matrix (cardiac jelly) located between myocardium and endocardium.

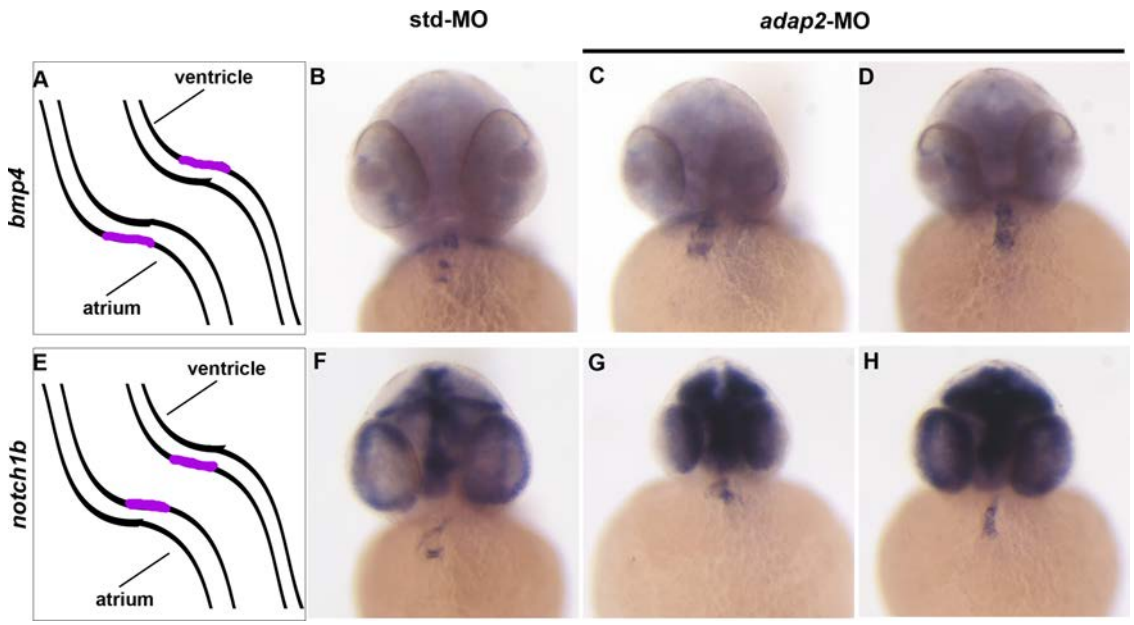

Figure 6 The expression of atrio-ventricular boundary markers is affected in *adap2* morphants. The analysis of *bmp4* and *notch1b* expression by in situ hybridisation was performed on std-MO and *adap2*-MO injected embryos at 2 dpf. (A and E) Schematic representation of *bmp4* and *notch1b* expression domain in zebrafish heart at 2 dpf. The myocardium and endocardium-specific territories of *bmp4* and *notch1b* expression are depicted in magenta. (B and F) Embryos injected with std-MO displaying a normal hybridisation signal. (C, D and G, H) Embryos injected with *adap2*-MO displaying expanded and disorganised *bmp4* and *notch1b* expression domains. Frontal views are shown.

NF1 microdeletion syndrome is caused by heterozygous deletions involving the *NF1* gene and, in the most common 1.4 Mb deletion, other 14 genes.[2] A more severe clinical phenotype has often been reported in NF1 patients carrying the microdeletion compared to patients with intragenic *NF1* mutations.[3] By reviewing the phenotype of 92 patients with NF1 microdeletion, we found that CVMs occurred at a significantly higher incidence in this patient population as compared to NF1 patients with intragenic mutations,[4] suggesting that the whole-gene deletion segment encompasses important genes involved in heart development. Subsequent expression studies indicated three possible candidate genes for CVMs that warranted further studies: *ADAP2* (formerly known as *CENTA2*), *SUZ12* and *UTP6* (previously called *C17ORF40*).[6]

Here, we analysed the spatio-temporal expression profile of the above mentioned genes during mouse embryonic and fetal development. Based on this analysis, *Adap2* seems to be expressed in heart starting from 9 dpc, during key phases of cardiac development, that is when the heart tube is elongating and looping, and atrial and ventricular septa, as well as AV valves, are forming.[16] Moreover, *Adap2* expression in heart continues even in the later stages of development, at least until 15.5 dpc. Of note, *Adap2* expression is not restricted to a particular cardiac compartment or structure, but rather seems to localise in atria and ventricles. *Suz12* was also detected in heart during mouse development, but its expression seems to be restricted to a short period around 10.5 dpc and to the heart atria. Differently, *Utp6* showed no expression in the developing heart at all.

Since the expression of *ADAP2* mouse ortholog in heart during fundamental stages of cardiac morphogenesis was suggestive of a role in heart development, we studied the possible role of *ADAP2* in heart development by employing zebrafish as a model system. Over the recent years, zebrafish has proven to be a valid model for studying cardiovascular development. Despite its apparent simplicity, the zebrafish heart shares common structural, developmental and genetics features with avian and mammalian heart.[17–19] Additionally, because of their small size, embryos receive enough oxygen by passive diffusion from external medium to survive and continue to develop in a relatively normal fashion for several days even in the complete absence of blood circulation, allowing a detailed phenotypic analysis of animals with severe cardiovascular defects that would be lethal in other organisms.[20]

The functional inactivation of *adap2*, the *ADAP2* zebrafish ortholog, obtained by the injection of two MO oligos targeting different *adap2* mRNA regions (translation start site and 5′-UTR), caused the same circulatory defects, proving the specificity of the phenotypes. We also designed a splice-blocking MO, which was predicted to cause exon 2 skipping, and to produce an altered form of *adap2* transcript with the generation of a premature stop codon. However, the injection of this MO at different doses did not cause any evident phenotypic defects. RT-PCR analysis, performed to test the efficacy of the splice-blocking MO, showed that only a fraction of *adap2* mRNA was incorrectly spliced. Consequently, we reason that the partial expression of the wild-type protein could be enough to prevent the occurrence of the phenotypic defects. This evidence, along with the presence in the embryo of the maternal transcript, which is targeted only by translation-blocking MOs, might explain the absence of alterations following the injection of this MO.

Our molecular results suggested *adap2* involvement in the cardiac jogging process, the morphogenetic process in which the heart cone is displaced to the left with respect to the anterior-posterior axis, which is one of the first evident breaks in left-right symmetry of the primitive zebrafish heart tube.[21] Moreover, *adap2* also appeared fundamental for the subsequent D-looping process, the bend of the heart tube to the right, which, by 36 hpf leads to the typical S-shaped heart, with the ventricle positioned on the right of the atrium. This was supported by the high number of *adap2* morphants, which at 2 dpf, when D-looping is normally completed, showed a linear heart,

a reduced loop or a reversed loop, all defects ascribable to alterations of the heart bending taking place during the D-looping process.

Functional inactivation of *adap2* also evidenced its important role during AV valve morphogenesis, since the earliest stages of endocardial cushion formation. Our results strongly suggest that a defective valvulogenesis results in impaired cardiac functionality, therefore, AV valve morphological alterations are most likely accounting for the in vivo blood circulation defects displayed by *adap2* morphants. Valve defects, including mitral valve prolapse, pulmonary valve stenosis and aortic valve anomalies, constitute a significant proportion of CVMs observed in patients with NF1 microdeletion syndrome.[3 4] Taking into account our findings on *ADAP2* role in valve morphogenesis, a correlation between *ADAP2* haploinsufficiency and the onset of valvular defects in NF1-microdeleted patients can be hypothesised. Additionally, the detachment between endocardium and myocardium observed in *adap2* morphants, particularly in the atrial chamber, could be caused by increased amounts of the extracellular matrix (cardiac jelly) juxtaposed between the two cardiac layers. Normal valve development involves multiple signalling pathways and extracellular matrix components take part in this process. Interestingly, dysregulation of components of the extracellular matrix seems to have a role in the myxomatous degeneration, the leaflet thickening and redundancy, typical of valvular abnormalities, such as mitral valve prolapse.[22]

ADAP2 is known to regulate microtubule stability[10] and the activity of ARF6, a GTPase involved in cellular motility, adhesion and polarity by regulating cytoskeleton remodelling and cortical actin formation.[9] The alteration of these functions might impair adhesion and migration properties of AV valve cells, explaining their disorganisation and the irregular valve architecture observed in *adap2* morphants.

During the early phases of valve morphogenesis, the myocardial component of AV junction is fundamental for the signalling events leading endocardial cells to begin the formation of cushions, which will be later remodelled to create flap-like valvular structures.[23] The marked alteration of *bmp4* myocardial expression in *adap2* morphants suggests a compromised signalling from myocardium to endocardium, which might result in the structural valve defects observed at 5 dpf.

Overall, our study points to *ADAP2* as a gene involved in heart development, and as a plausible candidate gene for the occurrence of CVMs in NF1-microdeleted patients and in the general population, constituting an advance towards a better comprehension of the complex phenotypic spectrum of the syndrome, as well as of the genetic basis of CVMs.

MATERIALS AND METHODS

Animals

The mice used were of the CD1 strain (Charles River Laboratories International) and were housed in the pathogen-free facility at the San Raffaele Scientific Institute (Milano, Italy). Zebrafish (*Danio rerio*) embryos, collected by natural spawning, were raised and maintained according to established techniques.[24] Embryos were staged according to Kimmel and colleagues,[25] and raised at 28°C in fish water (Instant Ocean, 0.1% Methylene Blue) in Petri dishes. Beginning from 24 hpf, embryos were cultured in fish water containing 0.003% PTU (1-phenyl-2-thiourea; SIGMA) to prevent pigmentation. The following lines were used: AB (obtained from the Wilson lab, University College London, London, UK); tg(*flk1*:EGFP)[13] (from the Stainier lab, University of California at San Francisco, USA), tg(*gata1*:dsRed)^{sd2}; tg(*flk1*:EGFP)S843 [14] (from the Santoro lab, Molecular Biotechnology Center, Università di Torino, Torino, Italy).

RT-PCR

RT-PCR was performed on total RNA extracted from oocytes, embryos (about 30 embryos per sample) at different developmental stages and adult organs using the TOTALLY RNA isolation kit (Ambion), treated with RQ1 RNase-Free DNase (Promega) and oligo(dT)-reverse transcribed using Super-Script II RT (Invitrogen), according to the manufacturer's instructions. The following primers were used for PCR reactions: adap2_fw 5′-GCTTAGACTTCTGGGATG-3′, adap2_rev 5′-CGAGATAA CGGTTTTCAAGGC-3′. PCR products were loaded and resolved onto 2% agarose gels.

In situ hybridisation

Probes were isolated by RT-PCR using specific primers (see online supplementary table S3) and cloned into the pCRII-TOPO vector (Invitrogen). Antisense and sense riboprobes were in vitro labelled with modified nucleotides (digoxigenin-UTP, Roche). WISH was performed on mouse embryos as described.[26] At least eight embryos per stage were analysed. Prehybridisation was performed in a formamide-tween20 solution, after which the DIG-labelled riboprobes were added to the embryos and incubated at 65°. In situ hybridisation on mouse cryostat sections was performed as described.[27]

WISH on zebrafish embryos was substantially carried out as described,[28] on embryos fixed for 2 h at room temperature in 4% paraformaldehyde/phosphate buffered saline, then rinsed with PBS-Tween, dehydrated in 100% methanol and stored at −20°C until processed for WISH.[29] A minimum of 20 embryos/time point were analysed.

The following probes were synthesised as described in the corresponding papers: *cmlc2* and *vmhc*,[30] *notch1b*[31] and *bmp4*.[32]

Images of stained embryos were taken with a Leica MZFLIII epifluorescence stereomicroscope equipped with a DFC 480 digital camera and IM50 Leica imaging software (Leica).

For histological sections, stained embryos were refixed in 4% paraformaldehyde, dehydrated, wax embedded, sectioned (8 µm) by a microtome (Leitz 1516) and stained with eosin. Images were taken with an Olympus BH2 microscope, equipped with a Leica DFC 320 digital camera and the IM50 software (Leica).

Morpholino injections and phenotype analysis

Antisense morpholinos (MOs; Gene Tools) were designed against the AUG translation start site region and the coding sequence, *adap2*-MO (5′-TTGTTCTTTTCCCGATTTGCCATAG-3′) and against the 5′-UTR region, UTR-*adap2*-MO (5′-AAAACACT CCTGTCGCGTCAGAATC-3′). As a control for unspecific effects, each experiment was performed in parallel with a std-MO (standard control oligo) with no target in zebrafish.

All morpholinos were diluted in Danieau solution[33] and injected at the 1–2-cells stage. Rhodamine dextran (Molecular Probes) was usually coinjected as a tracer. After injection, embryos were raised in fish water at 28°C and observed up to the stage of interest. For a better observation, the injected embryos were anaesthetised using 0.016% tricaine (Ethyl 3-aminobenzoate methanesulfonate salt, SIGMA) in fish water.

Images were acquired by using a Leica MZ FLIII epifluorescence microscope equipped with a Leica DCF 480 digital camera and the IM50 software (Leica). Confocal microscopy was performed with a Leica TCSNT confocal microscope equipped with an Ar/Kr laser (blocking filter BP 530/30 for EGFP and blocking filter LP 590 for ds Red).

For histological analysis 3 and 5 dpf zebrafish early larvae were fixed overnight at 4°C with bouin fixative. The samples were then dehydrated in a graded ethanol series, wax embedded, sectioned (8 μm) by a microtome (Leitz 1516) and stained with haematoxylin/eosin. Images were taken with a Leica DM6000 B microscope equipped with a Leica DCF480 digital camera and the LAS software.

Acknowledgements We thank U Fascio for his help in the acquisition of confocal images.

Contributors The study was conceived and designed by MV, SC, GG, PR, FC and SB. The experiments were carried out by MV, SC, GG, GRG and SM. The data were analysed by MV, SC, GG, PR, FC and SB. FC, PR and SB contributed reagents, materials and analysis tools. The paper was written and revised by MV, SC, GG, PR and FC.

Funding PR received an academic grant from Programma dell'Università per la Ricerca (PUR), University of Milan for this study.

Competing interests None.

Provenance and peer review Not commissioned; externally peer reviewed.

REFERENCES

1 Venturin M, Gervasini C, Orzan F, Bentivegna A, Corrado L, Colapietro P, Friso A, Tenconi R, Upadhyaya M, Larizza L, Riva P. Evidence for nonhomologous end joining and non allelic homologous recombination in atypical NF1 microdeletions. *Hum Genet* 2004;115:69–80.
2 Pasmant E, Sabbagh A, Spurlock G, Laurendeau I, Grillo E, Hamel MJ, Martin L, Barbarot S, Leheup B, Rodriguez D, Lacombe D, Dollfus H, Pasquier L, Isidor B, Ferkal S, Soulier J, Sanson M, Dieux-Coeslier A, Bièche I, Parfait B, Vidaud M, Wolkenstein P, Upadhyaya M, Vidaud D. NF1 microdeletions in neurofibromatosis type 1: from genotype to phenotype. *Hum Mutat* 2010;31:E1506–18.
3 Mautner VF, Kluwe L, Friedrich RE, Roehl AC, Bammert S, Högel J, Spöri H, Cooper DN, Kehrer-Sawatzki H. Clinical characterisation of 29 neurofibromatosis type-1 patients with molecularly ascertained 1.4 Mb type-1 NF1 deletions. *J Med Genet* 2010;47:623–30.
4 Venturin M, Guarnieri P, Natacci F, Stabile M, Tenconi R, Clementi M, Hernandez C, Thompson P, Upadhyaya M, Larizza L, Riva P. Mental retardation and cardiovascular malformations in NF1 microdeleted patients point to candidate genes in 17q11.2. *J Med Genet* 2004;41:35–41.
5 Lin AE, Birch PH, Korf BR, Tenconi R, Niimura M, Poyhonen M, Armfield Uhas K, Sigorini M, Virdis R, Romano C, Bonioli E, Wolkenstein P, Pivnick EK, Lawrence M, Friedman JM. Cardiovascular malformations and other cardiovascular abnormalities in neurofibromatosis 1. *Am J Med Genet* 2000;95:108–17.
6 Venturin M, Bentivegna A, Moroni R, Larizza L, Riva P. Evidence by expression analysis of candidate genes for congenital heart defects in the NF1 microdeletion interval. *Ann Hum Genet* 2005;69:508–16.
7 Kuzmichev A, Nishioka K, Erdjument-Bromage H, Tempst P, Reinberg D. Histone methyltransferase activity associated with a human multiprotein complex containing the Enhancer of Zeste protein. *Genes Dev* 2002;16:2893–905.
8 Pasini D, Bracken AP, Jensen MR, Lazzerini Denchi E, Helin K. Suz12 is essential for mouse development and for EZH2 histone methyltransferase activity. *EMBO J* 2004;23:4061–71.
9 Venkateswarlu K, Brandom KG, Yun H. PI-3-kinase-dependent membrane recruitment of centaurin-alpha2 is essential for its effect on ARF6-mediated actin cytoskeleton reorganisation. *J Cell Sci* 2007;120:792–801.
10 Zuccotti P, Cartelli D, Stroppi M, Pandini V, Venturin M, Aliverti A, Battaglioli E, Cappelletti G, Riva P. Centaurin-a2 Interacts with b-Tubulin and Stabilizes Microtubules. *PLoS ONE* 2012;7:e52867.
11 Champion EA, Lane BH, Jackrel ME, Regan L, Baserga SJ. A direct interaction between the Utp6 half-a-tetratricopeptide repeat domain and a specific peptide in Utp21 is essential for efficient pre-rRNA processing. *Mol Cell Biol* 2008;28:6547–56.
12 Piddubnyak V, Rigou P, Michel L, Rain JC, Geneste O, Wolkenstein P, Vidaud D, Hickman JA, Mauviel A, Poyet JL. Positive regulation of apoptosis by HCA66, a new Apaf-1 interacting protein, and its putative role in the physiopathology of NF1 microdeletion syndrome patients. *Cell Death Differ* 2007;14:1222–33.
13 Jin SW, Beis D, Mitchell T, Chen JN, Stainier DY. Cellular and molecular analyses of vascular tube and lumen formation in zebrafish. *Development* 2005;132:5199–209.
14 Santoro MM, Samuel T, Mitchell T, Reed JC, Stainier DY. Birc2 (clap1) regulates endothelial cell integrity and blood vessel homeostasis. *Nat Genet* 2007;39:1397–402.
15 Shaffer LG, Ledbetter DH, Lupski JR. Molecular cytogenetics of contiguous gene syndromes: Mechanisms and consequences. In: Scriver CR, Beaudet AL, Sly WS, Valle D, Childs B, Kinzler KW, Vogelstein B, eds. *The metabolic and molecular bases of inherited diseases*. New York: McGraw-Hill, 2001:6077–96.
16 Savolainen SM, Foley JF, Elmore SA. Histology atlas of the developing mouse heart with emphasis on E11.5 to E18.5. *Toxicol Pathol* 2009;37:395–414.
17 Weinstein BM, Fishman MC. Cardiovascular morphogenesis in zebrafish. *Cardiovas Res* 1996;31:E17–24.
18 Stainier DY, Fouquet B, Chen JN, Warren KS, Weinstein BM, Meiler SE, Mohideen MA, Neuhauss SC, Solnica-Krezel L, Schier AF, Zwartkruis F, Stemple DL, Malicki J, Driever W, Fishman MC. Mutations affecting the formation and function of the cardiovascular system in the zebrafish embryo. *Development* 1996;123:285–92.
19 Fishman MC, Stainier DY, Breitbart RE, Westerfield M. Zebrafish: Genetic and embryological methods in a transparent vertebrate embryo. *Meth Cell Biol* 1997;52:67–82.
20 Stainier DY, Fishman MC. Patterning the zebrafish heart tube: acquisition of anteroposterior polarity. *Dev Biol* 1992;153:91–101.
21 Chen JN, van Eeden FJ, Warren KS, Chin A, Nüsslein-Volhard C, Haffter P, Fishman MC. Left-right pattern of cardiac BMP4 may drive asymmetry of the heart in zebrafish. *Development* 1997;124:4373–82.
22 Hayek E, Gring GN, Griffin BP. Mitral valve prolapse. *Lancet* 2005;365:507–18.
23 Stainier DY. Zebrafish genetics and vertebrate heart formation. *Nat Rev Genet* 2001;2:39–48.
24 Westerfield M. *The Zebrafish Book*. Eugene, OR: University of Oregon Press, 1993.
25 Kimmel CB, Ballard WW, Kimmel SR, Ullmann B, Schilling TF. Stages of embryonic development of the zebrafish. *Dev Dyn* 1995;203:253–310.
26 Avilion AA, Bell DM, Lovell-Badge R. Micro-capillary tube in situ hybridisation: a novel method for processing small individual samples. *Genesis* 2000;27:76–80.
27 Strähle U, Blader P, Adam J, Ingham PW. A simple and efficient procedure for non-isotopic in situ hybridization to sectioned material. *Trends Genet* 1994;10:75–6.
28 Thisse C, Thisse B, Schilling TF, Postlethwait JH. Structure of the zebrafish snail1 gene and its expression in wild-type, spadetail and no tail mutant embryos. *Development* 1993;119:1203–15.
29 Jowett T, Lettice L. Whole-mount in situ hybridizations on zebrafish embryos using a mixture of digoxigenin- and fluorescein-labelled probes. *Trends Genet* 1994;10:73–4.
30 Yelon D, Horne SA, Stainier DY. Restricted expression of cardiac myosin genes reveals regulated aspects of heart tube assembly in zebrafish. *Dev Biol* 1999;214:23–37.
31 Westin J, Lardelli M. Three novel *Notch* genes in zebrafish: implications for vertebrate *Notch* gene evolution and function. *Dev Genes Evol* 1997;207:51–63.
32 Nikaido M, Tada M, Saji T, Ueno N. Conservation of BMP signaling in zebrafish mesoderm patterning. *Mech Dev* 1997;61:75–88.
33 Nasevicius A, Ekker SC. Effective targeted gene 'knockdown' in zebrafish. *Nat Genet* 2000;26:216–20.

ADAP2 in heart development: a candidate gene for the occurrence of cardiovascular malformations in NF1 microdeletion syndrome

Marco Venturin, Silvia Carra, Germano Gaudenzi, et al.

J Med Genet published online April 7, 2014
doi: 10.1136/jmedgenet-2013-102240

Notes

TABLES

Table S1: heart jogging defects in std-MO and *adap2*-MO injected embryos at 26 hpf as shown by *cmlc2* expression pattern analysis (Figure 4). n. = total number of injected embryos.

		Heart jog (%)			
Injected morpholino	**n.**	Left jog	No jog	Right jog	Total heart jogging defects
std-MO	53	98	2	0	2
adap2-MO	59	39	39	22	61

Table S2: heart looping defects in std-MO and adap2-MO injected embryos at 2 dpf as shown by cmlc2 expression pattern analysis (Figure 4). n. = total number of injected embryos.

		Heart loop (%)				
Injected morpholino	**n.**	D-loop	Reduced loop	No loop	Reversed loop	Total heart looping defects
std-MO	53	96	0	4	0	4
adap2-MO	49	22	18	47	12	77

Table S3: Primers Used to Generate the Probes for Whole-Mount *In Situ* Hybridization Experiments.

Name	**Sequence (5'-3')**	**Tm**
Adap2P_fw	CTCGTGCCTCTCATCACCAG	64°C
Adap2P_rev	CCAGTGTAGTCCAGGTTGTC	62°C
Suz12P_fw	AGCATAATGTCAATAGATAAAGC	60°C
Suz12P_rev	CATCTTCTGAATCTCCAACTG	60°C
Utp6P_fw	GCTCCAGGTGCTCATTGACTC	66°C
Utp6P_rev	GGTTGAGGCAGTCCATCCAC	64°C
adap2P_fw	CTTTCCAACTGCTAGTGATGTAG	66°C
adap2P_rev	CGCCAGACAGAGACAAGACTC	66°C

PART III

METHODS

ZEBRAFISH LINES AND MAINTENANCE

Zebrafish (*Danio rerio*) embryos were raised and maintained under standard conditions and national guidelines (Italian decree 4th March 2014, n.26). All experimental procedures were approved by IACUC (Institutional Animal Care and Use Committee).

Zebrafish AB wild-type strains were obtained from the Wilson lab, University College London, London, United Kingdom and the transgenic line tg(*islet1*:EGFP) was kindly provided by Dr. Deflorian (IFOM, Istituto FIRC di Oncologia Molecolare, Milan).

Regarding the generation of the mutant lines performed at Temple University, Philadelphia, PA (USA) at Dr. Gianfranco Bellipanni's lab, we used AB and Tubingen long-fin strains originally obtained from EkkWill Waterlife Resources (Gibbonston, FL, USA) and from ZIRC (Zebrafish International Resource Center; University of Oregon, Eugene, OR, USA). All procedures involving zebrafish were conducted in accordance with Institutional Animal Care and Use Committee (IACUC) policies.

Embryos were staged according to morphological criteria (Kimmel *et al.*, 1995) and embryonic ages are expressed in hours post-fertilization (hpf) and days post-fertilization (dpf).

ZEBRAFISH *haspin* ORTHOLOG IDENTIFICATION

The human *haspin* amino acid sequence was used as a query to identify *in silico* the zebrafish *haspin* gene. NCBI (http://www.ncbi.nlm.nih.gov/BLAST/), ClustalW (http://www.ebi.ac.uk/Tools/clustalw/) and SMART (http://smart.embl-heidelberg.de/) tools were used for basic handling and analysis of the nucleotide and protein sequences.

ZEBRAFISH *haspin* EXPRESSION ANALYSIS: RT-PCR AND *IN SITU* HYBRIDIZATION ASSAYS

Total RNA was isolated from embryos at different developmental stages and from different adult organs using the "SV Total RNA isolation System" (Promega, Madison, Wisconsin, USA).

After treatment with DNase I RNase-free (Roche, Basel, Switzerland) to avoid possible genomic contamination, 1 μg of RNA was reverse-transcribed using the "ImProm-II™ Reverse Transcription System" (Promega) and random primers according to the manufacturer's instructions.

According to the sequence information gained from bioinformatic analysis, we used different sets of primers for temporal expression analysis at different stages of development and in adult organs (see list of primers below) and performed cDNA amplification for detecting the expected bands using GoTaq polymerase (Promega), following the manufacturer's instructions. For a spatial expression pattern, we amplified a fragment of the zebrafish *haspin* coding sequence in order to use it as template to *in vitro* synthesize a RNA probe for *in situ* hybridization assays. We used GoTaq polymerase (Promega) following the manufacturer's instructions. Specific *gapdh* primers (see list of primers below) were used to check cDNA quality. For probe synthesis, we used as template an amplicon of 1166 base pairs, not including the conserved C-terminal kinase domain. Reaction products were analyzed by 1% agarose-gel electrophoresis. Amplicons were cloned in the pGEM-T vector system (Promega) according to manufacturer's instructions. These clones were then sent out for sequencing (Eurofins_Genomics-DNA sequencing service) and electropherograms were analyzed with ChromasPro software 1.42 (Technelysium Pty Ltd, Tewantin QLD, Australia) using the ENSEMBL sequence ENSDART00000134576 as reference. Sense and antisense RNA probes were respectively transcribed using T7 and SP6 RNA polymerase (Roche) on templates linearized with *SalI* or *NcoI* (New England Biolabs Inc, Ipswich, Massachusetts, USA). Probes were labeled with digoxigenin using the "DIG-RNA Labelling Kit" (Roche).

For all *in situ* hybridization experiments, embryos beyond 24 hpf were cultured in fish water containing 0.003% 1-phenyl-2-thiourea (Sigma-Aldrich, Saint Louis, Missouri, USA) before fixation to prevent pigmentation. When reaching the desired developmental stage, embryos were fixed overnight in 4% paraformaldehyde (Sigma-Aldrich) in PBS at 4°C, then dehydrated stepwise to methanol and stored at -20 °C.

Whole mount *in situ* hybridizations were essentially performed as described (Thisse and Thisse, 2014). Controls with sense ribo-probes were performed in parallel with antisense probes.

Images of stained embryos were taken on a Leica MZFLIII epifluorescence stereomicroscope equipped with a DFC 480 digital camera and LAS Leica imaging software (Leica, Wetzlar, Germany).

Some of the hybridized embryos were then embedded in paraffin (Paraplast plus, Bio Optica) and sectioned (8μm) on a microtome (Leitz 1516). The slides were mounted with Eukitt (Bio Optica) and all sections were observed using a Leica DM6000B microscope

equipped with a DFC 480 digital camera and LAS Leica imaging software (Leica, Wetzlar, Germany).

ZEBRAFISH *haspin* FULL LENGTH CLONING AND SEQUENCING, mRNA SYNTHESIS AND RESCUE EXPERIMENTS

Total RNA was isolated from a pool of embryos of the AB strain at tailbud stage using "TRIzol Reagent" (Ambion, Austin, Texas, USA) according to the manufacturer's instructions. Next, reverse-transcription was performed as described above. According to the sequence information gained from bioinformatic analysis, we amplified the full coding sequence of zebrafish *haspin* to confirm the sequence and to *in vitro* synthesize the corresponding transcript for rescue experiments. For amplification, we used a mixture of Taq DNA Polymerase (Thermo Fisher Scientific) and Pfu DNA Polymerase (Agilent Technologies, Santa Clara, CA, USA) to ensure accuracy during DNA synthesis. Reaction products were analyzed by 1% agarose-gel electrophoresis. All amplicons were first sub-cloned in the pJET 1.2 vector using the "CloneJET PCR Cloning Kit" (Thermo Fisher Scientific) and sequenced, to verify the absence of amplification errors, (Genewiz-DNA sequencing service). Next, they were cloned into the pCS2+ poly(A) vector, a commonly used zebrafish expression system, using the double restriction sites that we previously added to the primers used for amplification (*BamHI*, *XhoI;* New England Biolabs Inc). The obtained plasmids where then sent again for sequencing (Genewiz-DNA sequencing service) and used as template for generating sense mRNA, *in vitro* synthesized using the "mMessage mMachine kit" (Ambion) according to the manufacturer's instructions. The mRNA was then purified by phenol:chloroform extraction (Sigma-Aldrich), quantified and stored at -80°C. For rescue experiments, the synthesized mRNA, diluted in RNase-free water, was injected into one-or two-cell-stage embryos, separately from the ATG morpholino, to avoid *in vitro* hybridization of the two molecules prior to injection.

MOs-MEDIATED KNOCKDOWN, PHENOTYPE CHARACTERIZATION

Antisense morpholinos (GeneTools, Philomath, Oregon, USA) were designed against the AUG region of the zebrafish *haspin* coding sequence (*haspin* ATG MO, 5'-TTTTCCTCTTGCGTTCATCTTGGAC-3') and against the junction between exon 5 and intron 5/6 (*haspin* spl MO, 5'-GCATAATTACTTACAATTTGCTTGG-3'). A standard control oligo (Std-MO, 5'-CCTCTTACCTCAGTTACAATTTATA-3', against human *β-globin* gene)

with no target in zebrafish embryos, was also used, to check for non-specific effects due to the injection procedure.

All morpholinos were diluted in Danieau solution (Nasevicius and Ekker, 2000) and pressure-injected into 1-to-2 cell-stage embryos using Eppendorf FemtoJet Micromanipulator 5171. Rhodamine dextran (Molecular Probes, Life technology) was always co-injected as dye tracer.

For *in vivo* observations and imaging, embryos beyond 24 hpf were washed, dechorionated and anaesthetized with 0.016% tricaine (ethyl 3-aminobenzoate methanesulfonate salt; Sigma-Aldrich) before observations and picture acquisition.

For *in vivo* imaging of injected embryos we used a Leica MZFLIII epifluorescence stereomicroscope equipped with a DFC 480 digital camera and LAS Leica imaging software (Leica, Wetzlar, Germany).

RT-PCR analysis to determine efficacy of *haspin* spl MO was carried out on RNA isolated from 24 hpf morphant embryos using Go Taq polymerase (Promega) and specific primers, namely haspinspMOfor and haspinspMOrev (see list below). Amplicons were verified by agarose-gel electrophoresis and sequenced (Eurofins_Genomics-DNA sequencing service), to verify the expected exon skipping.

Antisense RNAs were *in vitro* transcribed for *otx3*, *fgf8*, *goosecoid (gsc)* and *chordin (chd)* ribo-probe synthesis. We used stock vectors present in our lab; these were linearized using the appropriate restriction enzymes and probes were *in vitro* transcribed using T7 or SP6 RNA polymerase (Roche). Probes were then labeled with digoxigenin using the “DIG-RNA Labelling Kit” (Roche). *In situ* hybridization assays were performed as mentioned above.

O-dianisidine staining was performed as described (Detrich *et al.*, 1995); pictures of the stained embryos were taken as mentioned above.

WESTERN BLOT EXPERIMENTS

All western blot experiments were essentially carried out as previously described (Bellipanni *et al.,* 2000). We used, as primary antibodies: rabbit antiH3Thr3PH (Merck Millipore) at 1/2500 dilution, mouse antiH3ser10PH (Abcam) at 1/5000 dilution, rabbit antiH3TOT (Merck Millipore) at 1/5000 dilution and rabbit antiαactin (Abcam) at 1/1500 dilution. Anti-mouse and anti-rabbit peroxidase-conjugated (Abcam) were used as secondary antibodies (1/10000 dilution).

ZEBRAFISH *haspin* MUTAGENESIS BY CRISPR-CAS9 SYSTEM

- Target selection

As described by (Hwang *et al*., 2013) and as already verified by Dr. Gianfranco Bellipanni and Dr. Darius Balciunas (Temple University, Philadelphia, USA; personal communication), the only requirement to be strictly followed for CRISPR target selection is the presence of a 5'-NGG-3' PAM site.

- sgRNAs synthesis

The sgRNAs were synthesized after a two steps PCR using the DR274 guide RNA expression vector as template (Addgene plasmid # 42250). DR274 was a gift from Keith Joung (Hwang *et al*., 2013). To synthesize our sgRNAs we designed specific short guide primers (see list below) containing, in addition to the sequence complementary to the target, a T7 promoter for *in vitro* transcription and a homology sequence to the sgRNA component of the DR274 vector. sgRNAs were *in vitro* transcribed using "MegaShortscript T7" kit (Thermo Fisher Scientific), according to manufacturer's instructions.

- *cas9* mRNA synthesis

We *in vitro* transcribed zebrafish-optimized *ncas9n* mRNA using pT3TS-nCas9n vector as template (Addgene plasmid # 46757). pT3TS-nCas9n was a gift from Wenbiao Chen (Jao *et al.*, 2013).

The vector was linearized using *XbaI* enzyme (New England Biolabs Inc.) and the mRNA was then *in vitro* transcribed using the "mMessage mMachine kit" (Ambion) according to the manufacturer's instructions. The mRNA was purified by phenol:chloroform extraction (Sigma-Aldrich), quantified and stored at -80°C.

- CRISPRS microinjection

The solution to inject was prepared by mixing sgRNAs together with the *cas9*mRNA and rhodamine dextran (Molecular Probes, Life technology) as a tracer, diluted in RNase-free water. This injection mix was pressure-injected into 1-to-2 cell-stage embryos using a Narishige micromanipulator. The optimal dose for each CRISPR was selected based on the evaluation of the toxicity and the phenotypic alterations resulting in the embryos, as well as the mortality rate.

- Mutations detection and screening

To extract genomic DNA from pools of embryos from adult fin clips for mutation detection, DNA extraction buffer (prepared as described by ZFIN community, see "https://zfin.org/zf_info/zfbook/chapt9/9.3.html", following "Large sample number") was added to the samples, that were then digested with Proteinase K (Sigma-Aldrich) at 65°C. Potassium acetate 8M was then used to remove proteins from DNA; after transfer of the supernatant phase to new clean tubes, DNA was precipitated using isopropanol and washed with 70% cold ethanol. Genomic DNA was resuspended in nuclease free water. PCR was then performed on genomic DNA using specific primers amplifying the region we targeted with our CRISPRs (see primers list below) and Taq DNA Polymerase (Thermo Fisher Scientific). To screen for mutations, PCR products were first of all processed using the "Surveyor Mutation Detection Kit" (IDT Technologies) according to manufacturer's instructions. After digestion with Surveyor nuclease, samples were analyzed by 2% agarose-gel electrophoresis to detect multiple bands derived from mismatches-directed cleavage. Surveyor-positive PCR samples from F1 pools of embryos that needed to be confirmed by Sanger sequencing were then purified using "DNA Clean-Up & Concentration Kit" (Zymo Research) according to manufacturer's instructions, and sent out for sequencing (Genewiz-DNA sequencing service). When screening for heterozygous F1 adult fish, surveyor-positive PCR amplicons derived from fin clips were first cloned in the pJET 1.2 vector using the "CloneJET PCR Cloning Kit" (Thermo Fisher Scientific) and then sequenced.

While screening for homozygous larvae or adult fish, PCR samples from F2 samples were directly purified as mentioned above and sent for sequencing (Genewiz-DNA sequencing service). All electropherograms were analyzed as mentioned above.

PRIMER SEQUENCES

For the sequences of primers used in our work, please refer to the list below.

-Primers for *haspin* probe synthesis:

Haspinishprobefor: 5'-AGTTGGAGCCTTGGATCTCC-3'

Haspinishproberev: 5'-GGCAGTCCTCTCTTCCTGTT-3'

-Primers for *haspin* temporal expression pattern on embryonic stages:

Haspseq2: 5'-AAGAGGATTCTCAGAGGCCA-3'

Haspinishproberev: 5’-GGCAGTCCTCTCTTCCTGTT-3’

-Primers for *haspin* full length amplification and cloning:
zFLHaspBamHIfrw:
5’-TGTCATGGATCCGTCCAAGATGAACGCAAGAGGAAAAAACGGG-3’
zFLHaspXhoIrev:
5’- TGTCATCTCGAGTCACTGAAAGAAACTGCACT-3’

-Primers for discerning both *haspin* isoforms temporal expression pattern on embryonic stages (first set of primers):
zhaspsplscreen frw: 5’-GCTGCTAATGAATGTGCTGG-3’
zhaspsplscreen rev: 5’-CTCTTCCTGTTTCTTGCTGC-3’

-Primers for discerning both *haspin* isoforms temporal expression pattern on adult organs (second set of primers):
zhaspsplscreenbis frw: 5’-TTGTCACAAGTCGCAGAAGACC-3’
zhaspsplscreenbis rev: 5’-GATGCTTTCGATGGTGTAGAGC-3’

-Primers for RT-PCR analysis to determine efficacy of *haspin* spl MO:
haspinspMOfor: 5’-AAGCCTCGAACCACAAAGAG-3’
haspinspMOrev: 5’-AACCTGTGTGTGTCTGAGCA-3’

-Short guide primers for sgRNAs CRISPR synthesis (composed of: T7 promoter; underlined sgRNA sequence, complementary to the target; homology to DR274):
sgRNAhaspinCRISPRE6:
5’-
CGCTAGCTAATACGACTCACTATA<u>GGAGGAGATCTCACTGATGG</u>GTTTTAGAGCTAGAAATAG-3’
sgRNAhaspinCRISPRATG:
5’-
CGCTAGCTAATACGACTCACTATAGG<u>TTTTCCTCTTGCGTTCATCT</u>GTTTTAGAGCTAGAAATAG-3’

-Primers for amplifying region targeted by CRISPR ATG (for mutation detection):
haspcrispATGscreenfrw: 5’-CTCAATTGCAGATTAGCAGAGC-3’
haspcrispATGscreenrev: 5’-CATCACTTTGGTCTTAGCAGTGC-3’

-Primers for amplifying region targeted by CRISPR E6 (for mutation detection):

haspcrispE6screenfrw: 5’-CTTTGTTCTAGGCTGTTCTTCACC-3’

haspcrispE6screenrev: 5’-CCCTCTTTCAGTTCTATGACTCTC-3’

-Primers for *gapdh* amplification:

gapdhfrw: 5’-GTGTAGGCGTGGACTGTGGT-3’

gapdhrev: 5’-TGGGAGTCAACCAGGACAAATA-3’

SUPPLEMENTARY FIGURES

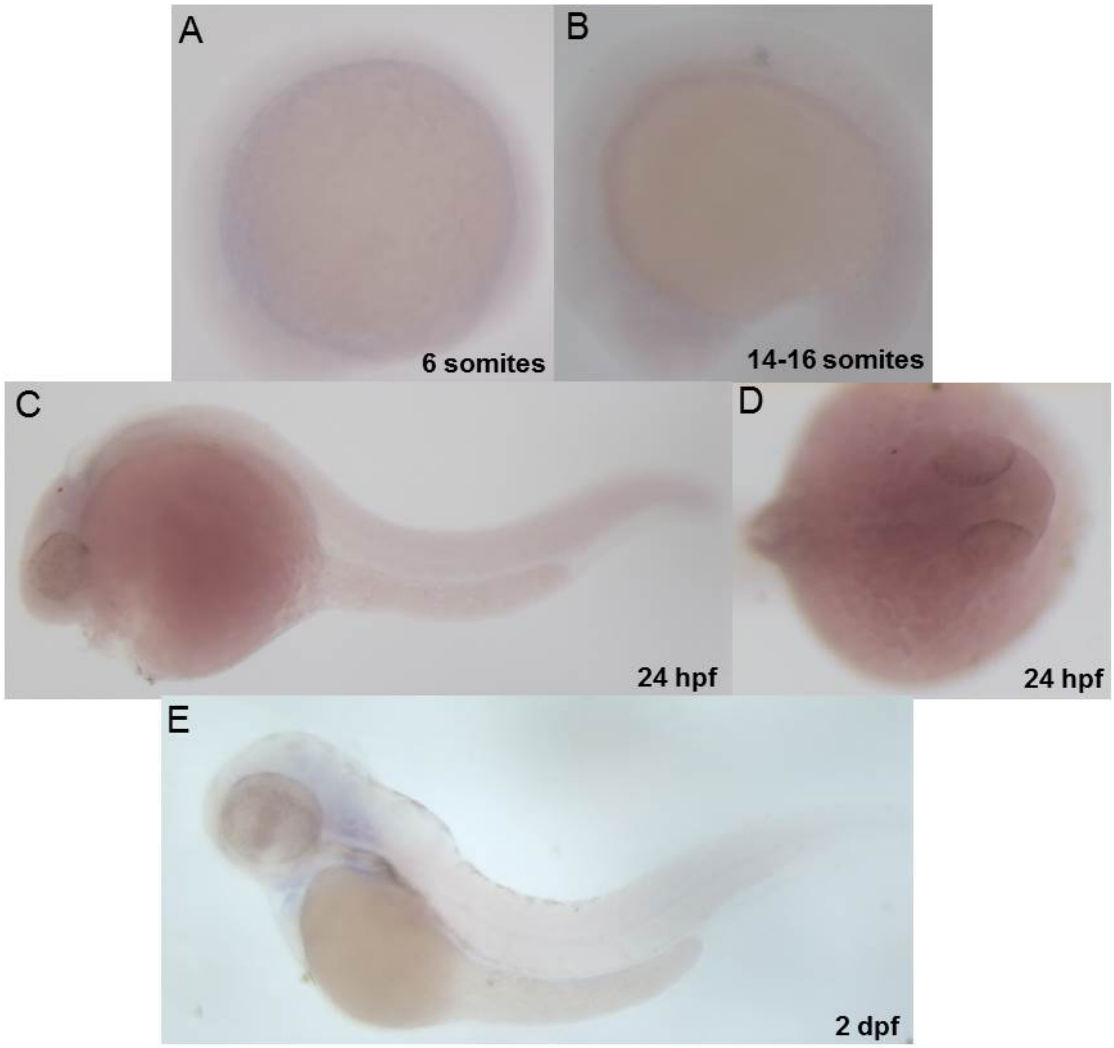

Suppl. fig. 1: *in situ* hybridization experiments conducted with *haspin* sense probe. No staining is detectable by hybridization with *haspin* sense probe. (A, B) Lateral view of embryos at somitogenesis stages with the cephalic region to the left. (C) Lateral view of a 24 hpf embryo with the cephalic region to the left. (D) Dorsal view of the cephalic region of a 24 hpf embryo from above. (E) Lateral view of a 2 dpf embryo with the cephalic region to the left.

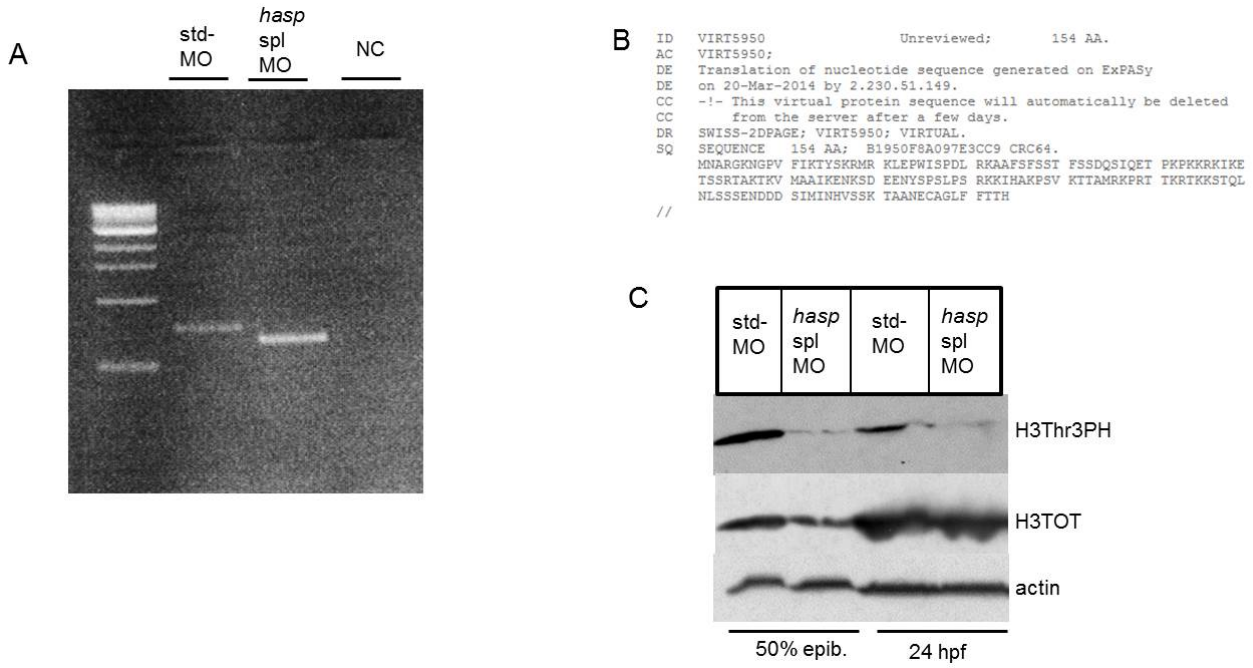

Suppl. figure 2: Effect of *haspin* spl MO microinjection. (A) RT-PCR analysis carried out on RNA isolated from *haspin* splicing morphant and std-morphants at 24hpf. Embryos were injected with 1.5 pmol/E for both MOs. The presence of a shorter aberrant transcript, compatible with the skipping of exon 5, is detectable in *haspin* morphants. Sanger sequencing of these bands confirmed this data. Negative control is shown in the right-most line. (B) Simulation of the translation of *haspin* coding sequence lacking exon 5 leads to the production of a truncated protein (only 154 aa) in which the functional C-term kinase domain is not included (analysis conducted with SMART tool). (C) Western blot assays performed on protein extracts from pools of embryos injected with *haspin* spl MO (1 pmol/E) at two different developmental stages. H3Thr3PH levels decrease in both stages analyzed after *haspin* spl MO micro-injection.

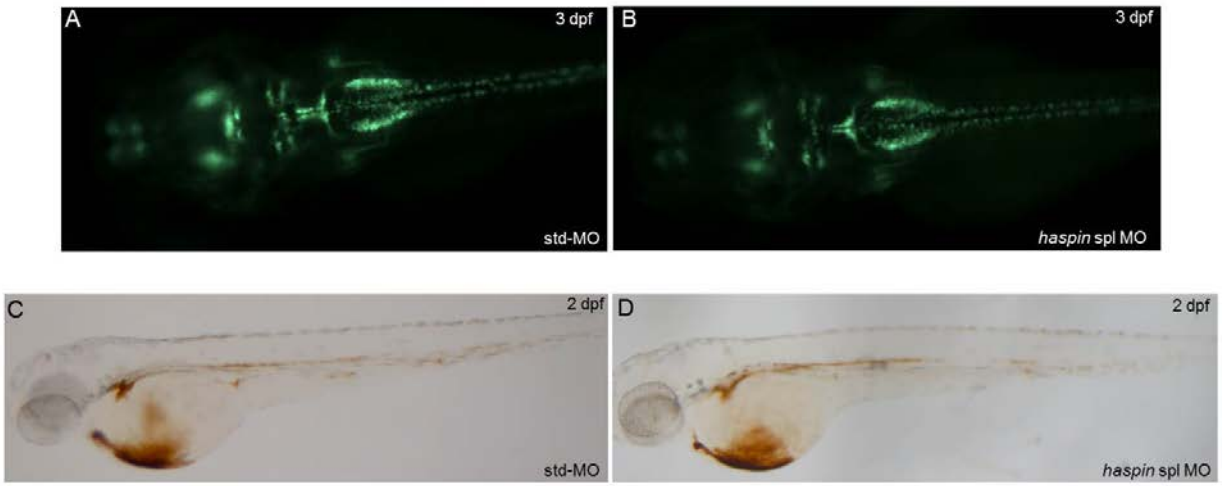

Suppl. figure 3: Phenotypic effect of *haspin* spl MO microinjection. (A,B) Dorsal view of 3 dpf embryos, with the cephalic region to the left, of the transgenic line *islet-1* EGFP, showing the patterning of the motor neurons of the hindbrain. No differences are detectable between controls (std-MO) and *haspin* spl morphants. Embryos were injected with 2 pmol/E for both MOs. (C,D) Lateral view of 2 dpf embryos, with the cephalic region to the left, stained with O-dianisidine in order to visualize hemoglobin. No differences are detectable between controls (std-MO) and *haspin* spl morphants. Embryos were injected with 2 pmol/E for both MOs.

APPENDIX

EMBRYONIC DEVELOPMENT OF ZEBRAFISH

The zebrafish eggs are small (400-500 µm), with a very large yolk mass. After the fertilization, several cytoplasmic rearrangements occur, and these events lead to the segregation of the cytoplasm to the animal pole, and the yolk mass to the vegetal pole. The segmentation (cleavage) is meroblastic and relative to the cytoplasm of the animal pole only. In this way, the formation of the "blastula" is observed. The blastula starts the gastrulation period, which is characterized by different cellular movements. Kimmel *et al*., (1995), distinguished the following developmental stages: zygote period (0-$^{3}/_{4}$ hpf), cleavage period ($^{3}/_{4}$-2$^{1}/_{4}$ hpf), blastula period (2$^{1}/_{4}$-5$^{1}/_{4}$ hpf), gastrula period (5$^{1}/_{4}$-10 hpf), segmentation period (10-24 hpf), pharingula period (24-48 hpf) and hatching period (48-72 hpf).

Zygote Period

The newly fertilized egg is in the zygote period until the first cleavage occurs, about 40 minutes after fertilization. The chorion swells and lifts away from the newly fertilized egg. Fertilization also activates cytoplasmic movements, easily evident within about 10 minutes. Nonyolky cytoplasm begins to stream toward the animal pole, segregating the blastodisc from the clearer yolk granule-rich vegetal cytoplasm. This segregation continues during early cleavage stages.

Cleavage Period

After the first cleavage the blastomeres divide at about 15-minute intervals. The cytoplasmic divisions are meroblastic; they only incompletely undercut the blastodisc, and the blastomeres, or a specific subset of them according to the stage, remain interconnected by cytoplasmic bridges. The six cleavages that comprise this period frequently occur at regular orientations and are synchronous. The cleavage period ends at 64-cell stage (2 hpf).

Blastula Period

We use the term blastula to refer to the period when the blastodisc begins to look ball-like, at the 128-cell stage, or eight zygotic cell cycle, and until the time of onset of gastrulation,

about cycle 14. Important processes occur during this blastula period; the embryo enters midblastula transition (MBT), the yolk syncytial layer (YSL) forms, and epiboly begins. Epiboly continues during the gastrulation period. Three different phases can be observed.

-Early-blastula: the marginal blastomeres lie against the yolk cell and remain cytoplasmatically connected to it throughout cleavage. Beginning during cycle 10, the marginal cells undergo a collapse, releasing their cytoplasm and nuclei together into the immediately adjoining cytoplasm of the yolk cell and forming the Yolk Syncytial Layer (YSL). After the YSL forms, the enveloping layer cells (EVL) that were in the second blastodisc tier, now lie at the marginal position and they are nonsyncytial.

-Mid-blastula: the YSL nuclei continue to undergo mitotic divisions in the midblastula, but the nuclear divisions are unaccompanied by cytoplasmic ones, and the yolk remains uncleaved and syncytial. After about three cycles, and coinciding with the beginning of epiboly, the YSL divisions abruptly cease. The YSL nuclei now begin to enlarge, possibly meaning that they are actively transcribing RNA. The YSL, an organ unique to teleosts, may be extraembryonic, making no direct contribution to the body of the embryo. At first the YSL has the form of a narrow ring around the blastodisc edge, but soon it spreads underneath the blastodisc, forming a complete “internal” syncytium (I-YSL), that persists throughout embryogenesis. In this position, the I-YSL might be presumed to be playing a nutritive role. Another portion of it, the E-YSL, is transiently “external” to the blastodisc edge, and appears to be a major motor for epiboly.

-Late-blastula: epiboly beginning in the late blastula is the thinning and spreading of both the YSL and the blastodisc over the yolk cell. During the early stages of this morphogenetic movement the blastodisc thins considerably, changing from a high-piled cell mound to a cup-shaped cell multiplayer of nearly uniform thickness. This is accomplished by the streaming outward, toward the surface, of the deepest blastomeres. As they move, they mix fairly indiscriminately among more superficial cells along their way, except for the EVL and the marginal blastomeres. These nonmixing marginal blastomeres will give rise to the mesoderm, and suggest the existence of a pattern established during early development. At 30% epiboly stage, the proper blastoderm begins to develop: it is uniform and formed by the EVL monolayer and a deep cells multilayer (Deep Enveloping Layer, DEL).

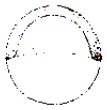

Gastrula Period

The beginning of involution defines the onset of gastrulation, and, so far as we have been able to tell, this occurs at 50%-epiboly. As a consequence, within minutes of reaching 50%-epiboly a thickened marginal region termed the "germ ring" appears, nearly simultaneously all around the blastoderm rim. Convergence movements then, nearly as rapidly, produce a local accumulation of cells at one position along the germ ring, the so-called embryonic shield. During these events, epiboly temporarily arrests, but after the shield forms, epiboly continues; the margin of the blastoderm advances around the yolk cell to cover it completely. The advance occurs at a nearly constant rate, over an additional 15% of the yolk cell each hour, and providing a useful staging index during most of gastrulation. Just as there was no blastocoele during the blastula period, there is no archenteron in the gastrula. Neither is there a blastopore; DEL cells involute at the blastoderm margin, which thus plays the role of the blastopore. Involution produces the germ ring by folding the blastoderm back upon itself. Hence, within the germ ring there are two germ layers: the upper, the epiblast, continues to feed cells into the lower, the hypoblast, throughout gastrulation. Between the two layers a fissure, termed "Brachet's cleft" is observed. Cells in the two layers are streaming in different directions. Except for the dorsal region, the epiblast cells generally stream toward the margin, and those reaching the margin move inward to enter the hypoblast. Then, as hypoblast cells, they stream away from the margin. The cells remaining in the epiblast when gastrulation ends correspond to the definitive ectoderm and will give rise to such tissues as epidermis, the central nervous system, neural crest, and sensory placodes. The hypoblast gives rise to derivatives classically ascribed to both the mesoderm and endoderm. At tail-bud stage (10 hpf), cell specifications processes are ending while cell differentiation mechanisms are turned on.

Segmentation Period

A wonderful variety of morphogenetic movements now occur, the somites develop, the rudiments of the primary organs become visible, the tail bud becomes more prominent and the embryo elongates. The AP and DV axes are unambiguous. The first cells differentiate morphologically, and the first body movements appear. Somites develop sequentially in the trunk and tail, and provide the most useful staging index. Anterior somites develop first and posterior ones last. Pronephric kidneys appear bilaterally deep to the third somite pair.

The notochord differentiates, also in an AP sequence. Some of its cells vacuolate and swell to become the structural elements of this organ, and others later form a notochord sheath, an epithelial monolayer that surrounds the organ. Endoderm develops on only the dorsal side of the embryo, beneath the axial and paraxial mesoderm. The epiblast, now exclusively ectodermal, undergoes extensive morphogenesis during the segmentation period. As gastrulation ends, the primordium of the central nervous system, the neural plate, is already fairly well delineated, because of its prominent thickness. The anterior region where the brain will form is particularly thick. Formation of the neural tube then occurs by a process known as "secondary neurulation". Secondary neurulation contrasts with "primary" neurulation, the version in vertebrates where a hollow tube forms from the neural plate by an uplifting and meeting together of neural folds. In teleosts the lumen of the neural tube, the neurocoele, forms by a late process of cavitation.

An intermediate and transient condensed primordium with no lumen, the neural keel, forms first. Because the times of neurulation and segmentation overlap so extensively the zebrafish does not have a distinct "neurula period" of development, such as occurs largely before segmentation in amphibian embryos.

Pharyngula Period

The pharyngula period (24-48 hpf) begins with the formation of the last somites (30/34 somites). At this time, the notochord is completely formed, and the brain is constituted by three lobes, which develop in an AP direction: forebrain, midbrain and hindbrain.

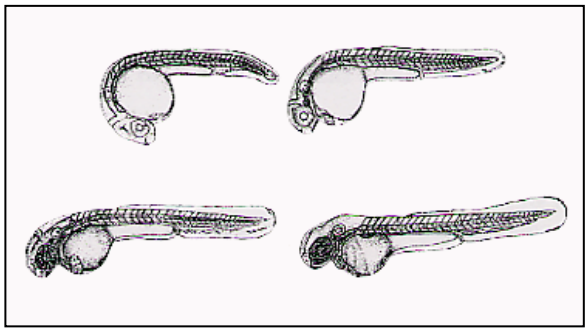

Hatching Period

During the last period, termed "hatching" (48-72 hpf), individuals within a single developing clutch hatch sporadically during the whole third day of development (at standard temperature), and occasionally later. At this time, we call these embryos "larvae"; morphogenesis of many organ rudiments is completing, and the embryo continues to grow at about the same rate.